NAVAL POSTGRADUATE SCHOOL

MONTEREY, CALIFORNIA

THESIS

ARTIFICIAL BOUNDARY CONDITIONS FOR FINITE ELEMENT MODEL UPDATE AND DAMAGE DETECTION

by

Emmanouil Damanakis

March 2017

Thesis Advisor:	Joshua H. Gordis
Second Reader:	Young W. Kwon

THIS PAGE INTENTIONALLY LEFT BLANK

REPORT DOCUMENTATION PAGE			Form Approved OMB No. 0704–0188
Public reporting burden for this collection of information is estimated to average 1 hour per response, including the time for reviewing instruction, searching existing data sources, gathering and maintaining the data needed, and completing and reviewing the collection of information. Send comments regarding this burden estimate or any other aspect of this collection of information, including suggestions for reducing this burden, to Washington headquarters Services, Directorate for Information Operations and Reports, 1215 Jefferson Davis Highway, Suite 1204, Arlington, VA 22202-4302, and to the Office of Management and Budget, Paperwork Reduction Project (0704-0188) Washington, DC 20503.			
1. AGENCY USE ONLY ***(Leave blank)***	**2. REPORT DATE** March 2017	**3. REPORT TYPE AND DATES COVERED** Master's thesis	
4. TITLE AND SUBTITLE ARTIFICIAL BOUNDARY CONDITIONS FOR FINITE ELEMENT MODEL UPDATE AND DAMAGE DETECTION			**5. FUNDING NUMBERS**
6. AUTHOR(S) Emmanouil Damanakis			
7. PERFORMING ORGANIZATION NAME(S) AND ADDRESS(ES) Naval Postgraduate School Monterey, CA 93943-5000			**8. PERFORMING ORGANIZATION REPORT NUMBER**
9. SPONSORING /MONITORING AGENCY NAME(S) AND ADDRESS(ES) N/A			**10. SPONSORING / MONITORING AGENCY REPORT NUMBER**
11. SUPPLEMENTARY NOTES The views expressed in this thesis are those of the author and do not reflect the official policy or position of the Department of Defense or the U.S. Government. IRB number N/A.			
12a. DISTRIBUTION / AVAILABILITY STATEMENT Approved for public release. Distribution is unlimited.			**12b. DISTRIBUTION CODE**

13. ABSTRACT (maximum 200 words)

In structural engineering, a finite element model is often used to estimate its dynamic or static behavior, and in conjunction with measured data, to monitor the health of a structure. This research is focusing on the use of experimental data for the improvement of a finite element model such that it accurately represents the structure, and in the localization of artificial damage in the model. The method of Artificial Boundary Conditions in model update and damage identification is used.

To update the finite element model, identified stiffness changes are typically applied at each element of the model. This research introduces and demonstrates a new method using the mean stiffness correction at every element, to produce improved prediction of natural frequencies. The use of this method in conjunction with a composite sensitivity matrix created from the application of artificial boundary conditions, and utilizing the higher modes, is shown to more accurately update the finite element model than the usual method.

Furthermore, this research demonstrates a new method for damage identification that uses subtraction of residual stiffness values, which can identify the damage regardless of location.

14. SUBJECT TERMS artificial boundary conditions, finite element model, model update, damage identification, natural frequencies, sensitivity matrix			**15. NUMBER OF PAGES** 169
			16. PRICE CODE
17. SECURITY CLASSIFICATION OF REPORT Unclassified	**18. SECURITY CLASSIFICATION OF THIS PAGE** Unclassified	**19. SECURITY CLASSIFICATION OF ABSTRACT** Unclassified	**20. LIMITATION OF ABSTRACT** UU

NSN 7540–01-280-5500 Standard Form 298 (Rev. 2–89)
Prescribed by ANSI Std. 239–18

THIS PAGE INTENTIONALLY LEFT BLANK

Approved for public release. Distribution is unlimited.

ARTIFICIAL BOUNDARY CONDITIONS FOR FINITE ELEMENT MODEL UPDATE AND DAMAGE DETECTION

Emmanouil Damanakis
Lieutenant, Hellenic Navy
B.S., Hellenic Naval Academy, 2008

Submitted in partial fulfillment of the
requirements for the degree of

MASTER OF SCIENCE IN MECHANICAL ENGINEERING

from the

NAVAL POSTGRADUATE SCHOOL
March 2017

Approved by: Joshua H. Gordis
Thesis Advisor

Young W. Kwon
Second Reader

Garth V. Hobson
Chair, Department of Mechanical and Aerospace Engineering

THIS PAGE INTENTIONALLY LEFT BLANK

ABSTRACT

In structural engineering, a finite element model is often used to estimate its dynamic or static behavior, and in conjunction with measured data, to monitor the health of a structure. This research is focusing on the use of experimental data for the improvement of a finite element model such that it accurately represents the structure, and in the localization of artificial damage in the model. The method of Artificial Boundary Conditions in model update and damage identification is used.

To update the finite element model, identified stiffness changes are typically applied at each element of the model. This research introduces and demonstrates a new method using the mean stiffness correction at every element, to produce improved prediction of natural frequencies. The use of this method in conjunction with a composite sensitivity matrix created from the application of artificial boundary conditions, and utilizing the higher modes, is shown to more accurately update the finite element model than the usual method.

Furthermore, this research demonstrates a new method for damage identification that uses subtraction of residual stiffness values, which can identify the damage regardless of location.

THIS PAGE INTENTIONALLY LEFT BLANK

TABLE OF CONTENTS

LIST OF FIGURES

THIS PAGE INTENTIONALLY LEFT BLANK

LIST OF TABLES

THIS PAGE INTENTIONALLY LEFT BLANK

LIST OF ACRONYMS AND ABBREVIATIONS

Abbreviations

ABC	Artificial Boundary Conditions
ASET	Analytic Set
DOF	Degree of Freedom
FE	Finite Element
FEM	Finite Element Model
FRF	Frequency Response Function
OSET	Omitted Set
PBC	Perturbed Boundary Condition

Symbols

$[\ ]$	Matrix
$\{\ \}$	Vector
$\{\ \}_{\text{exp}}$	Experimental Vector
$\{\ \}_{FE}$	Finite Element Vector

THIS PAGE INTENTIONALLY LEFT BLANK

ACKNOWLEDGMENTS

I dedicate this work to my wife, Stella, for her tremendous support, understanding, help, infinite patience, and unconditional love, who also brought to this world our beloved son.

I would also like to thank professor Joshua H. Gordis for his correct guidance, help, unlimited patience, and great professionalism, which helped me overcome any difficulties during our cooperation.

My special appreciation to professor Young W. Kwon for his excellence in teaching that made difficult concepts look like fundamental material, and his willingness to help whenever I need it.

Last, but not least, I would like to deeply thank my parents, Manoli and Maria, for the supplies that enabled me to achieve everything so far.

THIS PAGE INTENTIONALLY LEFT BLANK

I. INTRODUCTION

A. BACKGROUND

A large number of areas of engineering, such as structural engineering, and naval architecture, use the finite element method for analysis. In structural engineering, a finite element (FE) model is often used for the health monitoring of the structure and estimation of its dynamic or static behavior. Successful estimation and monitoring, therefore, require the finite element model to accurately represent the characteristics of the real structure. This is accomplished using a process called model update, which is discussed further in Chapter IV of this research. Then, using the damage identification technique, which is discussed in Chapter V, engineers can evaluate the health of the structure being modeled.

In this thesis, finite element models are used for structural dynamics modeling and simulation, and more specifically, for damage identification in a prototype structure after updating the finite element model. The prototype structure is restricted to a beam that will be discretized using the finite element method. The elements have specific properties that are discussed later on, so that when they are assembled, they represent the real structure as realistically as possible. The first stage of finite element method is to construct the elements, and the second stage is to assemble them into structural matrices.

Usually, dynamic characteristics of a prototype structure measured at spatially discrete points are used to characterize its behavior. Considering that the number of points at which response characteristics can be measured is small compared to the large number of points (degrees-of-freedom [DOF]) in a finite element model of the structure, and the frequency bandwidth of the test is limited, the measured characteristics are few. Although small in number, they are commonly used because they offer many useful data about the structure.

In recent decades, much research has been done in improving and developing methods to update a computer model using experimental data from a prototype structure. But, what does it mean to update a model? Conducting a vibration (modal) test of a structure can determine many of its modal features, such as frequencies, mass, stiffness, mode shapes and damping. However, that real measured data, usually do not match the predicted data from the finite element model. Thus, the updating process is used to make these modal parameters to match. Actually, the creation of a finite element model attempts to achieve modal parameters identical to those of the prototype structure. Ideally, the updating process will reveal physically realistic changes that need to be made to the finite element model such that the predicted modal parameters more closely match the measured values.

The updating process of the FE model is accomplished by modifying some of its parameters until it represents the prototype structure better. Thus, it is necessary to adjust some parameters of the finite element model until the estimated modal parameters, like natural frequencies and mode shapes, match the real measured data of the structure [1]. Usually, parameters like moduli of elasticity or density are modified. These ideas are further explained in Chapter II. So far the theory of model updating has been verified using simulated data (data predicted using a computer's software) [1].

To define the computer model accurately, a large number of parameters (physical and geometric data) may be required. Using the geometry and some material properties of a structure that are well known and easily measured (e.g., density), a similar finite element model consisting of these properties can be created. Nevertheless, the modal parameters of the finite element model are not similar to the real structure as formerly discussed; thus, the finite element model is inaccurate. Usually, there will be a mismatch in the measured modal parameters since the computer model is based on idealizations and assumptions.

It is crucial to acquire high quality dynamic property data from the experiment, which is not so difficult today since the technology has been improved and the equipment used is superior. However, only a small number of useful modal parameters are available from a modal test, order of magnitude $10^1 - 10^2$ times less than the parameters of the real structure [2] due to equipment constraints. Only a small number of modal parameters can be measured during an experimental test, which is proportional to the number of measurement equipment mounted on the structure. This parameter inequality leads to an underdetermined problem in that there are typically many more parameters in the finite element model that are of questionable accuracy.

Moreover, the ultimate purpose of model update is to use this model in the future for damage detection. In this process the updated model is used as a reference point, so that the new modal parameters of the prototype but damaged structure can be compared and the damage can be localized. This means that some parameters of the damaged structure are in error, although they are measured during the experiment. The damage identification process is used to find these parameters, which are unknown. This enhances the underdetermined problem that was discussed before.

B. LITERATURE REVIEW

As formerly said, there is confidence in the accuracy of the measured natural frequencies of the structure. Therefore, the resonant frequency data are used for FE model update and damage detection [3]. During the oscillation of a structure at one of its resonant frequencies, the point of the structure that is measured has maximum displacement. Consequently, by artificially exciting the structure and plotting the dynamic displacement over the frequency, the resonant frequencies of the structure can be accurately identified over the measured frequency domain. Unfortunately, the number of measurable natural frequencies is not large enough, since it is difficult to measure the higher natural frequencies of a real structure, to use this information in the updating process.

One technique to expand the resonant frequency dataset is to physically alter the boundary conditions of the structure [4]. This is feasible by applying an actual pin or adding mass at selected points of the structure. This technique is one of the first to alter the structure and is called “perturbed boundary condition (PBC)” [4]. It is obvious that each time a different boundary condition is applied a physical modification of the structure occurs. Taking into consideration the inexact characterization of joints, connections, and the inaccurate physical boundary conditions, the resonant frequency dataset may not be so accurate. Moreover, it is difficult, expensive, and time consuming to implement this technique in practice.

Recently another more effective method was proposed, the method of “artificial boundary conditions (ABC)” [2], [5]. The word artificial is used because altered boundary conditions are applied to the test data computationally. This artificial boundary condition is also applied to the finite element model [2]. There is no need to actually apply or modify the prototype structure; thus, this method is fast, cheap, and easy. Using this method, a large number of resonant frequency datasets can be extracted, and thus the expansion of the set of measured resonant frequencies is feasible [2]. The additional natural frequencies that correspond to any ABC system that is chosen can be obtained from any square frequency response function (FRF) matrix measured in a test. These measured frequencies correspond very accurately to the natural frequencies that would be calculated by physically applying the boundary conditions at the structure; see [2]. For example, for a structure with five points of measurement, there are 31 different structure configurations (ABC sets) to calculate the resonant frequencies. The artificial pins can be posed at any possible combination of the measured points. The only limit is in the number of measurement equipment that can be mounted on the structure, but even if this number is small, the number of possible structure configurations is large enough, as demonstrated in the previous example.

Alternatively, a recent study [6] uses anti-resonant frequencies rather than the resonant frequencies for model updating. In this study the location of the pin that was used in the generation of the anti-resonant frequency dataset was determined arbitrarily. An anti-resonant point is a point that does not move during the oscillation of the structure for a specific frequency. This frequency is called the anti-resonant frequency. Because a systematic approach for an effective structure configuration was not used, this technique is not easily applied to different structures. Moreover, the accurate measurement of the displacement of an anti-resonant point is susceptible to noise error because its value is close to zero. Thus, the identification of resonant frequencies is more accurate than the anti-resonant frequencies.

In [7], the genetic algorithm methodology is introduced in order to identify which artificial boundary condition frequencies are optimal for model updating. This methodology actually is used to optimize a globally given objective function. Moreover, in [8], the same methodology is used successfully for updating the computer model based on measured dynamic properties. However, this process is satisfactory for a small number of unknown parameters, a problem that is tackled by incorporating the eigensensitivity-based updating method.

A new method to identify the parameter-specific optimal artificial boundary condition set was introduced by Gordis [9]. This method is based on the QR (Q is an orthogonal matrix and R is an upper triangular matrix) decomposition with column pivoting. According to this method, to identify the damage in the structure, a square composite sensitivity matrix should be created. The concept and formulation of the sensitivity matrix is covered later in this thesis. Each row of each sensitivity matrix for the different artificial boundary condition set can identify the damage associated with a specific location. At the end of this method, the composite sensitivity matrix will have a different row for each location of potential damage to the model; thus, the damage identification is more effective and accurate.

Generally speaking, two different theories exist regarding how to create the elements of the finite element model. The first is the Euler-Bernoulli theory, and the second is the Timoshenko theory [10]. The main difference between these two theories is that in the Euler-Bernoulli's theory, the plane sections of the elements remain plane and normal to deformed longitudinal axis. In the Timoshenko's theory, by contrast, the plane sections of the elements remain plane but not normal to deformed longitudinal axis. Timoshenko's theory includes the rotatory inertia and shear deformation effects of the beam's elements.

C. SCOPE OF THESIS

This research seeks to extend the possibility of using experimental data for model updating and damage detection. Previous methods used for model update and damage identification using simulated data do not produce correct result using experimental data.

Initially an investigation is conducted to decide which data are best to be used for the needed purposes. Then, new methods for both model update and damage identification are introduced and investigated.

D. NOTES ON THESIS

In this thesis, the prototype structure which is used for the experiment is a beam. For simplicity reasons and brevity, a 2-D Euler-Bernoulli beam formulation is used to simulate the prototype structure.

The finite element model formulation and any other computational research is performed in MATLAB [11] . The Pulse Reflex software of Bruel & Kjaer Company [12] is used for recording the experimental data.

II. THEORY

A. GOVERNING VIBRATION EQUATION

In theory, a structure has an infinite number of degrees of freedom (DOF). Nevertheless, the finite element model is created with a finite number of degrees of freedom, (n), enough to simulate accurately the structure. A dynamic system under an excitation is described by the governing equation:

$$[M]\{\ddot{x}\}+[C]\{\dot{x}\}+[K]\{x\}=\{f(t)\}\ , \tag{2.1}$$

where $[M]$ is the mass matrix, $[K]$ is the stiffness matrix and $[C]$ is the damping matrix. Each matrix has size n x n. The vector $\{f(t)\}$ is the externally applied excitation on the structure. The displacement at the corresponding points of the structure is $\{x\}$, the first derivative of the displacement with respect to time is $\{\dot{x}\}$ (velocity), and the second derivative of the displacement with respect to time is $\{\ddot{x}\}$ (acceleration). The mass and stiffness matrices are easily derived while the damping matrix is not, since the mechanism of energy dissipation is not yet well understood. By omitting the damping matrix in Equation (2.1), the derivation of the undamped equation of motion is performed:

$$[M]\{\ddot{x}\}+[K]\{x\}=\{f(t)\}\ . \tag{2.2}$$

In the case of an unforced (free) vibration, the Equation (2.3) is obeyed:

$$[M]\{\ddot{x}\}+[K]\{x\}=0\ . \tag{2.3}$$

The general solution of Equation (2.3) is of the form:

$$\{x\}=\{\Phi\}e^{i\omega_j t}\ , \tag{2.4}$$

where ω_j are the resonant frequencies. Substituting (2.4) in (2.3) leads to:

$$[\mathrm{K}]\{\Phi\} = \omega^2 [\mathrm{M}]\{\Phi\}. \tag{2.5}$$

The solution of Equation (2.5) yields n eigenpairs, where the eigenvalues of the solution are the natural frequencies ω_j, and the eigenvectors of the solution are the natural modes $[\Phi]$.

The eigenvectors of the solution of (2.5) are arbitrarily scaled. Similarly, the eigenvectors are scaled such that:

$$[\Phi]^{\mathrm{T}} [\mathrm{M}][\Phi] = [\mathrm{I}] \ , \tag{2.6}$$

which results in

$$[\Phi]^{\mathrm{T}} [K][\Phi] = diag(\lambda_i) \ , \tag{2.7}$$

where Φ is the mass normalized eigenvector matrix.

Usually, if damping is taken into consideration, the assumption (2.8) is used:

$$[C] = \alpha * [K] + \beta * [M], \tag{2.8}$$

where α and β are real constants. This is proportional damping.

If this assumption has been made then the damping is proportional to stiffness and mass matrices, and if mass normalized mode shapes are used,

$$[\Phi]^{\mathrm{T}} [C][\Phi] = diag(2\zeta_i \omega_i), \tag{2.9}$$

where ζ_i is the damping ratio of each mode.

B. TWO DIMENSIONAL EULER–BERNOULLI BEAM

In this research, the finite element model is constructed by two–dimensional Euler–Bernoulli beam elements. Following, the derivation of the stiffness and mass element matrices is performed.

1. Stiffness Matrix Construction

From elementary theory, as in [13], a beam under shearing and rotational loading (Figure 1) has the lateral displacement of cubic order, so:

$$u = \begin{bmatrix} N_1 & N_2 & N_3 & N_4 \end{bmatrix} \begin{Bmatrix} y_1 \\ \theta_1 \\ y_2 \\ \theta_2 \end{Bmatrix}, \tag{2.10}$$

where u is the displacement of a general point in the bar and N_i are the shape functions.

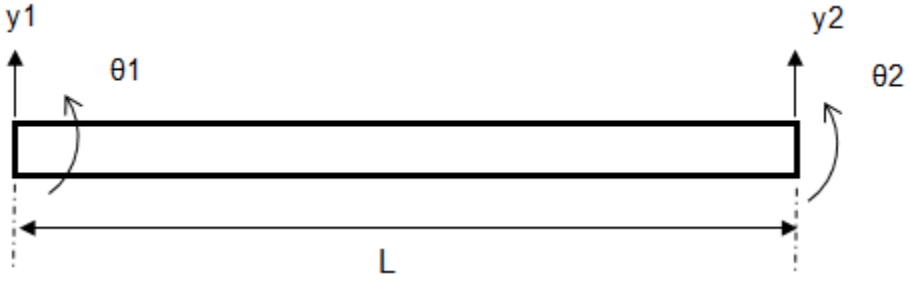

Figure 1. Beam under Shearing and Rotational Loading.

The shape functions are expressed as [13]:

$$N_1 = 1 - \frac{3x^2}{L^2} + \frac{2x^3}{L^3} \tag{2.11}$$

$$N_2 = x - \frac{2x^2}{L} + \frac{x^3}{L^2} \tag{2.12}$$

$$N_3 = \frac{3x^2}{L^2} - \frac{2x^3}{L^3} \tag{2.13}$$

$$N_4 = \frac{x^2}{L} + \frac{x^3}{L^2} . \tag{2.14}$$

Therefore, the strain displacement matrix [B] is [13]:

$$[\mathrm{B}] = [\partial]^{\mathrm{T}} [N] = \left[-\frac{6}{L^2} + \frac{12x}{L^3} \quad -\frac{4}{L} + \frac{6x}{L^2} \quad \frac{6}{L^2} - \frac{12x}{L^3} \quad -\frac{2}{L} + \frac{6x}{L^2} \right] . \tag{2.15}$$

So, the beam element stiffness matrix [13] is:

$$[K]_e = \int_V \left([\mathrm{B}]^{\mathrm{T}} [EI] [\mathrm{B}] \right) dV \ , \tag{2.16}$$

where dV is the volume of the element.

Combining (2.15) and (2.16) results in the stiffness element matrix:

$$[K]_e = \frac{EI}{L} \begin{bmatrix} 12/L^2 & 6/L & -12/L^2 & 6/L \\ 6/L & 4 & -6/L & 2 \\ -12/L^2 & -6/L & 12/L^2 & -6/L \\ 6/L & 2 & -6/L & 4 \end{bmatrix} . \tag{2.17}$$

2. Mass Matrix Construction

To simulate more realistically the prototype structure's mass undergoing acceleration, Equation (2.18) [13], which results in a continuous inertia distribution, is used:

$$[M]_e = \int_V \rho [N]^{\mathrm{T}} [N] dV \ , \tag{2.18}$$

where ρ is the material density.

Substituting the shape functions (2.11)–(2.14) into (2.18) and integrating over the volume leads to the element mass matrix:

$$[M]_e = \frac{\rho AL}{420}\begin{bmatrix} 156 & 22L & 54 & -13L \\ 22L & 4L^2 & 13L & -3L^2 \\ 54 & 13L & 156 & 22L \\ -13L & -3L^2 & 22L & 4L^2 \end{bmatrix}. \tag{2.19}$$

C. ANALYTICAL AND OMITTED COORDINATE SETS

We can express Equation (2.3) more explicitly as:

$$\begin{bmatrix} M_{11} & \cdots & M_{1n} \\ \vdots & \ddots & \vdots \\ M_{n1} & \cdots & M_{nn} \end{bmatrix}\begin{Bmatrix} \ddot{x}_1(t) \\ \vdots \\ \ddot{x}_n(t) \end{Bmatrix} + \begin{bmatrix} K_{11} & \cdots & K_{1n} \\ \vdots & \ddots & \vdots \\ K_{nn} & \cdots & K_{nn} \end{bmatrix}\begin{Bmatrix} x_1(t) \\ \vdots \\ x_n(t) \end{Bmatrix} = \begin{Bmatrix} f_1 \\ \vdots \\ f_n \end{Bmatrix}. \tag{2.20}$$

A continuous system of infinite degrees of freedom is approximated with the Equation (2.20) as a system of n degrees of freedom. During a real experimental test only a small number of measured degrees of freedom are available. The measured coordinates—i.e., the location where the instrumentation is placed and the degrees of freedom that they can measure (displacement or rotation)—are called the analytic set (ASET). The rest of the unmeasured degrees of freedom are the omitted coordinate set (OSET).

Assuming steady-state harmonic excitation and response, Equation (2.20) becomes:

$$\left[\begin{pmatrix} K_{11} & \cdots & K_{1n} \\ \vdots & \ddots & \vdots \\ K_{n1} & \cdots & K_{nn} \end{pmatrix} - \Omega^2 \begin{pmatrix} M_{11} & \cdots & M_{1n} \\ \vdots & \ddots & \vdots \\ M_{n1} & \cdots & M_{nn} \end{pmatrix}\right]\begin{Bmatrix} x_1(t) \\ \vdots \\ x_n(t) \end{Bmatrix} = \begin{Bmatrix} f_1 \\ \vdots \\ f_n \end{Bmatrix}, \tag{2.21}$$

where Ω is the frequency of the harmonic excitation. Equation (2.21) includes measured and unmeasured degrees of freedom. By taking into account ASET and OSET coordinate sets, Equation (2.21) can be so partitioned and becomes:

$$\left[\begin{pmatrix} K_{\alpha\alpha} & K_{\alpha o} \\ K_{o\alpha} & K_{oo} \end{pmatrix} - \Omega^2 \begin{pmatrix} M_{aa} & M_{\alpha o} \\ M_{o\alpha} & M_{oo} \end{pmatrix}\right] \begin{Bmatrix} x_\alpha \\ x_o \end{Bmatrix} = \begin{Bmatrix} f_a \\ f_0 \end{Bmatrix} , \tag{2.22}$$

where the subscript “a” denotes the analytical coordinates and the subscript “o” denotes the omitted coordinates. Assuming no excitation on the omitted coordinates, Equation (2.22) results in:

$$\left[\begin{pmatrix} K_{\alpha\alpha} & K_{\alpha o} \\ K_{o\alpha} & K_{oo} \end{pmatrix} - \Omega^2 \begin{pmatrix} M_{aa} & M_{\alpha o} \\ M_{o\alpha} & M_{oo} \end{pmatrix}\right] \begin{Bmatrix} x_\alpha \\ x_o \end{Bmatrix} = \begin{Bmatrix} f_a \\ 0 \end{Bmatrix} . \tag{2.23}$$

Generally speaking, Equation (2.23) represents a system of two sets of equations. The solution is of the form:

$$[K_{o\alpha}]\{x_a\} + [K_{oo}]\{x_o\} - \Omega^2 \left[[M_{o\alpha}]\{x_a\} + [M_{oo}]\{x_o\}\right] = 0 . \tag{2.24}$$

Solving for $\{x_0\}$ results in:

$$\{x_0\} = \left[\mathrm{I} - \Omega^2 K_{00}^{-1} \mathrm{M}_{00}\right]^{-1} \left[-\mathrm{K}_{00}^{-1} \mathrm{K}_{o\alpha} + \Omega^2 K_{00}^{-1} M_{o\alpha}\right] \{x_a\} . \tag{2.25}$$

It is generally known that:

$$[A]^{-1} = \frac{1}{Det[A]} Adj[A] , \tag{2.26}$$

where $Det[A]$ is the determinant and $Adj[A]$ is the adjoint of matrix $[A]$. So from (2.25)

$$\left[\mathrm{I}-\Omega^2 K_{00}^{-1}\mathrm{M}_{00}\right]^{-1}=\frac{1}{Det\left[\mathrm{I}-\Omega^2 K_{00}^{-1}\mathrm{M}_{00}\right]}Adj\left[\mathrm{I}-\Omega^2 K_{00}^{-1}\mathrm{M}_{00}\right]\ , \tag{2.27}$$

it is obvious that for some values of Ω,

$$Det\left[\mathrm{I}-\Omega^2 K_{00}^{-1}\mathrm{M}_{00}\right]=0\,. \tag{2.28}$$

Therefore, the inverse matrix does not exist for those frequencies.

This means that the solutions, Ω, of Equation (2.29):

$$\left[K_{oo}\right]-\Omega^2\left[M_{oo}\right]=0\ , \tag{2.29}$$

are the natural frequencies of the OSET system. Thus, when the ASET coordinates are constrained to the ground, the eigensolution of Equation (2.29) can be derived.

D. REDUCED ORDER MODEL

The impedance of a structure or dynamic stiffness, (Z), is the resistance in motion of this structure, when subjected to a harmonic excitation, and it is dependent on the frequency of the harmonic excitation. The inverse of the impedance, $(\mathrm{Z})^{-1}$, is called the frequency response function (FRF). The symbol that usually is used to represent the inverse of the impedance is (H). In a real experiment only a small number of degrees of freedom can be measured, since the number of transducers is finite, and thus, a reduced order model arises. The impedance of the reduced order model is nonlinearly dependent on the impedance of the full order model with infinite number of degrees of freedom [2]. This results in the following FRF matrix (2.30):

$$\left[\mathrm{H}\right]=\begin{bmatrix}H_{aa} & H_{ao}\\ H_{oa} & H_{oo}\end{bmatrix}\ , \tag{2.30}$$

where as previously defined, the “a” subscript denotes the analytic measurements and the “o” subscript denotes the omitted measurements. Consequently, $[H_{aa}]$ represents an exact dynamic reduced model [2]. The impedance of the structure is related to the frequency response function, as mentioned before, with the inverse operation. Thus:

$$\begin{bmatrix} Z_{aa} & Z_{oa} \\ Z_{ao} & Z_{oo} \end{bmatrix} \begin{bmatrix} H_{aa} & H_{oa} \\ H_{ao} & H_{oo} \end{bmatrix} = \begin{bmatrix} I & 0 \\ 0 & I \end{bmatrix} . \tag{2.31}$$

Solving for $[H_{aa}]$ results in:

$$[H_{aa}] = \left[Z_{aa} - Z_{ao} Z_{oo}^{-1} Z_{oa} \right]^{-1} . \tag{2.32}$$

Rearranging Equation (2.22) in terms of impedance results in:

$$\begin{bmatrix} Z_{aa} & Z_{ao} \\ Z_{oa} & Z_{oo} \end{bmatrix} \begin{Bmatrix} x_a \\ x_o \end{Bmatrix} = \begin{Bmatrix} f_a \\ 0 \end{Bmatrix} . \tag{2.33}$$

Solving Equation (2.32) for $\{f_a\}$ results in [5]:

$$\{f_a\} = \left[Z_{aa} - Z_{ao} Z_{oo}^{-1} Z_{oa} \right] \{x_a\} . \tag{2.34}$$

From a comparison of Equations (2.32) and (2.34), it is obvious that the term $\left[Z_{aa} - Z_{ao} Z_{oo}^{-1} Z_{oa} \right]$ is common. This implies that the measured frequency response function extracted from a real modal experiment is equivalent to the inverse of an impedance matrix extracted from a dynamically reduced model. Furthermore, the elements of the term, Z_{oo}^{-1}, will be singular at the natural frequencies of the OSET. Thus, from Equation (2.32) the elements of the term, $H_{aa}{}^{-1}$, will also be very large (singular) at the same natural frequencies [2]. We may conclude that, by using artificial boundary conditions on the finite element

model, we can extract the same natural frequencies as we would if actual boundary conditions had been applied at the same locations.

E. CAUCHY'S INTERLACE THEOREM

Consider a matrix A, of dimension nxn, and a submatrix H, of dimension mxm. In general, Cauchy's interlace theorem is used to identify the relationship of the eigenvalues between the submatrix H and matrix A. From the analysis made in [14], we can assume that the matrix A has eigenvalues: $\alpha_1 \le \alpha_2 \le \cdots \le \alpha_n$ and the submatrix H has eigenvalues: $\theta_1 \le \theta_2 \le \cdots \le \theta_m$.

Then for j = 1, 2, … , m:

$$\alpha_j \le \theta_j \le \alpha_{j+n-m} \Leftrightarrow \alpha_{-(j+n-m)} \le \theta_{-j} \le \alpha_{-j} ,$$

and for k = 1,2, … ,n

$$\theta_{k-n+m} \le \alpha_k \le \theta_k \Leftrightarrow \theta_{-k} \le \alpha_{-k} \le \theta_{-(k-n+m)} .$$

This simply means that eigenvalues of H submatrix $\{\theta\}$ are an inner bound on eigenvalues of matrix A. To demonstrate the previous concept, a simple example is provided. Assume the following matrix A :

$$A = \begin{bmatrix} 0 & \kappa & 0 \\ \kappa & 0 & \tau \\ 0 & \tau & 0 \end{bmatrix}, \text{ with eigenvalues } \begin{matrix} \alpha_1 = -\sqrt{\left(\kappa^2 + \tau^2\right)} \\ \alpha_2 = 0 \\ \alpha_3 = \sqrt{\left(\kappa^2 + \tau^2\right)} \end{matrix} ,$$

and the submatrix:

$$\mathrm{H} = \begin{bmatrix} 0 & \kappa \\ \kappa & 0 \end{bmatrix} , \text{ with eigenvalues } \begin{matrix} \theta_1 = -\kappa \\ \theta_2 = \kappa \end{matrix} .$$

Then the following is true:

$$\alpha_1 \le \theta_1 \le \alpha_2 \le \theta_2 \le \alpha_3 \ .$$

In Figure 2, a graphical representation is also provided.

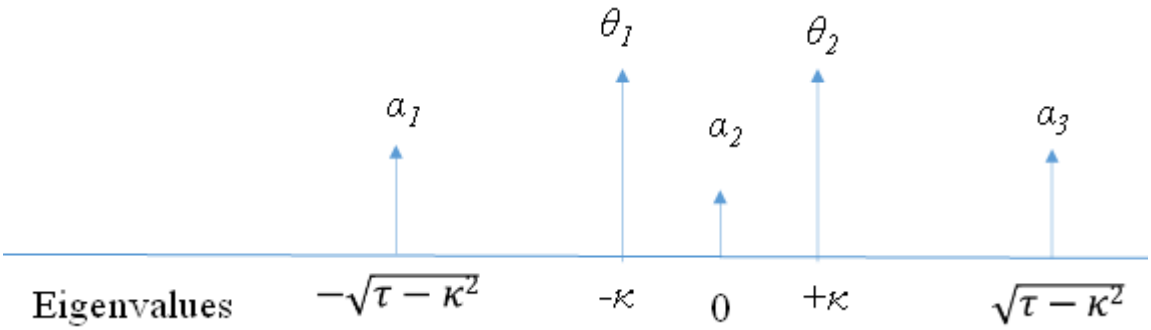

Figure 2. Graphical Representation of Cauchy's Theorem.

This theorem is going to be used later to validate the experimental set up process, and the measured natural frequencies.

F. FREQUENCY RESPONSE FUNCTION

As previously outlined, the inverse of impedance, $(Z)^{-1}$, is the frequency response function. This frequency response function is determined experimentally by measuring the excitation of a DOF and the response of the same, or any other DOF, at the same time. By examining the FRF much modal information can be extracted, including the amplitude and the phase of the response at a specific DOF, the natural frequencies, the damping ratios, and the mode shapes of the structure. If the excitation force is applied at the same DOF as the response DOF, then this FRF is called a driving point FRF, and the plot of such FRF always has an anti-resonant frequency after each resonant frequency. It is obvious that the measurement is made in time domain initially, but through fast Fourier analysis (FFT), the measured time histories are converted to frequency domain. As previously said:

$$\left[Z(\Omega)\right] = \left[H(\Omega)\right]^{-1} \ . \qquad (2.35)$$

In terms of impedance, Equation (2.21) can be written as:

$$\begin{bmatrix} Z_{11} & \cdots & Z_{1n} \\ \vdots & \ddots & \vdots \\ Z_{n1} & \cdots & Z_{nn} \end{bmatrix} \begin{Bmatrix} x_1(t) \\ \vdots \\ x_n(t) \end{Bmatrix} = \begin{Bmatrix} f_1 \\ \vdots \\ f_n \end{Bmatrix} , \tag{2.36}$$

where impedance is in the frequency domain and is equal to:

$$\left[Z(\Omega) \right] = \left[K - \Omega^2 M + j\Omega C \right] . \tag{2.37}$$

Assume a coordinate transformation, which is of the form:

$$\{x\} = [\Phi]\{q\} , \tag{2.38}$$

where $[\Phi]$ is the mode shape matrix and $\{q\}$ is modal coordinate.

Taking into consideration (2.6), we substitute (2.38) in (2.36) which results in:

$$[Z][\Phi]\{q\} = \{f\} . \tag{2.39}$$

Substituting (2.37) into (2.39) and premultiplying by $[\Phi]^{\mathrm{T}}$ results in:

$$\left[[\Phi]^{\mathrm{T}} [K][\Phi] - \Omega^2 [\Phi]^{\mathrm{T}} [M][\Phi] + j\Omega [\Phi]^{\mathrm{T}} [C][\Phi] \right] \{q\} = [\Phi]^{\mathrm{T}} \{f\} . \tag{2.40}$$

From (2.6), (2.7), and (2.9), the previous equation (2.40) becomes:

$$\left[\omega_i^2 - \Omega^2 + 2j\zeta\Omega\omega_i \right] \{q\} = [\Phi]^T \{f\} . \tag{2.41}$$

However, in Equation (2.41) the first term is the modal impedance matrix [Z], which is diagonal. Solving for $\{q\}$ and substituting back to (2.38) results in:

$$\{x\} = [\Phi] \frac{1}{\left[\omega_i^2 - \Omega^2 + 2j\zeta\Omega\omega_i\right]} [\Phi]^T \{f\} \ . \tag{2.42}$$

Thus, the frequency response function can also be defined as:

$$\left[H(\Omega)\right] = [\Phi] \frac{1}{\left[\omega_i^2 - \Omega^2 + 2j\zeta\Omega\omega_i\right]} [\Phi]^T \ , \tag{2.43}$$

or in summation form:

$$\left[\mathrm{H}(\Omega)\right] = \sum_{k=1}^{\text{modes}} \frac{\left\{\Phi^k\right\}\left\{\Phi^k\right\}^T}{\omega_k^2 - \Omega^2 + 2j\zeta\Omega\omega_k} \ . \tag{2.44}$$

Depending on the DOF at which the excitation force is applied, and the DOF where the response is measured, Equation (2.44) can be written as:

$$\mathrm{H}_{ij}(\Omega) = \sum_{k=1}^{\text{modes}} \frac{\Phi_i^k \Phi_j^k}{\omega_k^2 - \Omega^2 + 2j\zeta\Omega\omega_k} \ , \tag{2.45}$$

where the subscript “i” denotes the measured DOF by applying an excitation force at “j” DOF.

G. SYNTHESIS FOR ARTIFICIAL BOUNDARY CONDITIONS

Assuming the free-free beam of Figure 3, with N nodes, the frequency response function equation of steady-state response is:

$$\{X(\Omega)\} = [H(\Omega)]\{F(\Omega)\} \ , \tag{2.46}$$

where $\{X(\Omega)\}$ is the displacement of each node, $[H(\Omega)]$ is the FRF matrix, and $\{F(\Omega)\}$ is the amplitude of the force at each node. All of the quantities in

Equation (2.46) are dependent on frequency (Ω); however, from now on, the frequency-dependency will be omitted for clarity.

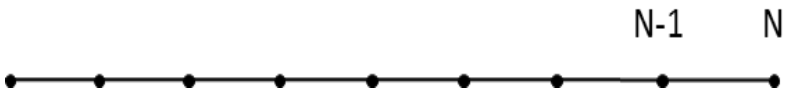

Figure 3. Nodes of Free-Free Beam.

By applying artificial boundary conditions (pins) at nodes $C_1 - C_K$, $K \le N$, Figure 4, Equation (2.46) can be rewritten as:

$$\begin{Bmatrix} X_i \\ X_c \end{Bmatrix} = \begin{bmatrix} H_{ii} & H_{ic} \\ H_{ci} & H_{cc} \end{bmatrix} \begin{Bmatrix} F_i \\ F_c \end{Bmatrix} , \tag{2.47}$$

where the subscript “c” denotes the nodes with the artificial pin, and the subscript “i” denotes the rest of the nodes.

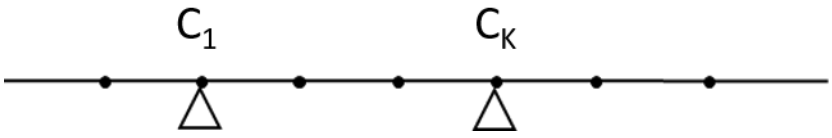

Figure 4. Beam with Boundary Conditions.

The imposition of boundary conditions restrains the displacement of the corresponding node. Thus:

$$\{X_c\} = \{0\} . \tag{2.48}$$

Using Equation (2.48), the bottom row of Equation (2.47) yields:

$$\{X_c\} = [H_{ci}]\{F_i\} + [H_{cc}]\{F_c^*\} = \{0\} , \tag{2.49}$$

where the superscript "*" at the force vector indicates that these are forces of synthesis. Solving for that force vector, (2.49) becomes:

$$\left\{F_c^*\right\} = -\left[H_{cc}\right]^{-1}\left[H_{ci}\right]\left\{F_i\right\} \ . \tag{2.50}$$

The top row of Equation (2.47) results in:

$$\left\{X_i^*\right\} = \left[H_{ii}\right]\left\{F_i\right\} + \left[H_{ic}\right]\left\{F_c^*\right\} \ . \tag{2.51}$$

Substituting Equation (2.50) in (2.51) yields:

$$\left\{X_i^*\right\} = \left[\left[H_{ii}\right] - \left[H_{ic}\right]\left[H_{cc}\right]^{-1}\left[H_{ci}\right]\right]\left\{F_i\right\}. \tag{2.52}$$

Finally, the synthesized FRF matrix for the artificially constrained beam is:

$$\left[H_{ii}^*\right] = \left[H_{ii}\right] - \left[H_{ic}\right]\left[H_{cc}\right]^{-1}\left[H_{ci}\right]. \tag{2.53}$$

Equation (2.53) is called the synthesis equation. By applying an artificial boundary condition at a structure, and using the synthesis equation, the structure's new natural frequencies are calculated.

H. SENSITIVITY METHODS

In structural dynamics, a method known as sensitivity analysis, which applies small changes in the design parameters, is used to predict the amount of change in the dynamic response characteristics of a structure. A change in the parameter of a structure alters the structure's dynamic response. However, the magnitude of this alteration depends on the magnitude of the alteration of the parameter, and which parameter is altered. This dependency is quantified using sensitivity analysis. Usually, physical parameters of the structure, like bending rigidity (EI), density, thickness, and so forth, are stated as design or updating parameters, and are subjected to changes.

Assuming a change in an eigenvalue $\lambda_i = \omega_i^2$, with respect to a parameter p_j, then the sensitivity, S_{ij}, allows the prediction of the rate of that change using equation (2.54):

$$S_{ij} = \frac{\partial \lambda_i}{\partial p_j} \ . \tag{2.54}$$

By slightly modifying (perturbing) an updating parameter of the structure, the eigenvalues of the structure change. Rewriting Equation (2.54) using the eigenvalues of the perturbed system, λ_i^*, results in:

$$\lambda_i^* = \lambda_i + S_{ij}(\mathrm{p}_j^* - \mathrm{p}_j) \ , \tag{2.55}$$

where p_j^* is the perturbed value of the updating parameter.

Sensitivity methods are typically used in relating errors in finite element predictions of natural frequencies to physical parameters in the model. This method is called sensitivity-based finite element model (FEM) updating and it is discussed further later. Conducting a vibration test of a structure, the experimental measured values of natural frequencies, $\omega_i^{(\mathrm{x})}$ (or eigenvalue, $\lambda_i^{(\mathrm{x})}$), can be obtained. From the finite element model, the predictions of these natural frequencies, $\omega_i^{(\mathrm{a})}$ (or eigenvalue, $\lambda_i^{(\mathrm{a})}$), have been calculated. Using the sensitivity for mode “i” and for parameter “j”, the relation of the error between the measured and the predicted value can be identified from:

$$\lambda_i^{(\mathrm{x})} - \lambda_i^{(\mathrm{a})} = \Delta\lambda_i = S_{ij}\Delta p_j \ . \tag{2.56}$$

In general, the modal parameters of the structure, like mode shapes, natural frequencies, eigenvalue sensitivity, and eigenvector sensitivity, are the inputs of the system that will be solved. The unknown is the difference of the updating parameters. So, the following system (2.57) has to be assembled:

$$\{\Delta\lambda\} = [S]\{\Delta p\}, \tag{2.57}$$

where $\{\Delta p\}$ is a set of alterations of the updating parameters, $\{\Delta\lambda\}$ is a set of differences between dynamic behavior in the analytical and the experimental models, and $[S]$ is the sensitivity matrix of the finite element model.

Different sensitivity analysis techniques exist. Generally speaking, they can be divided into techniques using frequency response functions and techniques using modal data (eigenvalues and eigenvectors).

1. Methods Using Frequency Response Data

Often, an actual experiment of a prototype structure results in a small number of resonant frequencies in the measured frequency range. To address this issue, researchers can use response data directly from the experiment. A major advantage of this technique is that there is no need to perform modal identification, which can be inaccurate and is time consuming. This alternative method uses the differences between analytical predictions and experimental measurements of frequency response functions in order to identify the sensitivity of a structural parameter [15], [16]. In this case, Equation (2.57) becomes:

$$\left[S(\omega)\right]\{\Delta p\} = \{\Delta H(\omega)\}, \tag{2.58}$$

where

$$\{\Delta H(\omega)\} = \{H(\omega)\}_{FE} - \{H(\omega)\}_{\exp}, \tag{2.59}$$

where $\{H(\omega)\}_{FE}$ is the frequency response function calculated by the finite element model, and $\{H(\omega)\}_{\exp}$ is the frequency response function measured by the experiment.

At a given frequency point the sensitivity of the “i” DOF due to a change of the “j” updating parameter is given by [17]:

$$S(\omega)_{ij} = \{H(\omega)\}_{FE}^{T}\left(\left[-\omega^2 \frac{\partial}{\partial p_j}[M] + \frac{\partial}{\partial p_j}[K]\right]\{H(\omega)\}_{\exp}\right) . \tag{2.60}$$

To find the minimum difference between the finite element predictions and the experimental values at specific frequencies, an iterative solution is used by changing an updating parameter.

Then the number of sensitivity matrices that will be used is specified by the user, and an overdetermined system arises:

$$\begin{bmatrix} S(\omega_1) \\ S(\omega_2) \\ \vdots \\ S(\omega_n) \end{bmatrix}\{p\} = \begin{Bmatrix} \Delta H(\omega_1) \\ \Delta H(\omega_2) \\ \vdots \\ \Delta H(\omega_n) \end{Bmatrix} . \tag{2.61}$$

However, it is very important to choose the most useful frequency points for the updating process; otherwise, Equation (2.58), even if it seems overdetermined, can have linear dependent rows and ends up being underdetermined.

2. Methods Using Eigenvalues And Eigenvectors

Next, methods using eigenvalues and eigenvectors are provided.

a. Eigenvalue Sensitivity Method

To match the dynamic behavior predictions of the finite element model with the dynamic behavior of the structure, a more common procedure is typically used. This procedure is based on the alteration of certain updating parameters of the finite element model, such that the natural frequencies of the model more closely match the experimental natural frequencies.

According to the eigenvalue sensitivity method, the following procedure is followed [18]:

$$\left[\mathrm{K}-\lambda_i M\right]\{\phi_i\}=\{0\}, \tag{2.62}$$

where λ_i and $\{\phi_i\}$ are the solutions to Equation (2.5), and $\{\phi_i\}$ from (2.6) is mass normalized.

Differentiating (2.62) with respect to an updating parameter “p” leads to:

$$\left[\frac{\Delta \mathrm{K}}{\Delta p}-\lambda_i\frac{\Delta \mathrm{M}}{\Delta p}-\frac{\Delta\lambda_i}{\Delta p}\right]\{\phi_i\}+\left[\mathrm{K}-\lambda_i M\right]\left\{\frac{\Delta\phi_i}{\Delta p}\right\}=\{0\}\ . \tag{2.63}$$

Premultiplying (2.63) by $\{\phi_i\}^T$ results in:

$$\{\phi_i\}^T\left[\frac{\Delta \mathrm{K}}{\Delta p}\right]\{\phi_i\}-\lambda_i\{\phi_i\}^T\left[\frac{\Delta \mathrm{M}}{\Delta p}\right]\{\phi_i\}-\left[\frac{\Delta\lambda_i}{\Delta p}\right]\{\phi_i\}^T[\mathrm{M}]\{\phi_i\}+\{\phi_i\}^T\left[\mathrm{K}-\lambda_i M\right]\left\{\frac{\Delta\phi_i}{\Delta p}\right\}=\{0\}. \tag{2.64}$$

Using Equations (2.62) and (2.6), Equation (2.64) is reduced to:

$$\{\phi_i\}^T\left[\frac{\Delta \mathrm{K}}{\Delta p}\right]\{\Phi_i\}-\lambda_i\{\phi_i\}^T\left[\frac{\Delta \mathrm{M}}{\Delta p}\right]\{\phi_i\}-\left[\frac{\Delta\lambda_i}{\Delta p}\right]=\{0\}\ . \tag{2.65}$$

Rearranging (2.65) leads to:

$$\frac{\Delta\lambda_i}{\Delta p}=\{\phi_i\}^T\left[\frac{\Delta \mathrm{K}}{\Delta p}-\lambda_i\frac{\Delta \mathrm{M}}{\Delta p}\right]\{\phi_i\}\ . \tag{2.66}$$

Depending on which parameter is altered, the stiffness or mass, Equation (2.66) can be further reduced. In this research, only changes to the stiffness parameter are demonstrated, and so Equation (2.66) is reduced to:

$$\frac{\Delta\lambda_i}{\Delta p_j}=\{\phi_i\}^T\left[\frac{\Delta \mathrm{K}}{\Delta p_j}\right]\{\phi_i\}\ , \tag{2.67}$$

where “Δp” represents the difference of the updating parameter between experimental and analytical, “ΔK” is the difference of the stiffness global matrix between the initial and the perturbed structure, and the subscript “i” is the rate of change at this eigenvector due to a change at “j” updating parameter.

The right-hand side of Equation (2.67) is the sensitivity of the structure; thus:

$$S_{stiffness} = \{\phi_i\}^T \left[\frac{\Delta \mathrm{K}}{\Delta p}\right]\{\phi_i\}. \tag{2.68}$$

By constraining the structure at a specific DOF through the use of the artificial boundary condition approach, i.e., applying the boundary condition computationally, we find the stiffness sensitivity values near that DOF are much higher in comparison to the rest [19]. This concept was used in [9] in order to determine which rows of the stiffness sensitivity matrix should be used in the damage identification process of the finite element model.

b. Eigenvector Sensitivity Method

The development of the eigenvector sensitivity matrix derivation is generally attributed to Fox and Kapoor [20], with a significant later contribution by Nelson [21] and his simplified method. The reader can refer to [22] for more literature about contributors to the specific subject.

Substituting Equation (2.67) into (2.63) results in [23]:

$$\left[\mathrm{K} - \lambda_i M\right]\left[\frac{\Delta \phi_i}{\Delta p}\right] = -\left[\frac{\Delta \mathrm{K}}{\Delta p} - \frac{\Delta \lambda_i}{\Delta p}\mathrm{M}\right]\{\phi_i\}. \tag{2.69}$$

If all the eigenvectors are available, then the derivative at the left-hand side can be written as:

$$\left[\frac{\Delta\phi_i}{\Delta p}\right] = [\Phi]\{c\}, \tag{2.70}$$

which indicates that the derivative is a linear combination of eigenvector matrix $[\Phi]$ and some constant coefficients $\{c\}$ that have to be determined. Combining (2.69) and (2.70) and premultiplying with $[\Phi]^T$ yields:

$$[\Phi]^{\mathrm{T}}\left[\mathrm{K} - \lambda_i M\right][\Phi]\{c\} = -[\Phi]^{\mathrm{T}}\left[\frac{\Delta \mathrm{K}}{\Delta p} - \frac{\Delta\lambda_i}{\Delta p}\mathrm{M}\right]\{\phi_i\}. \tag{2.71}$$

However, it is known that:

$$[\Phi]^{\mathrm{T}}\left[\mathrm{K} - \lambda_i M\right][\Phi] = [\Lambda - \lambda_i \mathrm{I}], \tag{2.72}$$

where [Λ] is the diagonal eigenvalue matrix. From matrix algebra, the Equation (2.72) implies that, there is a unique solution for all the coefficients except from the i^{th} coefficient. The solution is of the form:

$$c_{\mathrm{K}} = -\frac{\{\phi_k\}^{\mathrm{T}}\left[\frac{\Delta \mathrm{K}}{\Delta p} - \frac{\Delta\lambda_i}{\Delta p}\mathrm{M}\right]\{\phi_i\}}{\lambda_k - \lambda_i}, \qquad \kappa \neq i \ . \tag{2.73}$$

In the case that the model has closely spaced eigenvalues, then the prediction of changes in eigenvectors will not be available, because, as is obvious from Equation (2.73), in these cases numerical ill-conditioning will occur. Thus, the eigenvector derivative is not useful.

Substituting (2.73) into (2.70) yields to:

$$\left\{\frac{\Delta\phi_i}{\Delta p}\right\} = \sum_{k\neq i} c_k \{\phi_k\} + c_i \{\phi_i\} = \{P_i\} + c_i \{\phi_i\}, \tag{2.74}$$

where $\{P_i\}$ vector is uniquely determined. However, as mentioned before, not all the coefficients are known yet. In order to determine c_i coefficient, the differentiation of Equation (2.6) is required:

$$\frac{\partial}{\partial p}\left(\{\phi_i\}^{\mathrm{T}}[\mathrm{M}]\{\phi_i\}=1\right), \tag{2.75}$$

which results in:

$$2\{\phi_i\}^{\mathrm{T}}[\mathrm{M}]\left\{\frac{\partial\phi_i}{\partial p}\right\}+\{\phi_i\}^{\mathrm{T}}\left[\frac{\partial \mathrm{M}}{\partial p}\right]\{\phi_i\}=0. \tag{2.76}$$

Assuming no changes in mass, Equation (2.76) becomes:

$$\{\phi_i\}^{\mathrm{T}}[\mathrm{M}]\left\{\frac{\partial\phi_i}{\partial p}\right\}=0. \tag{2.77}$$

Combining Equations (2.74) and (2.77) finally leads to:

$$c_i=-\{\phi_i\}^{\mathrm{T}}[\mathrm{M}]\{P_i\}\ . \tag{2.78}$$

The most important conclusion in Nelson's research [21] is that any vector that satisfies Equation (2.69) can be used instead of the unknown $\{P_i\}$ vector. That is valid, since the eigenvector derivative is orthogonal to the eigenvector [23]. Following, a process to identify a non-trivial solution for the unknown vector $\{P_i\}$ is demonstrated [23]:

$$\begin{bmatrix}(\mathrm{K}-\lambda_i\mathrm{M})_{11} & (\mathrm{K}-\lambda_i\mathrm{M})_{1k} & (\mathrm{K}-\lambda_i\mathrm{M})_{13}\\ (\mathrm{K}-\lambda_i\mathrm{M})_{k1} & (\mathrm{K}-\lambda_i\mathrm{M})_{2k} & (\mathrm{K}-\lambda_i\mathrm{M})_{k1}\\ (\mathrm{K}-\lambda_i\mathrm{M})_{31} & (\mathrm{K}-\lambda_i\mathrm{M})_{3k} & (\mathrm{K}-\lambda_i\mathrm{M})_{33}\end{bmatrix}\begin{Bmatrix}x_1\\ x_k\\ x_3\end{Bmatrix}=\begin{Bmatrix}0\\0\\0\end{Bmatrix}. \tag{2.79}$$

Solving for a non-zero x_k results in:

$$\begin{bmatrix} (\mathrm{K}-\lambda_i \mathrm{M})_{11} & (\mathrm{K}-\lambda_i \mathrm{M})_{13} \\ (\mathrm{K}-\lambda_i \mathrm{M})_{k1} & (\mathrm{K}-\lambda_i \mathrm{M})_{k3} \\ (\mathrm{K}-\lambda_i \mathrm{M})_{31} & (\mathrm{K}-\lambda_i \mathrm{M})_{33} \end{bmatrix} \begin{Bmatrix} x_1 \\ x_2 \end{Bmatrix} = -x_k \begin{Bmatrix} (\mathrm{K}-\lambda_i \mathrm{M})_{1k} \\ (\mathrm{K}-\lambda_i \mathrm{M})_{kk} \\ (\mathrm{K}-\lambda_i \mathrm{M})_{3k} \end{Bmatrix} . \tag{2.80}$$

However, the k[th] row can be eliminated since it is linearly dependent on the (n-1) remaining rows, which results in a (n-1) system:

$$\begin{bmatrix} (\mathrm{K}-\lambda_i \mathrm{M})_{11} & (\mathrm{K}-\lambda_i \mathrm{M})_{13} \\ (\mathrm{K}-\lambda_i \mathrm{M})_{31} & (\mathrm{K}-\lambda_i \mathrm{M})_{33} \end{bmatrix} \begin{Bmatrix} x_1 \\ x_2 \end{Bmatrix} = -x_k \begin{Bmatrix} (\mathrm{K}-\lambda_i \mathrm{M})_{1k} \\ (\mathrm{K}-\lambda_i \mathrm{M})_{3k} \end{Bmatrix} . \tag{2.81}$$

Substituting in (2.81) the arbitrary $\{P_i\}$ results in:

$$\begin{bmatrix} (\mathrm{K}-\lambda_i \mathrm{M})_{11} & (\mathrm{K}-\lambda_i \mathrm{M})_{13} \\ (\mathrm{K}-\lambda_i \mathrm{M})_{31} & (\mathrm{K}-\lambda_i \mathrm{M})_{33} \end{bmatrix} \begin{Bmatrix} P_1 \\ P_3 \end{Bmatrix} = -\begin{Bmatrix} \left(\left[\frac{\Delta \mathrm{K}}{\Delta p} - \frac{\Delta \lambda_i}{\Delta p} \mathrm{M} \right] \{\phi_i\} \right)_1 \\ \left(\left[\frac{\Delta \mathrm{K}}{\Delta p} - \frac{\Delta \lambda_i}{\Delta p} \mathrm{M} \right] \{\phi_i\} \right)_3 \end{Bmatrix} , \tag{2.82}$$

which has a unique solution:

$$\begin{Bmatrix} \frac{\partial \phi_i}{\partial p} \end{Bmatrix} = \begin{Bmatrix} P_1 \\ 0 \\ P_3 \end{Bmatrix} + c_i \phi_i . \tag{2.83}$$

From Equation (2.82) P_1, P_3 are evaluated, and from Equation (2.83) the remaining term c_i is evaluated. So by calculating the eigenvalue sensitivities, Blelloch [23] proposes an algorithm based on the Equations (2.69)–(2.83) for calculating the eigenvector sensitivities.

I. COMPOSITE SENSITIVITY MATRIX

In this research, Equation (2.67) is thoroughly used. Initially for the model updating method, as updating parameters, the stiffness value (EI) of each finite

element is used. The examinable output of Equation (2.67) is the difference of the experimental and estimated natural frequencies. So, equation (2.84) arises:

$$\left\{\Delta\omega^2\right\} = \left\{\omega^2{}_{\exp} - \omega_{ana}^2\right\} = [S]\{\Delta EI\} \ , \tag{2.84}$$

where $\omega_{\exp}$ is the experimentally measured natural frequency, ω_{ana} is the FEM estimated natural frequency, and vector ΔEI contains the change in stiffness of each element, corresponding to either errors in the finite element model or damage in the test article. To match the experimental natural frequencies with the predicted, we must apply the changes of vector ΔEI at the FEM. The number of rows of the sensitivity matrix represents the number of used modes, and the number of columns represents the number of potential damage locations.

For a specific structural configuration, the sensitivity matrix is used to relate the amount of change at structural dynamic properties (natural frequencies) due to a change at an updating parameter (stiffness). For example, using the sensitivity matrix, the new natural frequencies of the structure are calculated, by perturbing the stiffness of an element at the FEM. By applying an artificial boundary condition (pin), the structural configuration changes. Now if the stiffness value of the same element is perturbed by the same amount, the natural frequencies will be different. That change depends on the distance of the perturbed element from the pin. Thus, in this case the sensitivity matrix is different from the initial configuration. That is the case for every different structural configuration. This concept is further demonstrated in a later chapter.

The creation of the sensitivity matrix is one of the most important and difficult procedures. In [9] it was shown that the QR decomposition process can create a reliable composite sensitivity matrix. This sensitivity matrix might have rows from different ABC sets. The formed sensitivity matrix must include rows from ABC sets that can identify damage at each element of the finite element. This is expressed mathematically as [2]:

$$\begin{Bmatrix} \Delta\omega^{2(0)}_{BASE} \\ \Delta\omega^{2(1)}_{ABC1} \\ \vdots \\ \Delta\omega^{2(k)}_{ABCk} \end{Bmatrix} = \begin{pmatrix} S^{(0)}{}_{BASE} \\ S^{(1)}{}_{ABC1} \\ \vdots \\ S^{(k)}{}_{ABCk} \end{pmatrix} \begin{Bmatrix} dEI_1 \\ \vdots \\ dEI_n \end{Bmatrix}, \tag{2.85}$$

where subscript “base” means the initial finite element configuration with no artificial boundary conditions.

If the stiffness value (EI) of an element in the finite element model has been decreased, simulating the occurrence of damage in a structure, then the resonant frequencies will also change. This decrease in stiffness simulates damage to the structure at the specific element (location). Consequently, using Equation (2.85) where $\{\Delta\omega^2\}$ has changed but is known, we have the same sensitivity matrix [S], and solving for {dEI}, we can identify the damage.

J. CONCLUDING REMARKS

The background to the creation of a finite element model, for a Bernoulli-Euler 2-D beam, has been set out. The artificial boundary condition theory and the synthesis of the impedance matrix have also been described in this chapter. This theory is thoroughly used and demonstrated in this research. This chapter has also demonstrated so far the theory behind the different sensitivity methods, emphasizing the use of eigenvalues in the sensitivity matrix derivation, the method used in this thesis.

Finally, the basic concept of model updating and damage identification has been highlighted, and the significance of the creation of a reliable sensitivity matrix has been made clear.

III. EXPERIMENTAL SETUP AND INITIAL INVESTIGATION

A. DIFFICULTIES USING EXPERIMENTAL DATA

The methods analyzed in Chapter II, for model updating and damage detection, have been thoroughly verified using computational (simulated) data. That means data usually obtained from a vibration test of a potentially damaged structure are replaced by simulated versions from a finite element model of the structure, with damage represented as a reduction in bending rigidity (EI) at a specific element. However, when experimental data are used, there are some issues that make the process difficult, and often the theory does not work as expected. These issues can be noise from the experiment that alters the measured data, limited number of measured locations, limited bandwidth of measurement, simulation of connections or boundary conditions, and even the finite element model used. This thesis, investigates a way to overcome these difficulties, starting with the difficulties associated with model update.

B. EXPERIMENTAL SETUP

The prototype structure used in this research was an Aluminum 6061 beam with properties shown in Table 1.

Table 1. Properties of Prototype Structure

Length cm (in)	182.88 (72)
Width cm (in)	4.9 (1.93)
Height cm (in)	0.947 (0.373)
Modulus of elasticity MPa (psi)	68947.5729 (10000000)
Density Kg/m^3 (lbm/in^3)	2698.79 (0.0975)

To avoid potential discrepancies from boundary conditions, the beam is tested as free-free, meaning that no boundary conditions applied.

The beam was modeled using 16 2-D Bernoulli-Euler beam elements, and the measurement points on the structure matched the node points of the finite element model.

The odd-numbered DOF of the finite element model are translation, and the even-numbered DOF are rotation. Response transducers (accelerometers) are set up at all the translational DOF, except from the first and the last DOF, corresponding to the actual ends of the beam (1,33 DOF). In total, 15 transducers were used and were placed at nodes 2–16. Henceforth, these nodes are referred to as “all” or the “rest” unless something different is mentioned.

The experiment was conducted by exciting all nodes using a modal hammer. Each time the frequency response function of all the nodes was measured using the Reflex Pulse software of Kjaer, Bruel company [12]. To proceed from one node to another an average of five successful measurements was taken. After each excitation, an external absorber was applied at the beam to absorb the remaining energy of the excitation, and enough time was given for the beam to come to rest in order to get as accurate a measurement as possible.

The beam was hung from the ceiling using elastic cords at the nodal points (locations with zero displacement) of its first vibrating mode. Great consideration was given in the way that the beam was attached at the cords, so that they did not restrain any movement of the beam. Moreover, the height from which the bar hung from the ceiling was long enough so that the frequency of the pendulum mode of the whole system was extremely small and far from the first elastic mode frequency of the beam.

Last, but not least, special care was given such that the cables of the transducers did not contact or restrain the movement of the beam and did not add mass on the system.

The resolution of the hammer test was set to 0.3125 Hz, and the measured bandwidth was 0–1000 Hz. From the measured FRF’s the frequencies corresponding to the peak values of response were identified and used as the

natural frequencies. Generally speaking, these values are not exactly the same as the resonant frequencies, but they are very close due to the very low levels of damping.

C. CREATION OF FINITE ELEMENT MODEL

The stiffness matrix for each element was created using Equation (2.18) and then added to form a global stiffness matrix. In the same way, the global mass matrix was created using Equation (2.20). However, the mass of the transducers and their mass moment of inertia are significant; thus, the global mass matrix must be altered. Each transducer was represented as a translational mass and rotational moment of inertia and added at the diagonal elements of the global mass matrix. In this case, the first two modes of a free–free beam are 0 since they are rigid body modes. In the rest of the analysis, the first flexible mode is referred to as mode 1.

The measured FRF is a matrix of size 15x15, since there are 15 transducers, for all the measured frequencies (3201 points). In this case, in order to create the FRF of the free–free beam and identify the peak values that correspond to the resonant frequencies, the average value of the diagonal elements of each matrix was taken.

An initial check of how accurately the finite element model represents the beam in terms of resonant frequencies resulted in the following (Table 2 and Figure 5):

Table 2. Initial FE Resonant Frequencies.

	Experimental Resonant Frequencies (Hz)	FE Model Resonant Frequencies (Hz)	Absolute Error
Mode 1	13.75	14.351	0.601
Mode 2	38.125	39.555	1.430
Mode 3	75	77.544	2.544
Mode 4	124.06	128.209	4.149
Mode 5	185	191.619	6.619
Mode 6	258.43	267.883	9.453
Mode 7	343.75	357.179	13.429
Mode 8	441.56	459.762	18.202
Mode 9	551.56	575.953	24.393
Mode 10	672.5	706.076	33.576
Mode 11	805.93	850.205	44.275
Mode 12	950.62	1007.102	56.482

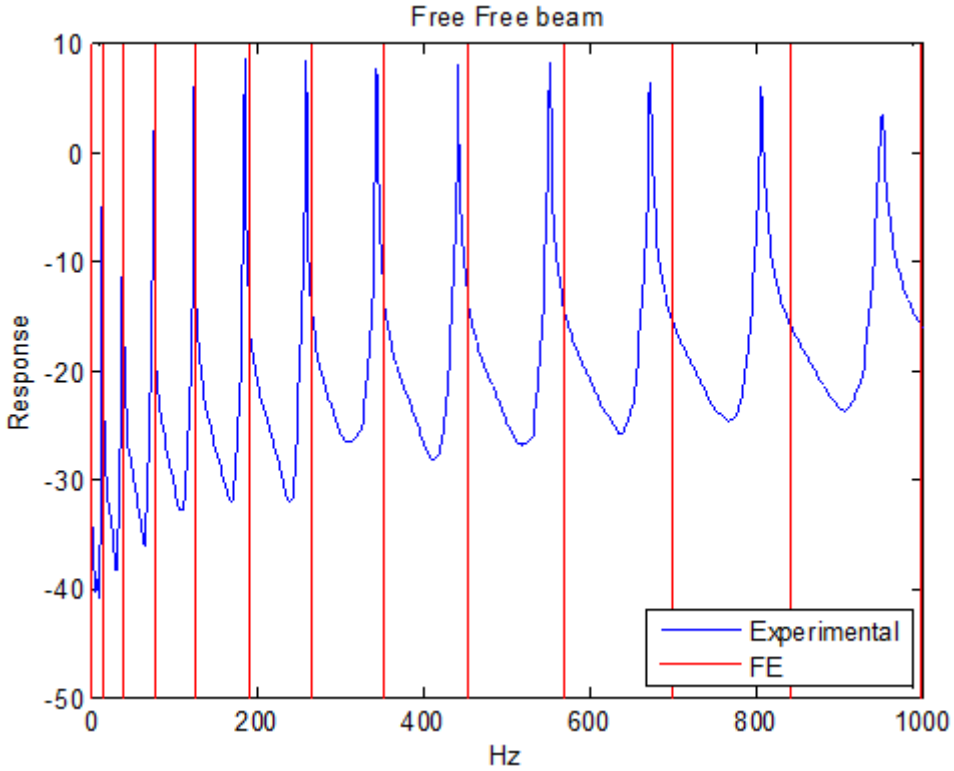

Figure 5. Experimental and Initial FE Model Resonant Frequencies.

In Figure 5, the blue curve is the average of the diagonal elements of the measured frequency response function (H). The red lines are the values of the estimated natural frequencies of the FE model.

It is obvious from Table 2 and Figure 5 that the finite element model simulates well the beam for the lower modes of vibration. However, as the frequency is increased, the error rate also increases, and the resonant frequencies do not match very well.

Thus, a small change in the stiffness of the beam was made. The initial value of modulus of elasticity was decreased by 3 percent. The results of that change are provided in Table 3 and Figure 6.

Table 3. Modified FE Model Resonant Frequencies.

	Experimental Resonant Frequencies (Hz)	Modified FE Model Resonant Frequencies (Hz)	Initial Absolute Error	New Absolute Error
Mode 1	13.75	14.135	0.601	0.385
Mode 2	38.125	38.958	1.430	0.833
Mode 3	75	76.372	2.544	1.372
Mode 4	124.06	126.272	4.149	2.212
Mode 5	185	188.723	6.619	3.723
Mode 6	258.43	263.834	9.453	5.404
Mode 7	343.75	351.781	13.429	8.031
Mode 8	441.56	452.813	18.202	11.253
Mode 9	551.56	567.248	24.393	15.688
Mode 10	672.5	695.404	33.576	22.904
Mode 11	805.93	837.355	44.275	31.425
Mode 12	950.62	991.881	56.482	41.261

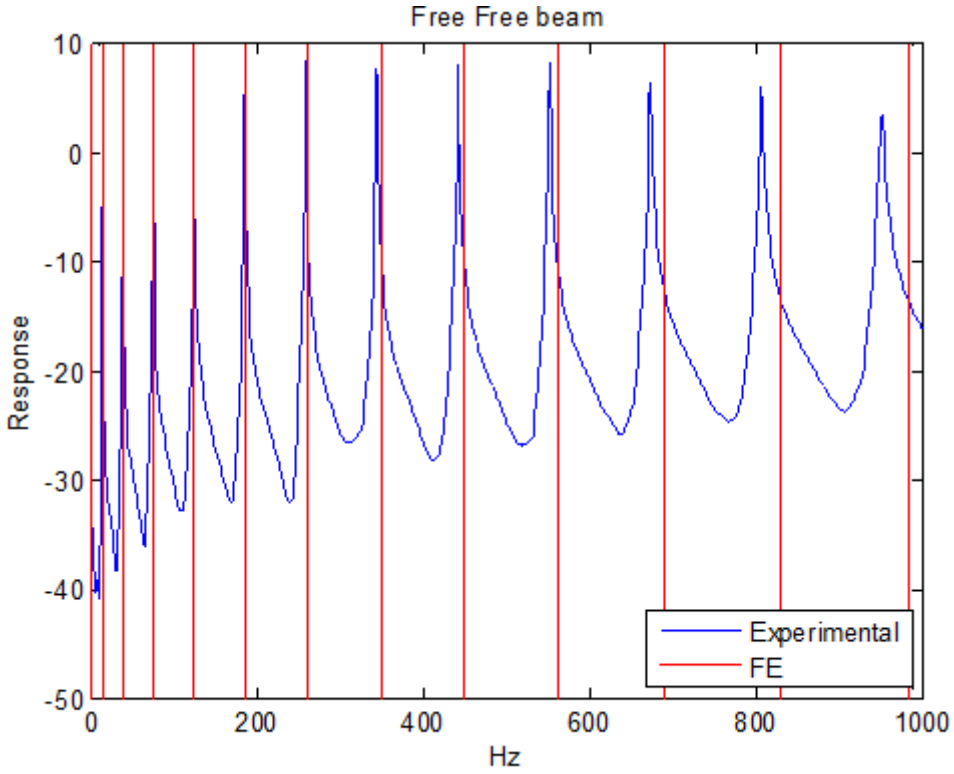

Figure 6. Experimental and Modified FE Model Resonant Frequencies.

Now the FE model represents more accurately the real structure. This finite element model is defined as a baseline and used for the rest of the research.

D. CREATION OF COMPOSITE SENSITIVITY MATRIX

As discussed previously, to procced with the model updating method a composite sensitivity matrix has to be created. This step is one of the most difficult and crucial for successfully detecting damage. Based on previous research, [9], the QR decomposition technique is used to create the sensitivity matrix. After such a matrix is created, it has to be validated using simulated data to verify its functionality. The way to validate such a matrix is to apply damage at a known location of the finite element model (slightly altering the stiffness value), then to calculate the new natural frequencies of the damaged FE model and from Equation (2.85), solve for the changes in stiffness as follows:

$$\{\Delta EI\} = [S_{composite}] \setminus \{\Delta\omega^2\}. \quad (3.1)$$

If the vector $\{\Delta EI\}$ has all values close to zero except for the value that corresponds to the damaged element in the FE model, then the composite sensitivity matrix is good. This process must be repeated for each potential location of damage. This concept is used for damage identification and is further discussed in a later chapter.

Consequently, an investigation is performed to create a reliable composite sensitivity matrix. Initially, the comparison of a composite sensitivity matrix created using lower modes (1–6), and one created using higher modes (7–12) is performed to identify which modes are more effective.

At the beginning, the creation of sensitivity matrices using structural configurations with one pin (ABC1) is investigated. In this experiment, there are 15 different ABC1 structural configuration cases since there are fifteen transducers, and therefore, 15 possible locations where the pin can be applied artificially.

From Figures 5 and 6, it is obvious that only the first 12 vibration modes are available. That means only these natural frequencies can be used for the creation of the sensitivity matrix. Therefore, the dimensions of the sensitivity matrices for each ABC case created from the FE model are 12x14. The number 12 indicates the number of modes used for the creation of the corresponding row, where the number 14 indicates the location of possible damage (or element).

First, a composite sensitivity matrix is created using modes 1–6 (lower modes) as follows:

$$[S_L] = \begin{bmatrix} S_{1,3}^{ABC_1} \\ S_{3,11}^{ABC_1} \\ S_{1,14}^{ABC_1} \\ S_{6,1}^{ABC_1} \\ S_{3,3}^{ABC_1} \\ S_{2,15}^{ABC_1} \\ S_{3,14}^{ABC_1} \\ S_{2,11}^{ABC_1} \\ S_{1,12}^{ABC_1} \\ S_{2,6}^{ABC_1} \\ S_{6,14}^{ABC_1} \\ S_{1,2}^{ABC_1} \\ S_{2,12}^{ABC_1} \\ S_{5,9}^{ABC_1} \end{bmatrix},$$

where $S_{i,j}^{ABC_1}$ means that this sensitivity matrix was created by applying a single artificial boundary condition at the free-free beam, the subscript “i” shows which row was chosen from the specific sensitivity matrix (i.e., the mode used for the creation of that row), and the subscript “j” shows which case of ABC1 was used (i.e., the location of the pin).

The composite sensitivity matrix is a full rank, square matrix with the values shown in Table 4:

Table 4. Composite Sensitivity Matrix Using Modes 1–6.

$$[S_L] = \begin{bmatrix}
0.0000 & 0.0001 & 0.0010 & 0.0041 & 0.0083 & 0.0123 & 0.0146 & 0.0145 & 0.0121 & 0.0084 & 0.0046 & 0.0018 & 0.0004 & 0.0000 \\
0.0144 & 0.1681 & 0.4166 & 0.4016 & 0.1249 & 0.0306 & 0.2437 & 0.3452 & 0.1319 & 0.0534 & 0.1892 & 0.1239 & 0.0414 & 0.0032 \\
0.0000 & 0.0002 & 0.0011 & 0.0028 & 0.0053 & 0.0079 & 0.0100 & 0.0108 & 0.0100 & 0.0078 & 0.0048 & 0.0020 & 0.0003 & 0.0000 \\
1.8309 & 2.8669 & 0.9237 & 3.5107 & 0.6249 & 3.4236 & 1.0864 & 2.6499 & 2.0712 & 1.5819 & 3.0351 & 0.8503 & 4.1767 & 1.0393 \\
0.0263 & 0.3821 & 0.5255 & 0.1372 & 0.0111 & 0.1015 & 0.1700 & 0.0901 & 0.0085 & 0.0788 & 0.2009 & 0.1900 & 0.0730 & 0.0061 \\
0.0006 & 0.0095 & 0.0349 & 0.0660 & 0.0787 & 0.0604 & 0.0252 & 0.0025 & 0.0109 & 0.0417 & 0.0661 & 0.0617 & 0.0325 & 0.0055 \\
0.0161 & 0.1804 & 0.4150 & 0.3450 & 0.0706 & 0.0718 & 0.3200 & 0.3301 & 0.0828 & 0.0584 & 0.3167 & 0.3839 & 0.1455 & 0.0082 \\
0.0003 & 0.0052 & 0.0200 & 0.0402 & 0.0520 & 0.0448 & 0.0225 & 0.0031 & 0.0096 & 0.0570 & 0.0678 & 0.0262 & 0.0057 & 0.0003 \\
0.0000 & 0.0005 & 0.0021 & 0.0054 & 0.0097 & 0.0139 & 0.0164 & 0.0164 & 0.0137 & 0.0095 & 0.0051 & 0.0020 & 0.0004 & 0.0000 \\
0.0002 & 0.0030 & 0.0129 & 0.0313 & 0.0559 & 0.0320 & 0.0024 & 0.0254 & 0.0644 & 0.0831 & 0.0685 & 0.0356 & 0.0095 & 0.0006 \\
0.7510 & 3.2107 & 0.7400 & 2.1307 & 1.5047 & 1.2117 & 2.4015 & 0.5345 & 2.7591 & 0.5908 & 2.1073 & 0.9945 & 4.8475 & 3.4580 \\
0.0000 & 0.0003 & 0.0020 & 0.0048 & 0.0078 & 0.0100 & 0.0108 & 0.0100 & 0.0079 & 0.0053 & 0.0028 & 0.0011 & 0.0002 & 0.0000 \\
0.0003 & 0.0047 & 0.0175 & 0.0335 & 0.0403 & 0.0310 & 0.0121 & 0.0011 & 0.0137 & 0.0544 & 0.1174 & 0.0953 & 0.0217 & 0.0013 \\
0.1714 & 1.0167 & 0.5619 & 0.2475 & 0.9133 & 0.1956 & 0.7322 & 1.3320 & 0.6066 & 3.0508 & 0.8551 & 2.0515 & 3.6899 & 0.6214
\end{bmatrix}$$

Then, to simulate damage at a specific location on the beam, a reduction of the stiffness value is applied at the corresponding finite element. In this case, a reduction of 10 percent of the stiffness value is recursively applied at each element (i.e., potential damage location). Using the estimated natural frequencies from the damaged and the undamaged finite element model, the vector $\{\Delta\omega^2\}$ is created. Finally, using this information the results of Equation (3.1) are shown in Figures 7–11. In all figures, the y-axis represents the actual value of $\{\Delta EI\}$ difference, and the x-axis, the number of the element.

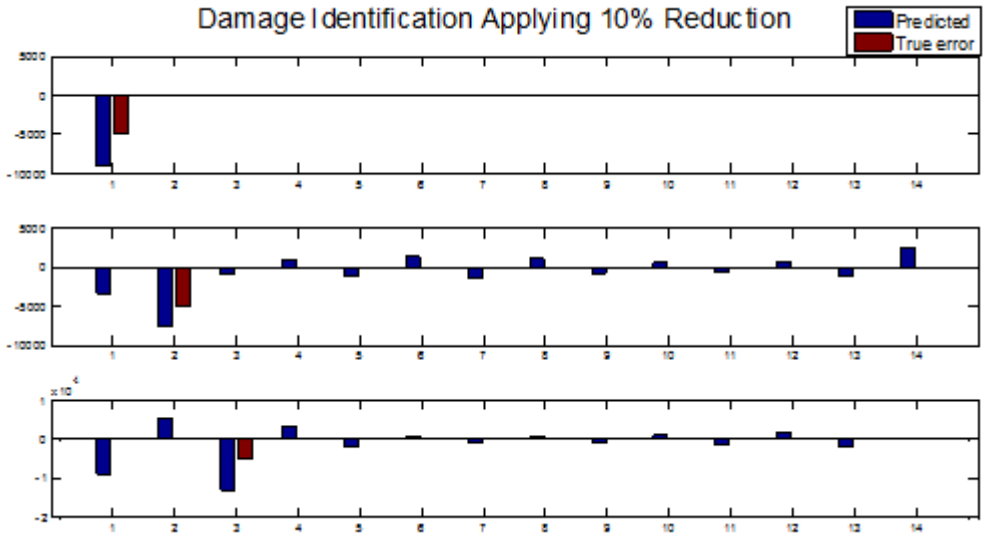

Figure 7. Damage Identification for Elements 1–3, Using $[S_L]$.

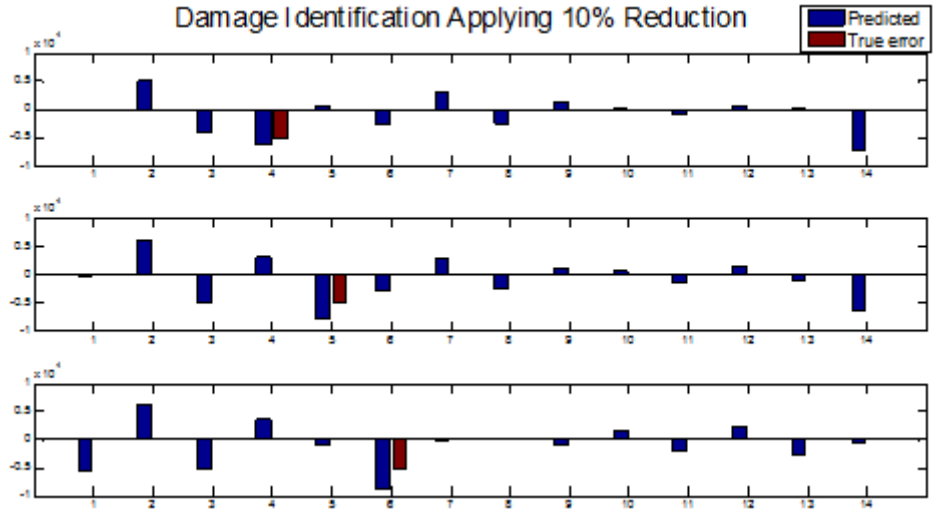

Figure 8. Damage Identification for Elements 4–6, Using $[S_L]$.

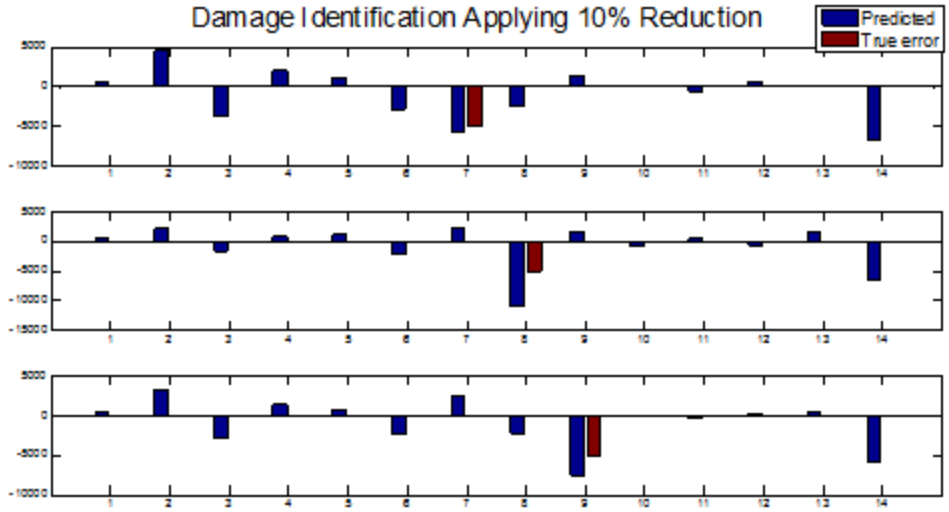

Figure 9. Damage Identification for Elements 7–9, Using $[S_L]$.

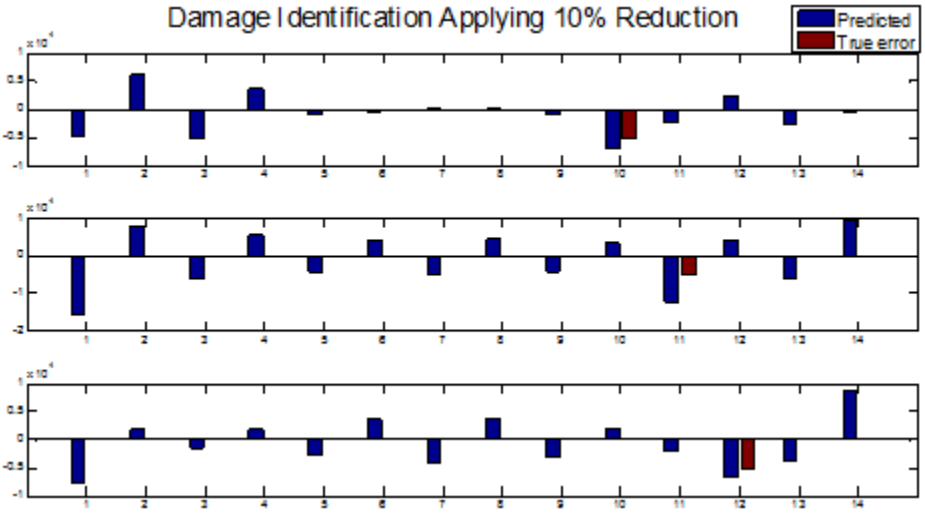

Figure 10. Damage Identification for Elements 10–12, Using $[S_L]$.

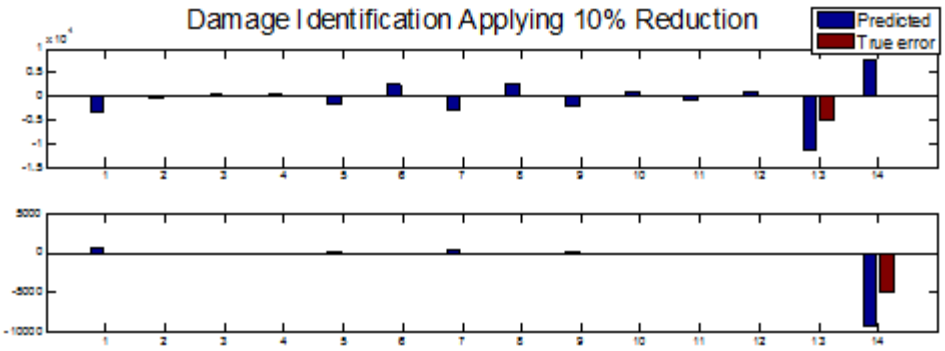

Figure 11. Damage Identification for Elements 12–14, Using $[S_L]$.

Obviously, the damage is not identified clearly in each element. Therefore, the use of lower modes is not very effective.

Subsequently a composite sensitivity matrix using modes 7–12 (higher modes) is created. However, damage at element 13 can only be identified from lower modes, based on QR decomposition. Thus, we purposely use a row created from a higher mode that can identify the damage at element 10. It is expected that the damage identification process will not identify the damage at element 13. Again, this is a full rank, square matrix, which is created as follows:

$$[S_H] = \begin{bmatrix} S_{8,9}^{ABC_1} \\ S_{11,10}^{ABC_1} \\ S_{11,2}^{ABC_1} \\ S_{7,15}^{ABC_1} \\ S_{7,14}^{ABC_1} \\ S_{9,6}^{ABC_1} \\ S_{8,1}^{ABC_1} \\ S_{9,14}^{ABC_1} \\ S_{9,11}^{ABC_1} \\ S_{7,2}^{ABC_1} \\ S_{8,13}^{ABC_1} \\ S_{7,13}^{ABC_1} \\ S_{8,4}^{ABC_1} \\ S_{8,7}^{ABC_1} \end{bmatrix},$$

with values shown in Table 5:

Table 5. Composite Sensitivity Matrix Using Modes 7–12.

$$[S_H] = \begin{bmatrix} 3.2018 & 5.1490 & 3.5242 & 3.0747 & 5.0194 & 1.9423 & 4.8399 & 5.2310 & 5.5031 & 9.0418 & 6.4362 & 7.3108 & 10.6255 & 6.6098 \\ 39.6268 & 27.0537 & 27.1423 & 31.7803 & 33.9220 & 30.6725 & 26.6180 & 27.2915 & 28.2988 & 15.9595 & 10.1528 & 8.8250 & 8.8025 & 12.8905 \\ 11.2225 & 20.9336 & 19.4895 & 21.1117 & 25.3792 & 26.1669 & 22.1908 & 19.5392 & 22.2666 & 26.2016 & 25.3356 & 20.8980 & 20.1712 & 30.3681 \\ 2.7115 & 6.4851 & 1.9992 & 5.4423 & 2.2655 & 5.2095 & 2.5452 & 4.9119 & 2.8552 & 4.5903 & 3.1868 & 4.2502 & 3.5346 & 3.9072 \\ 2.1390 & 5.8007 & 1.3666 & 5.0829 & 1.3268 & 5.1535 & 1.2912 & 5.1832 & 1.2637 & 5.2541 & 1.1744 & 4.3593 & 3.6705 & 4.3267 \\ 23.1877 & 18.3052 & 28.9516 & 14.1861 & 16.5852 & 10.6601 & 3.6830 & 2.4489 & 5.2284 & 3.4893 & 2.7791 & 5.2908 & 3.3661 & 4.2632 \\ 7.2757 & 4.1018 & 9.5548 & 3.2415 & 8.7487 & 5.4999 & 5.6340 & 8.6499 & 3.2790 & 9.5928 & 3.9890 & 7.3043 & 7.9453 & 5.9657 \\ 10.6582 & 9.0658 & 13.5782 & 6.3110 & 10.2763 & 12.5990 & 5.6654 & 12.2019 & 10.7797 & 6.0621 & 13.6323 & 7.8783 & 7.4895 & 6.4093 \\ 11.7909 & 10.5454 & 15.1913 & 6.6272 & 12.5466 & 13.2867 & 6.3767 & 15.0726 & 9.2898 & 8.4188 & 6.1905 & 4.1901 & 3.4054 & 3.7812 \\ 4.3267 & 3.6705 & 4.3593 & 1.1744 & 5.2541 & 1.2637 & 5.1832 & 1.2912 & 5.1535 & 1.3268 & 5.0829 & 1.3666 & 5.8007 & 2.1390 \\ 5.9732 & 7.2930 & 7.5432 & 3.5130 & 9.2711 & 3.7920 & 7.1811 & 7.0048 & 3.9107 & 9.2179 & 3.5357 & 8.7243 & 10.9694 & 9.5864 \\ 3.2874 & 7.3635 & 2.6227 & 5.9512 & 3.2122 & 5.3830 & 3.8458 & 4.7191 & 4.5334 & 4.0763 & 4.8622 & 2.8681 & 3.5287 & 1.2065 \\ 1.1147 & 1.4542 & 3.9361 & 4.6182 & 7.1119 & 8.3360 & 4.6762 & 10.7090 & 3.4277 & 10.4726 & 5.0805 & 7.6090 & 9.4194 & 6.4827 \\ 6.6098 & 10.6255 & 7.3108 & 6.4362 & 9.0418 & 5.5031 & 5.2310 & 4.8399 & 1.9423 & 5.0194 & 3.0747 & 3.5242 & 5.1490 & 3.2018 \end{bmatrix}$$

Performing damage identification in the same way as previously, yields the following results (Figures 12–16):

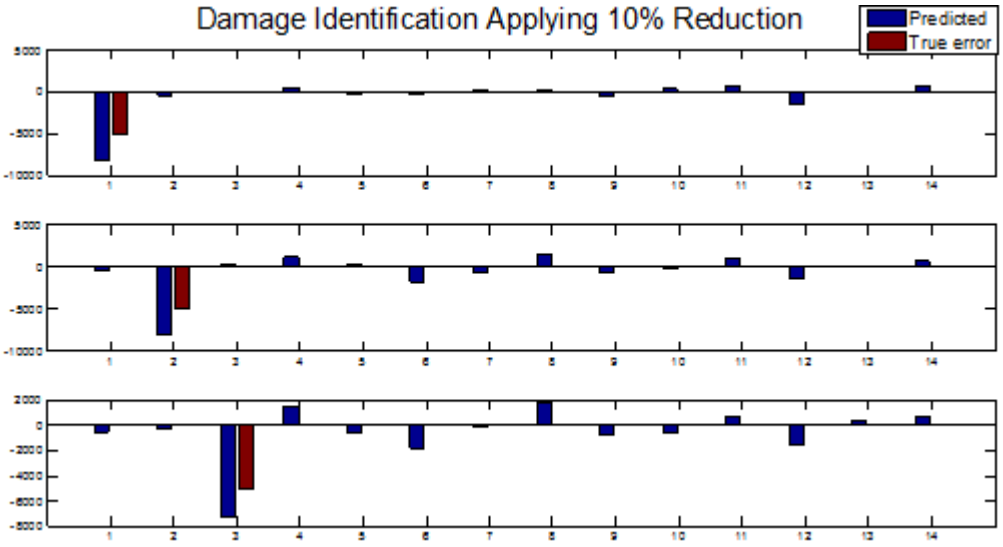

Figure 12. Damage Identification for Elements 1–3, Using $\left[S_H\right]$.

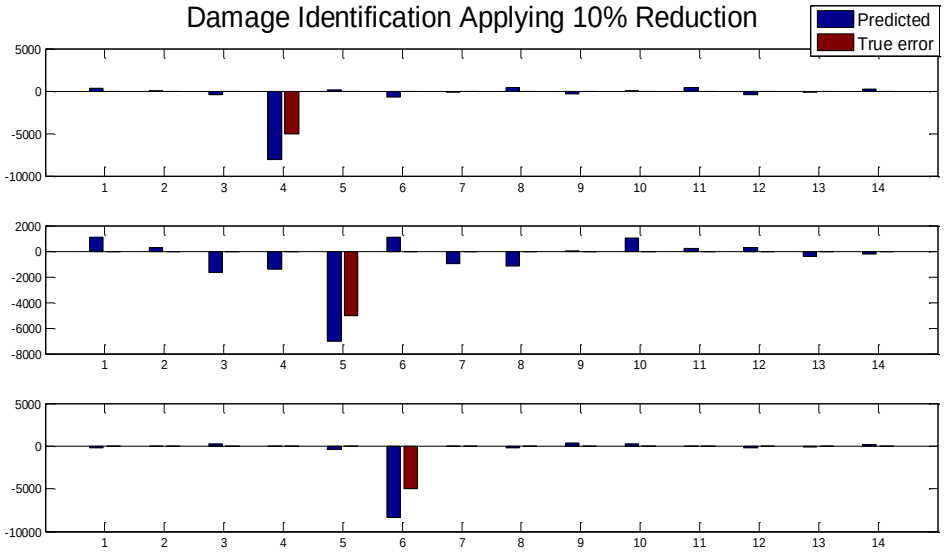

Figure 13. Damage Identification for Elements 4–6, Using $\left[S_H\right]$.

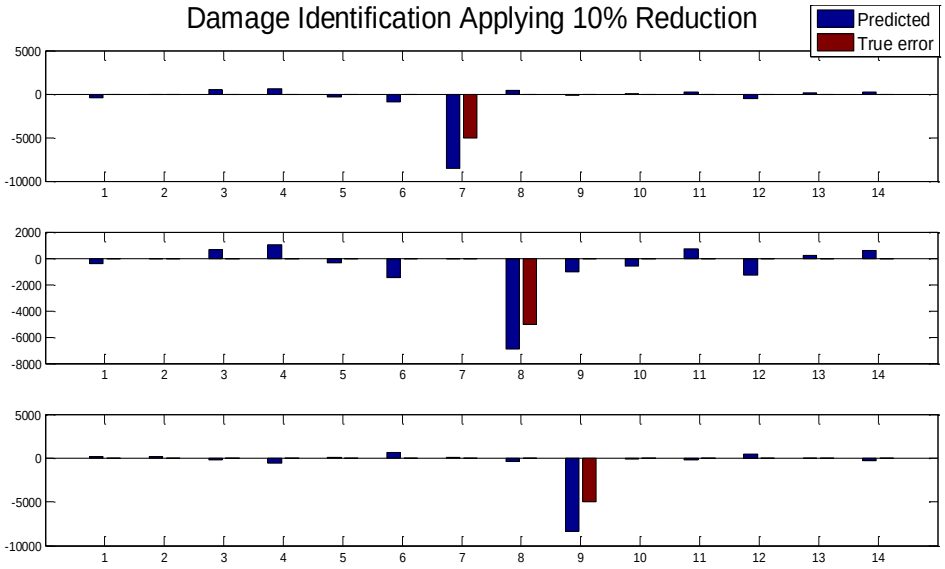

Figure 14. Damage Identification for Elements 7–9, Using $\left[S_H\right]$.

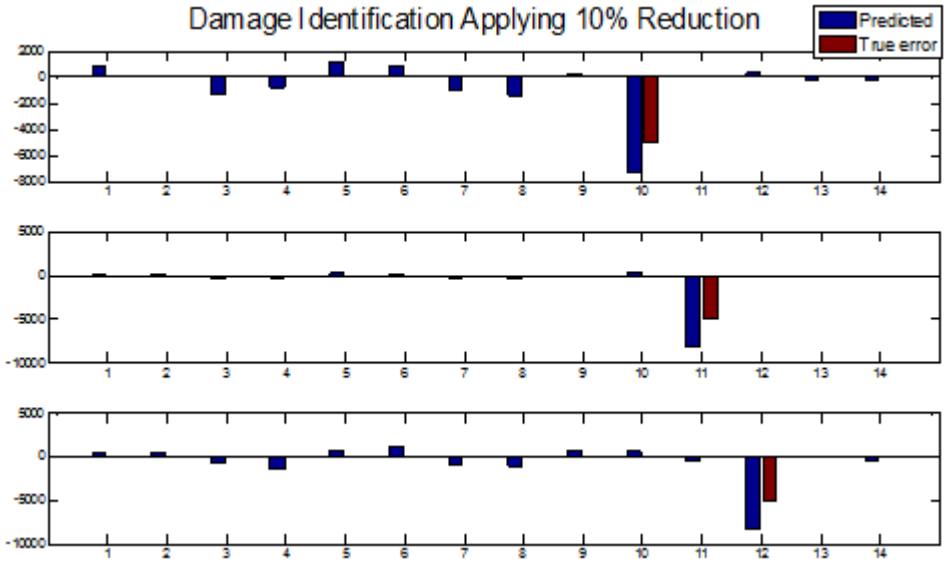

Figure 15. Damage Identification for Elements 10–12, Using $\left[S_H\right]$.

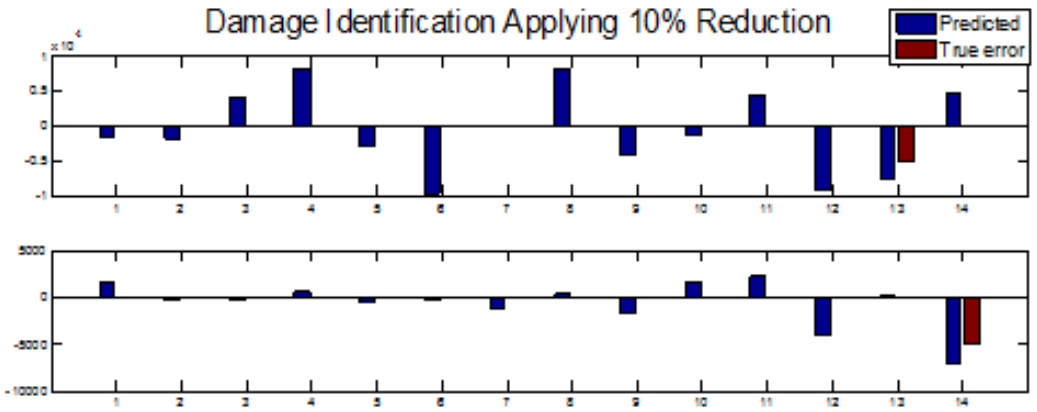

Figure 16. Damage Identification for Elements 13–14, Using $\left[S_H\right]$.

Now the damage identification process can be conducted at each element with no difficulties, except at element 13 as expected. By changing the thirteenth row, $S_{8,4}^{ABC_1}$, of the sensitivity matrix with the row $S_{1,11}^{ABC_1}$, which can identify the damage at element 13 based on QR decomposition, the damage is identified as Figure 17 shows. Therefore, the use of a composite sensitivity matrix based on higher modes is more efficient, as long as it has been created based on QR decomposition.

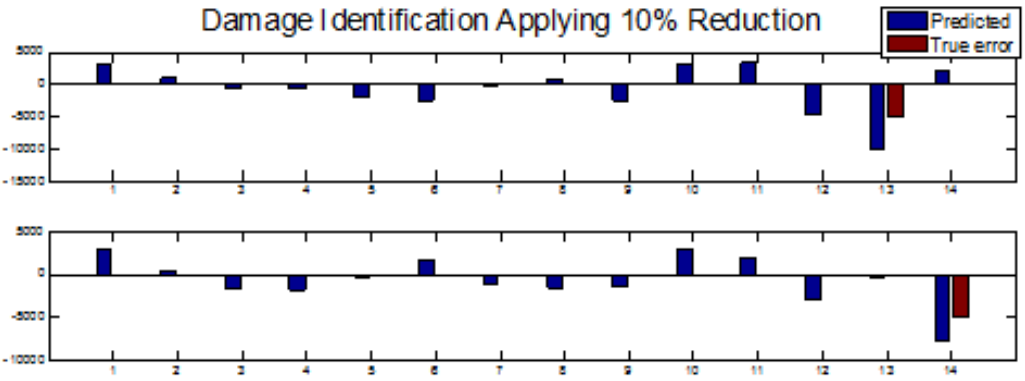

Figure 17. Damage Identification for Elements 13–14, Based on QR Decomposition and Using $\left[S_H\right]$.

Next, the use of two pins (ABC2) for the creation of a composite sensitivity matrix is investigated. Moreover, the next composite sensitivity matrix $\left[S_{Sym}\right]$, is created from rows of sensitivity matrices, which were created by symmetrical structural configurations. Symmetrical structural configurations for a free-free beam include, one pin at the middle of the beam (case 8), two pins at the first and last node of beam, and so forth. The first case of ABC2 is to apply one pin at the first node, and the other pin, at the second node of the finite element model. Then the first pin remains at the first node, and each time the second pin shifts a node until the last one, and the first 15 cases of ABC2 are created. After this, pins are applied at the second and third node, and the same process is repeated until all the possible cases (105 cases) have been investigated. Based again on the QR decomposition, this composite sensitivity matrix is a full rank, square matrix as follows:

$$\left[S_{Sym}\right]=\begin{bmatrix} S_{2,9}^{ABC_1} \\ S_{5,9}^{ABC_1} \\ S_{6,14}^{ABC_1} \\ S_{9,14}^{ABC_1} \\ S_{3,26}^{ABC_1} \\ S_{10,26}^{ABC_1} \\ S_{4,37}^{ABC_1} \\ S_{9,37}^{ABC_1} \\ S_{2,47}^{ABC_1} \\ S_{3,47}^{ABC_1} \\ S_{7,56}^{ABC_1} \\ S_{10,56}^{ABC_1} \\ S_{8,64}^{ABC_1} \\ S_{2,71}^{ABC_1} \end{bmatrix},$$

with the values shown in Table 6:

Table 6. Composite Sensitivity Matrix Based on Symmetrical Structure Configurations.

$$\left[S_{Sym}\right] = \begin{bmatrix}
0.0013 & 0.0182 & 0.0626 & 0.1059 & 0.1055 & 0.0582 & 0.0101 & 0.0101 & 0.0582 & 0.1055 & 0.1059 & 0.0626 & 0.0182 & 0.0013 \\
0.2083 & 1.4526 & 1.2254 & 0.1570 & 1.1293 & 0.6358 & 0.9956 & 0.9956 & 0.6358 & 1.1293 & 0.1570 & 1.2254 & 1.4526 & 0.2083 \\
1.5834 & 2.7237 & 0.6612 & 3.2340 & 0.6601 & 2.7248 & 1.5788 & 1.5788 & 2.7248 & 0.6601 & 3.2340 & 0.6612 & 2.7237 & 1.5834 \\
11.4461 & 5.7307 & 12.7780 & 9.6626 & 6.5022 & 13.5642 & 7.9077 & 7.9077 & 13.5642 & 6.5022 & 9.6626 & 12.7780 & 5.7307 & 11.4461 \\
0.0081 & 0.1473 & 0.3917 & 0.3271 & 0.0623 & 0.0809 & 0.3347 & 0.3347 & 0.0809 & 0.0623 & 0.3271 & 0.3917 & 0.1473 & 0.0081 \\
8.2838 & 12.0128 & 10.0543 & 18.8195 & 15.0737 & 9.7465 & 17.1862 & 17.1862 & 9.7465 & 15.0737 & 18.8195 & 10.0543 & 12.0128 & 8.2838 \\
0.0389 & 0.5393 & 0.4985 & 0.0333 & 0.2525 & 0.3215 & 0.0767 & 0.0767 & 0.3215 & 0.2525 & 0.0333 & 0.4985 & 0.5393 & 0.0389 \\
21.3278 & 17.6994 & 10.4556 & 3.5460 & 2.1296 & 4.9770 & 2.9044 & 2.9044 & 4.9770 & 2.1296 & 3.5460 & 10.4556 & 17.6994 & 21.3278 \\
0.0006 & 0.0103 & 0.0459 & 0.0619 & 0.0371 & 0.0155 & 0.0024 & 0.0024 & 0.0155 & 0.0371 & 0.0619 & 0.0459 & 0.0103 & 0.0006 \\
0.0026 & 0.0416 & 0.1732 & 0.1470 & 0.0130 & 0.0280 & 0.0867 & 0.0867 & 0.0280 & 0.0130 & 0.1470 & 0.1732 & 0.0416 & 0.0026 \\
1.8418 & 4.1231 & 1.6117 & 4.4874 & 4.2618 & 6.3425 & 5.8585 & 5.8585 & 6.3425 & 4.2618 & 4.4874 & 1.6117 & 4.1231 & 1.8418 \\
5.6745 & 3.5487 & 5.1647 & 12.2198 & 22.6236 & 17.8427 & 31.3632 & 31.3632 & 17.8427 & 22.6236 & 12.2198 & 5.1647 & 3.5487 & 5.6745 \\
2.0025 & 3.2156 & 2.1215 & 1.7149 & 7.6713 & 8.4915 & 13.6926 & 13.6926 & 8.4915 & 7.6713 & 1.7149 & 2.1215 & 3.2156 & 2.0025 \\
0.0000 & 0.0002 & 0.0011 & 0.0031 & 0.0067 & 0.0120 & 0.0051 & 0.0051 & 0.0120 & 0.0067 & 0.0031 & 0.0011 & 0.0002 & 0.0000
\end{bmatrix}$$

In observing the $\left[S_{Sym}\right]$ matrix, we note the first column and the last are the same and so forth. The columns of this matrix are symmetrical to an imaginary line passing through its middle (between the seventh and eighth columns) and having direction parallel to the y-axis. Damage identification this time results in antisymmetric values of ΔEI as Figures 18–22 show.

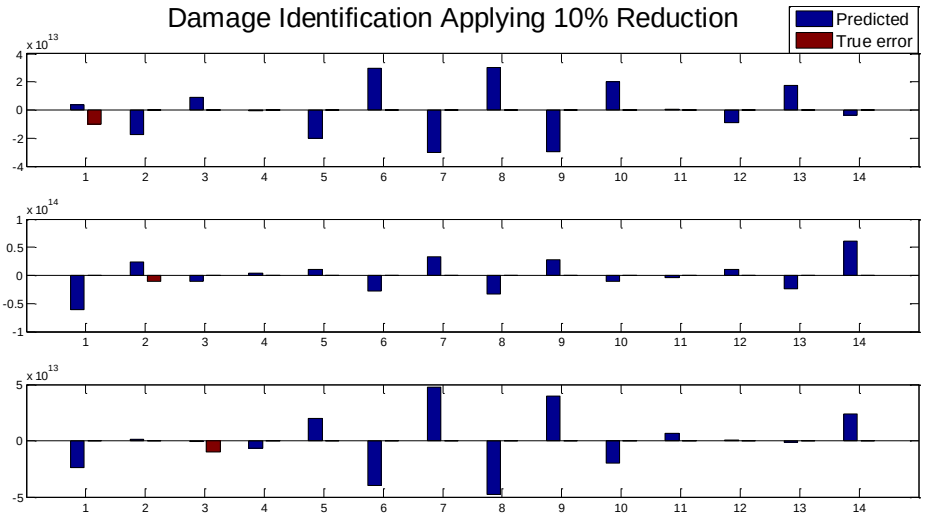

Figure 18. Damage Identification for Elements 1–3, Using $\left[S_{Sym}\right]$.

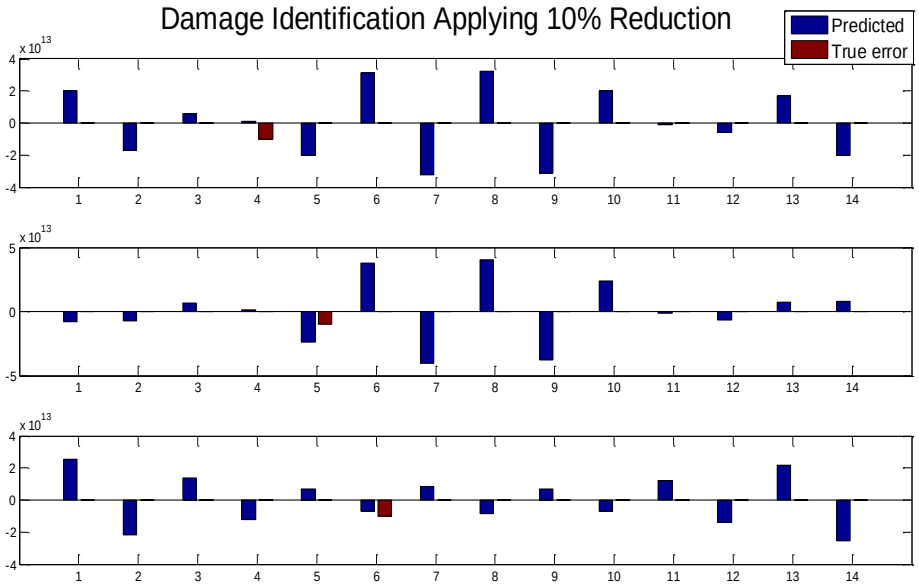

Figure 19. Damage Identification for Elements 4–6, Using $\left[S_{Sym} \right]$.

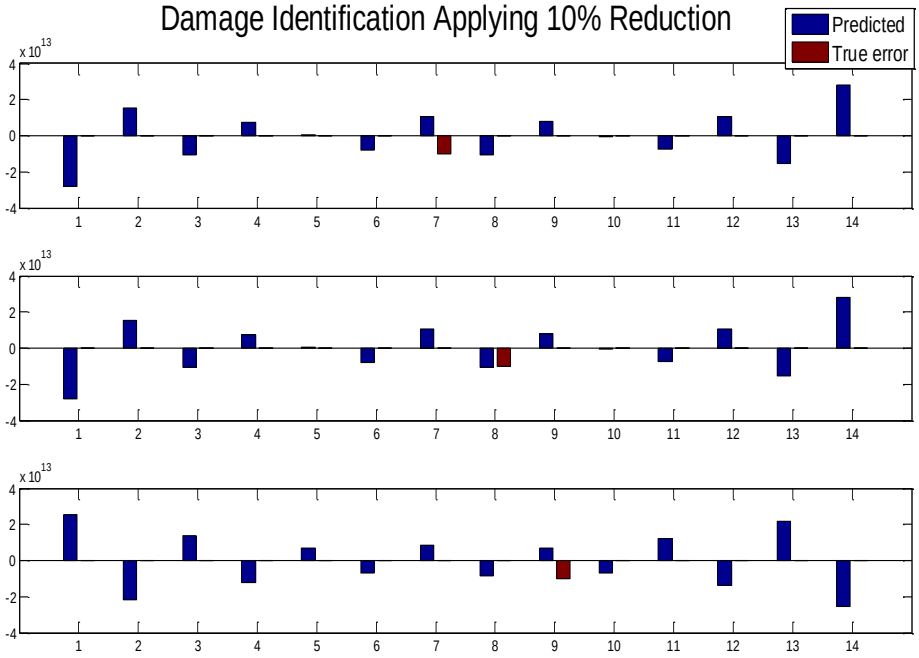

Figure 20. Damage Identification for Elements 7–9, Using $\left[S_{Sym} \right]$.

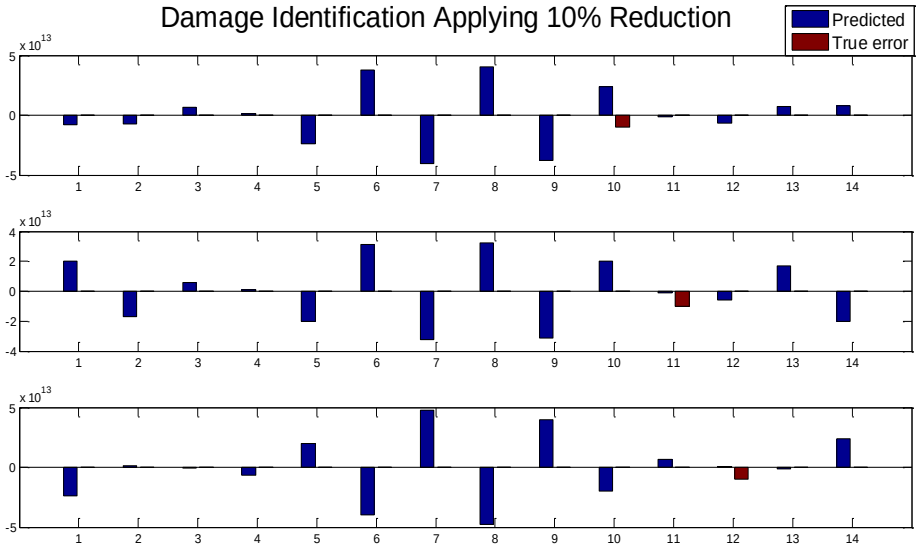

Figure 21. Damage Identification for Elements 10–12, Using $\left[S_{Sym}\right]$.

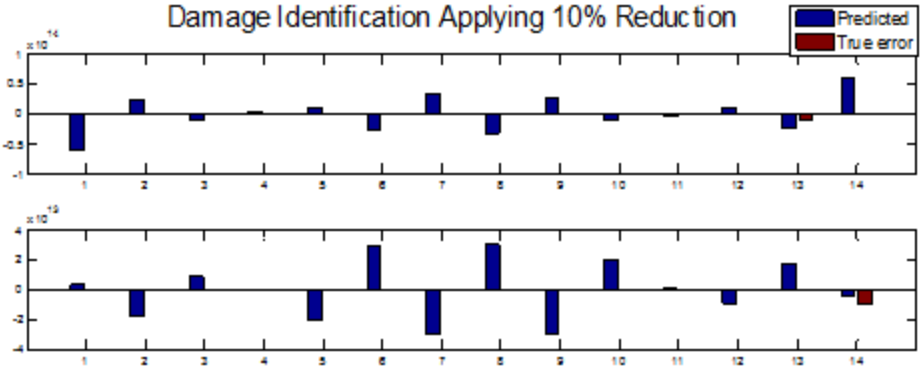

Figure 22. Damage Identification for Elements 13–14, Using $\left[S_{Sym}\right]$.

The error at the finite element model cannot be identified in any case. A further investigation of these results has to be made, thus a change at matrix $\left[S_H\right]$ is performed. The first row ($S_{8,9}^{ABC_1}$) was able to identify damage at the first element, and is changed with a row from a symmetrical structure configuration (

$S_{6,8}^{ABC_1}$) that could still identify the damage at that element. Conducting again damage identification, we find the results are clearly worse, as shown in Figures 23–27.

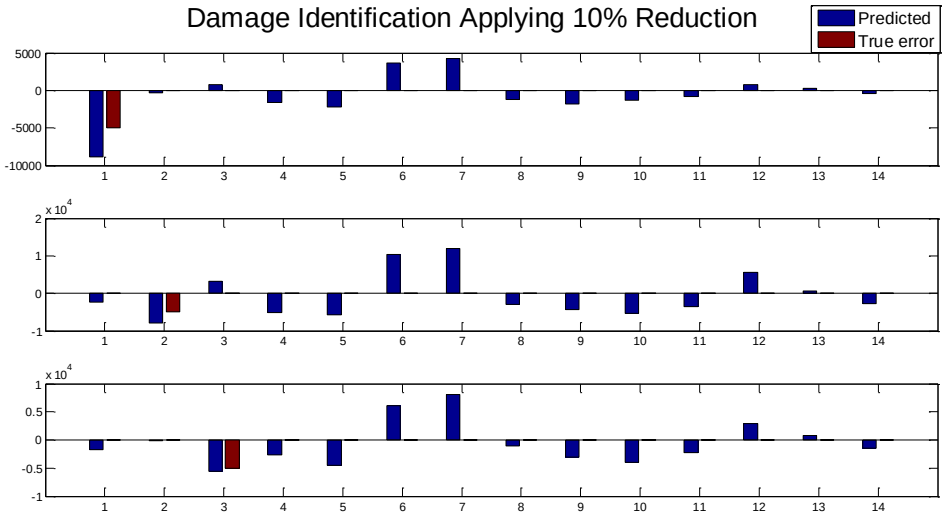

Figure 23. Damage Identification for Elements 1–3, Using $\left[S_H^{'} \right]$.

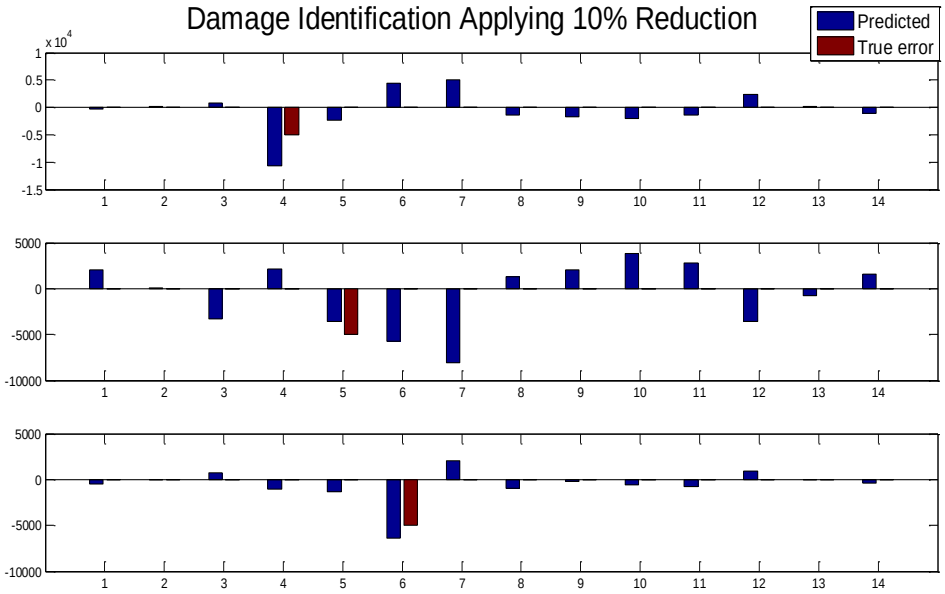

Figure 24. Damage Identification for Elements 4–6, Using $\left[S_H^{'} \right]$.

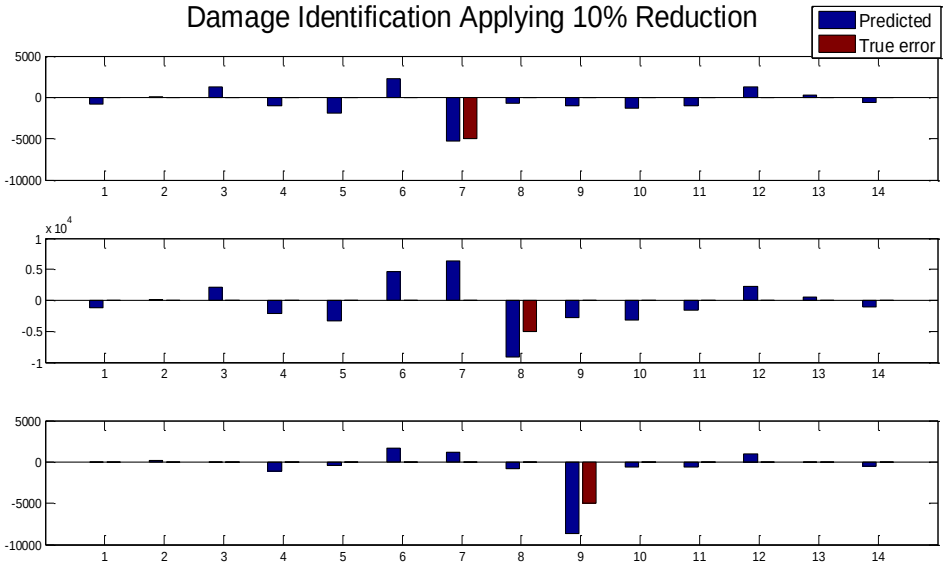

Figure 25. Damage Identification for Elements 7–9, Using $\left[S_H^{'} \right]$.

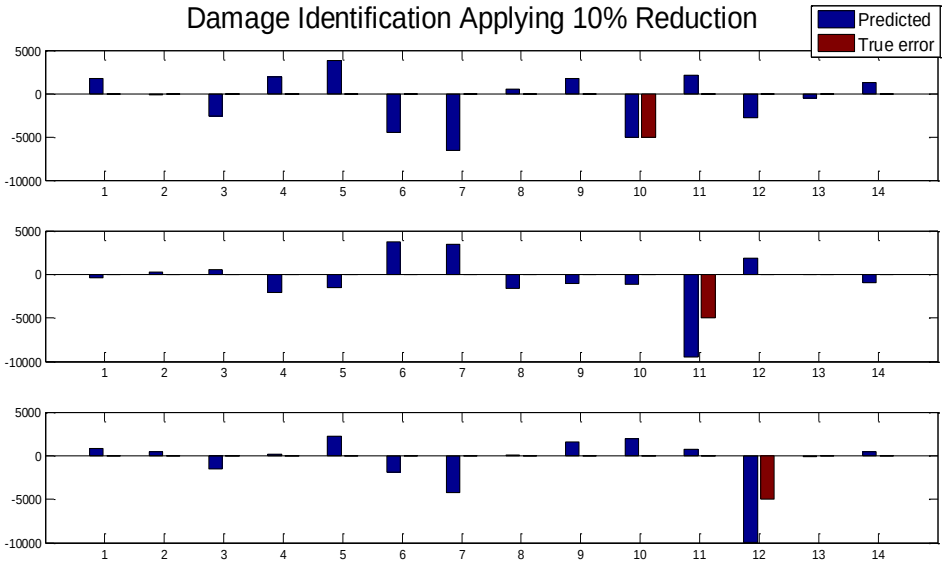

Figure 26. Damage Identification for Elements 10–12, Using $\left[S_H^{'}\right]$.

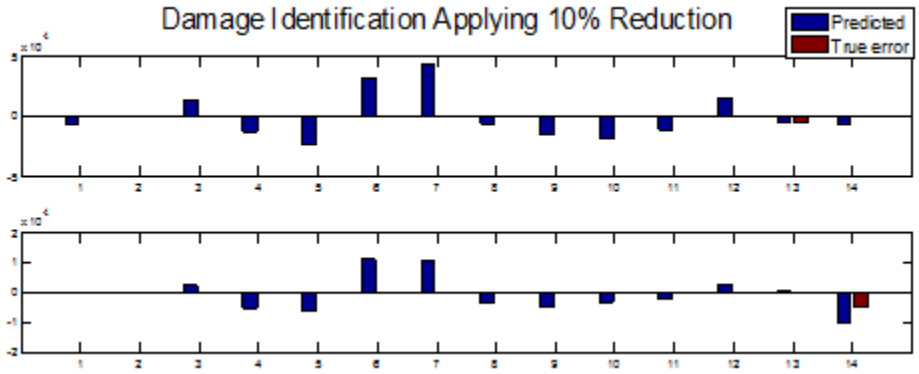

Figure 27. Damage Identification for Elements 13–14, Using $\left[S_H^{'}\right]$.

Thus, a very important conclusion is reached in this case. The use of data that originated from symmetrical structural configurations is not useful. The reason for that is the first value of each row of the sensitivity matrix is the same as the last value of the same row, and so forth. Thus, each row provides half the information as compared to a row created by an asymmetrical structure configuration. The sensitivity matrix of a symmetrical structural configuration is rank deficient. However, because of the use of different rows of different

sensitivity matrices found from different ABC configurations, the composite sensitivity matrix is not rank deficient but still has “coupled sensitivity information” across each row.

Finally, a full rank, square composite sensitivity matrix based on mixed modes, ABC sets, and QR decomposition is created as follows.

$$[S_G] = \begin{bmatrix} S_{9,4}^{ABC_1} \\ S_{5,3}^{ABC_2} \\ S_{4,6}^{ABC_1} \\ S_{1,3}^{ABC_2} \\ S_{2,10}^{ABC_1} \\ S_{1,7}^{ABC_1} \\ S_{1,3}^{ABC_1} \\ S_{8,3}^{ABC_1} \\ S_{2,78}^{ABC_2} \\ S_{2,85}^{ABC_2} \\ S_{2,12}^{ABC_2} \\ S_{4,4}^{ABC_1} \\ S_{6,13}^{ABC_1} \\ S_{7,95}^{ABC_2} \end{bmatrix},$$

Table 7. Composite Sensitivity Matrix Using Mixed Modes and ABC Sets.

$$[S_G] = \begin{bmatrix}
3.5834 & 2.7008 & 7.1602 & 10.5646 & 8.0180 & 16.9323 & 11.2927 & 8.9548 & 17.0901 & 10.4761 & 9.6268 & 17.0339 & 10.6314 & 13.9808 \\
1.5402 & 3.7993 & 0.6784 & 1.7034 & 0.8041 & 0.1958 & 0.9922 & 0.3464 & 0.4149 & 0.9888 & 0.1688 & 0.7363 & 1.0644 & 0.1648 \\
0.0633 & 0.5956 & 0.9564 & 0.2983 & 0.4416 & 0.6273 & 0.0455 & 0.3252 & 0.3199 & 0.0393 & 0.2352 & 0.5329 & 0.3068 & 0.0317 \\
0.0000 & 0.0003 & 0.0009 & 0.0011 & 0.0008 & 0.0006 & 0.0004 & 0.0003 & 0.0001 & 0.0001 & 0.0000 & 0.0000 & 0.0000 & 0.0000 \\
0.0006 & 0.0095 & 0.0356 & 0.0685 & 0.0831 & 0.0644 & 0.0254 & 0.0024 & 0.0320 & 0.0559 & 0.0313 & 0.0129 & 0.0030 & 0.0002 \\
0.0000 & 0.0001 & 0.0008 & 0.0023 & 0.0050 & 0.0090 & 0.0097 & 0.0067 & 0.0043 & 0.0024 & 0.0011 & 0.0004 & 0.0001 & 0.0000 \\
0.0000 & 0.0001 & 0.0010 & 0.0041 & 0.0083 & 0.0123 & 0.0146 & 0.0145 & 0.0121 & 0.0084 & 0.0046 & 0.0018 & 0.0004 & 0.0000 \\
9.5864 & 10.9694 & 8.7243 & 3.5357 & 9.2179 & 3.9107 & 7.0048 & 7.1811 & 3.7920 & 9.2711 & 3.5130 & 7.5432 & 7.2930 & 5.9732 \\
0.0000 & 0.0000 & 0.0000 & 0.0001 & 0.0003 & 0.0005 & 0.0008 & 0.0088 & 0.0243 & 0.0136 & 0.0063 & 0.0022 & 0.0004 & 0.0000 \\
0.0000 & 0.0000 & 0.0000 & 0.0001 & 0.0001 & 0.0002 & 0.0003 & 0.0004 & 0.0217 & 0.0526 & 0.0254 & 0.0090 & 0.0018 & 0.0001 \\
0.0003 & 0.0047 & 0.0175 & 0.0335 & 0.0403 & 0.0310 & 0.0121 & 0.0011 & 0.0137 & 0.0544 & 0.1174 & 0.0953 & 0.0217 & 0.0013 \\
0.0205 & 0.2127 & 0.4859 & 0.1391 & 0.6360 & 0.7854 & 0.1061 & 0.5242 & 0.9964 & 0.2793 & 0.2878 & 1.1191 & 0.7851 & 0.0894 \\
1.1690 & 4.6946 & 0.9545 & 3.4149 & 1.7733 & 2.3347 & 2.9701 & 1.2318 & 3.8688 & 0.6826 & 3.5307 & 0.9586 & 1.8323 & 0.2863 \\
3.5315 & 7.9478 & 2.8017 & 6.4430 & 3.4137 & 5.8540 & 4.0771 & 5.1829 & 4.6497 & 4.0991 & 3.8655 & 2.0862 & 2.4239 & 0.8229
\end{bmatrix}$$

Then the damage identification process is conducted again, Figures 28–32.

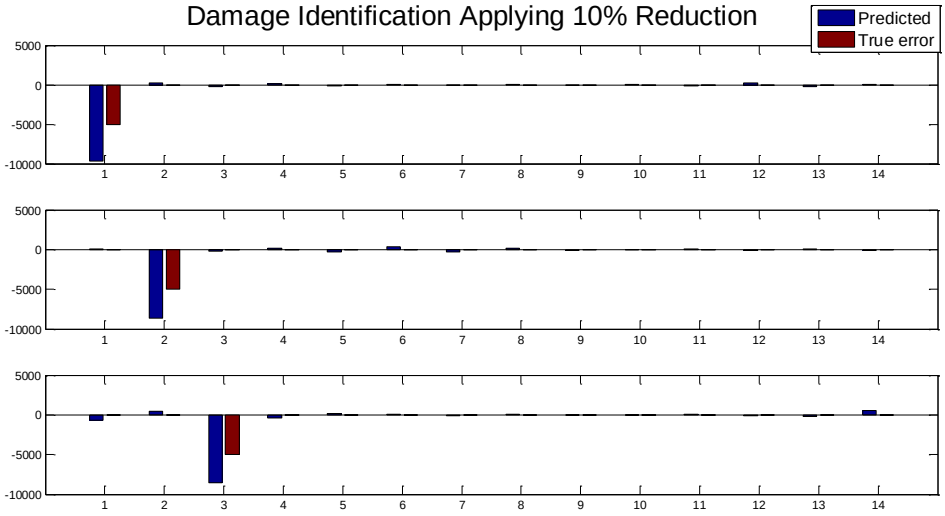

Figure 28. Damage Identification for Elements 1–3, Using $[S_G]$.

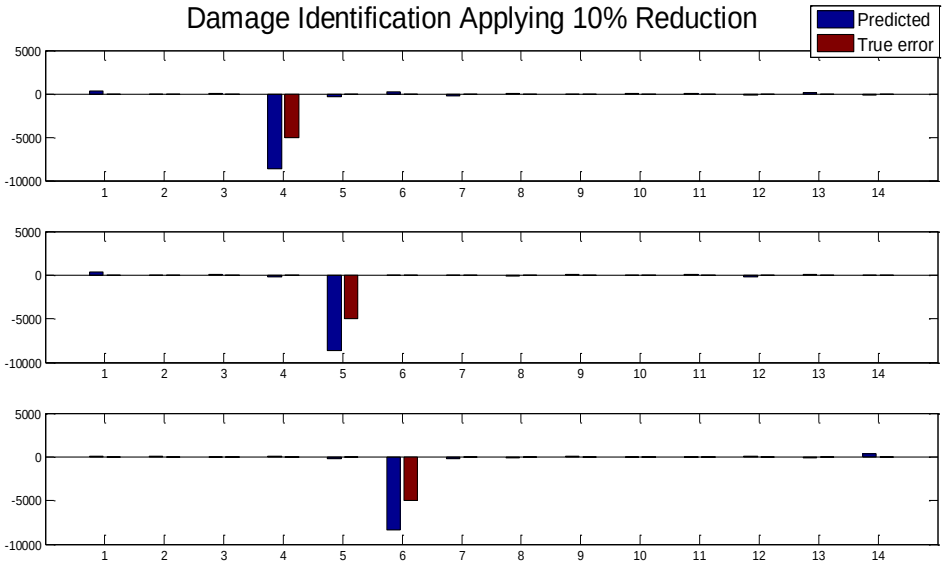

Figure 29. Damage Identification for Elements 4–6, Using $[S_G]$.

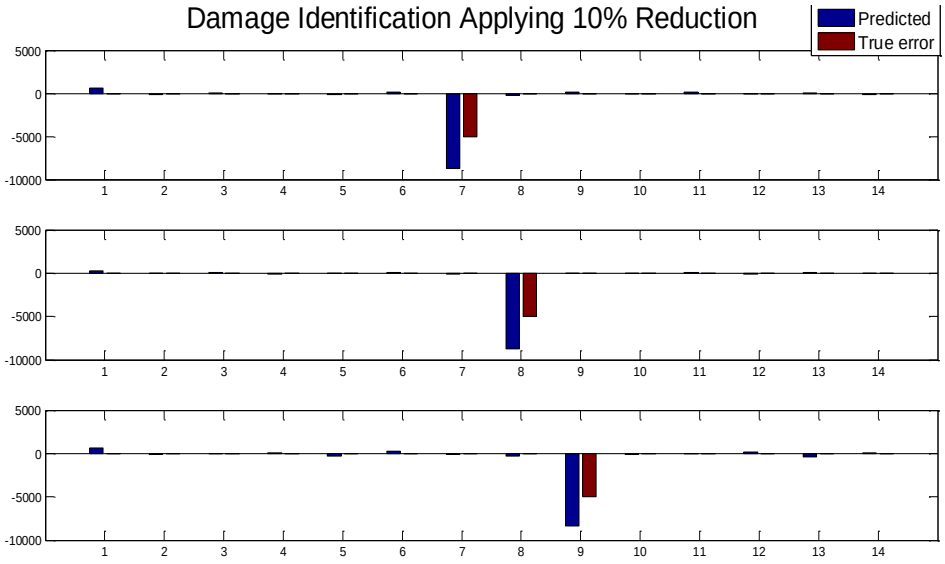

Figure 30. Damage Identification for Elements 7–9, Using $[S_G]$.

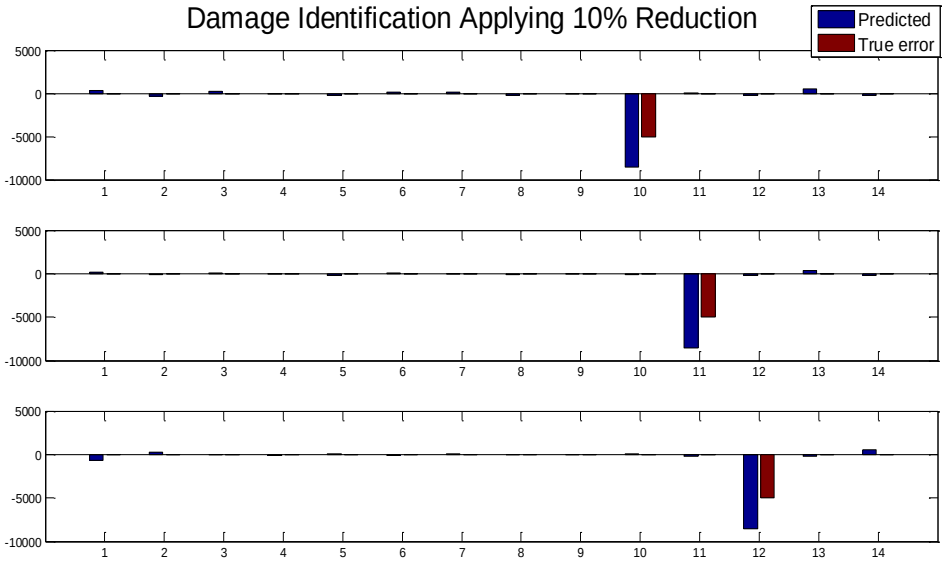

Figure 31. Damage Identification for Elements 10–12, Using $[S_G]$.

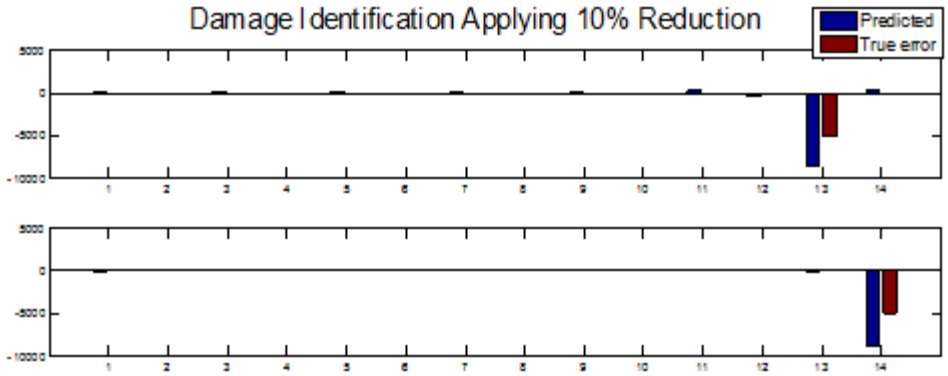

Figure 32. Damage Identification for Elements 10–12, Using $[S_G]$.

It is obvious that this is the best composite matrix to identify the damage at each element. This matrix is used later on for damage identification using experimental data.

E. CALCULATION OF EXPERIMENTAL NATURAL FREQUENCIES FOR ABC SETS USING SYNTHESIS

The previous chapter demonstrated the use of simulated data for damage identification. Initially, the same concept is used to update the finite element model. However, this time, experimental natural frequencies are used. The vector $\{\Delta\omega^2\}$ of equation:

$$\{\Delta EI\} = [\mathrm{S}_{composite}] \setminus \{\Delta\omega^2\}, \tag{3.1}$$

is formed as $\{\Delta\omega^2\} = \omega^2_{\exp} - \omega^2_{FE}$, where the subscript “exp” denotes experimental data, and the subscript “FE” denotes finite element data. From the experiment, a frequency response function for the free-free beam is measured. This FRF is a 15x15 matrix. However, the use of natural frequencies from other ABC sets is needed. Thus, the synthesis equation, Equation (2.53),

$$\left[H^*_{ii}\right] = \left[H_{ii}\right] - \left[H_{ic}\right]\left[H_{cc}\right]^{-1}\left[H_{ci}\right],$$

which was derived in Chapter II, Section G, is used. Applying a pin at the beam (ABC1) results in an FRF that is a 14x14 matrix, and using Equation (2.34) the natural frequencies of ABC1 sets can be evaluated. Again, the average of the diagonal elements of the FRF matrix is used. For reasons of simplicity and brevity, only four cases of ABC1 sets are demonstrated in Figures 33–36.

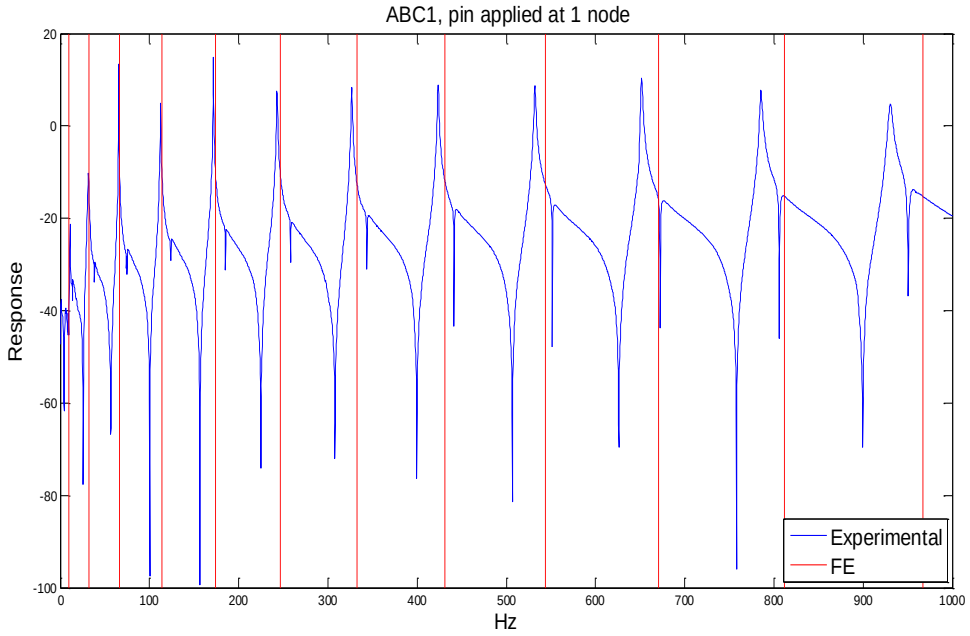

Figure 33. Frequency Response Function for ABC1 with Pin at Node 1.

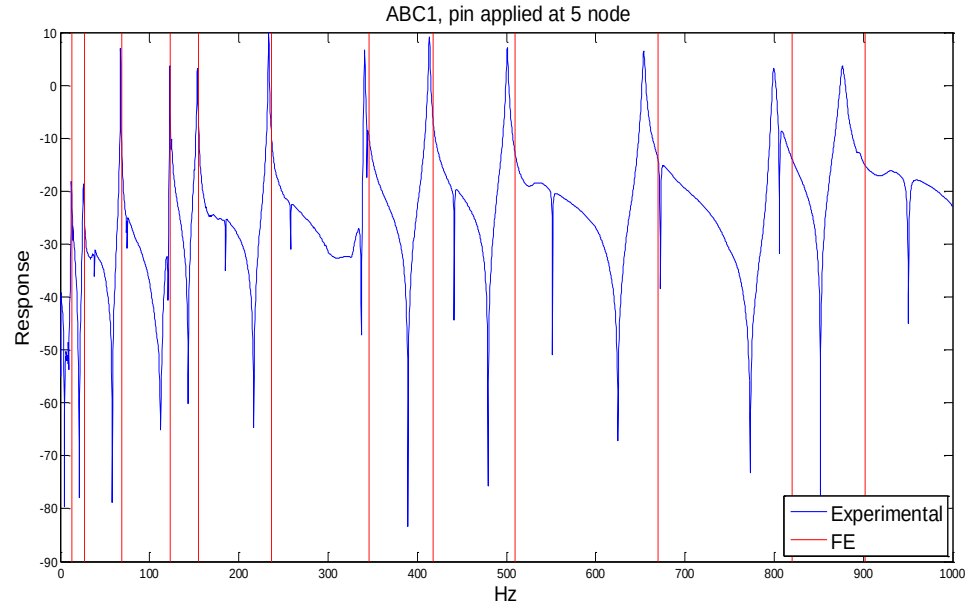

Figure 34. Frequency Response Function for ABC1 with Pin at Node 5.

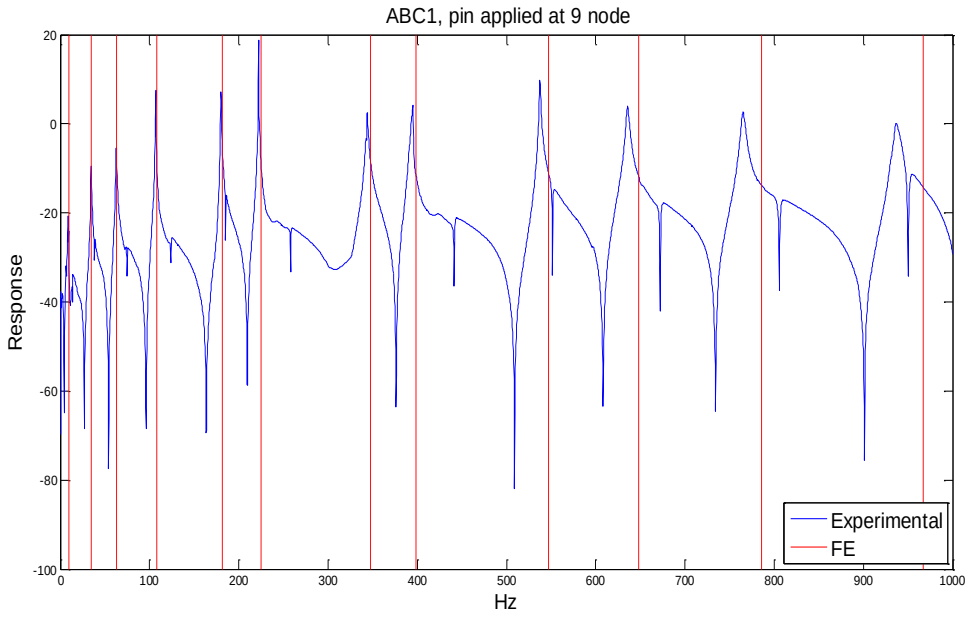

Figure 35. Frequency Response Function for ABC1 with Pin at Node 9.

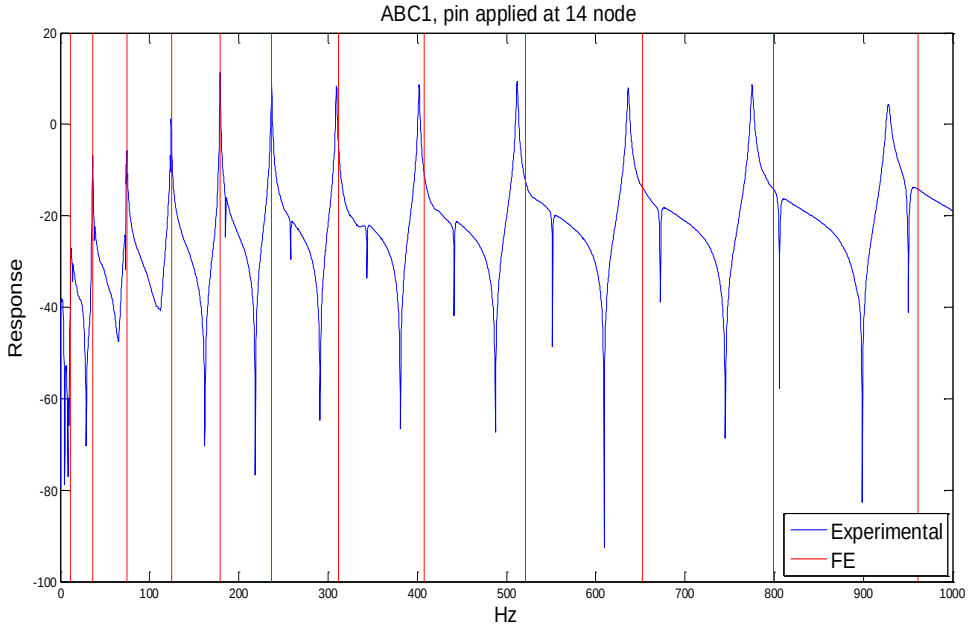

Figure 36. Frequency Response Function for ABC1 with Pin at Node 14.

In Figures 33–36, the blue curve is the resulting frequency response function using the synthesis equation, Equation (2.53). The corresponding

frequencies of the peak values are used as the natural frequencies for the corresponding ABC set. The red lines are the estimated natural frequencies from the finite element model.

Next, the creation of the FRF matrix for ABC2 sets is performed by applying two pins on the free-free beam. This time the resulting FRF matrix is 13x13, and the average of the diagonal elements of the matrix is used. The possible cases for ABC2 are 105, so only a few cases are demonstrated in Figures 37–40.

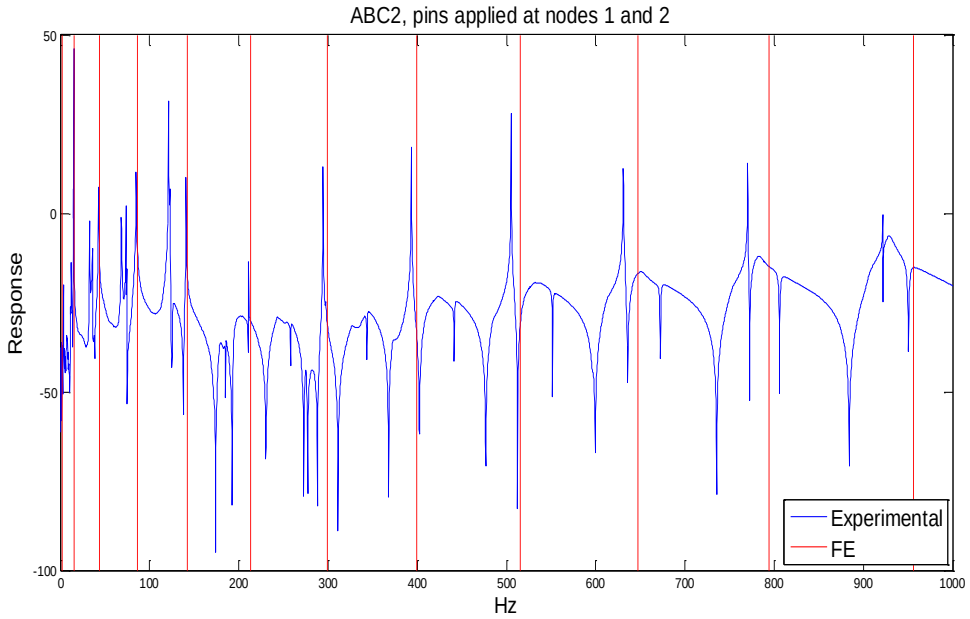

Figure 37. Frequency Response Function for ABC2 with Pins at Nodes 1, 2.

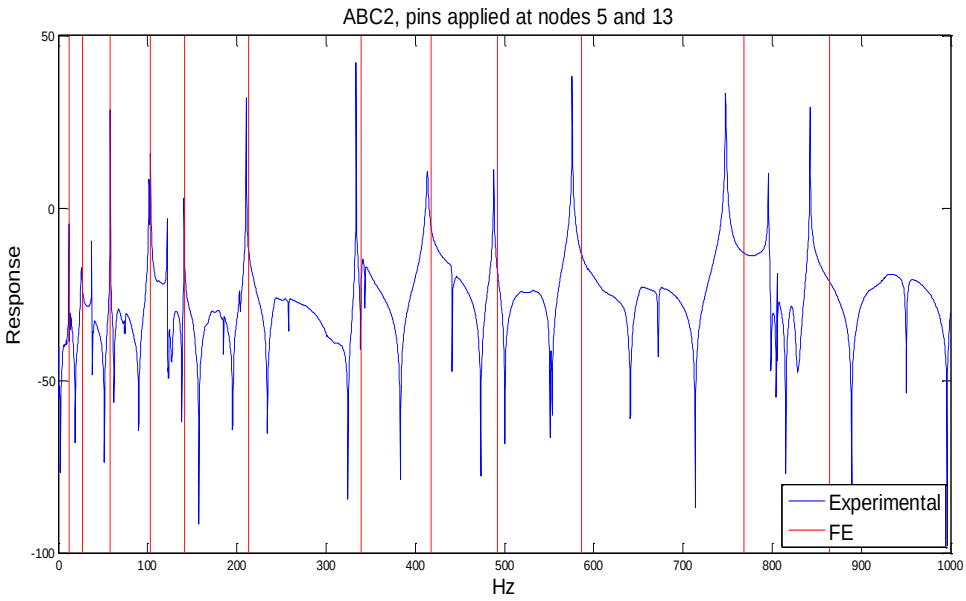

Figure 38. Frequency Response Function for ABC2 with Pins at Nodes 5, 13.

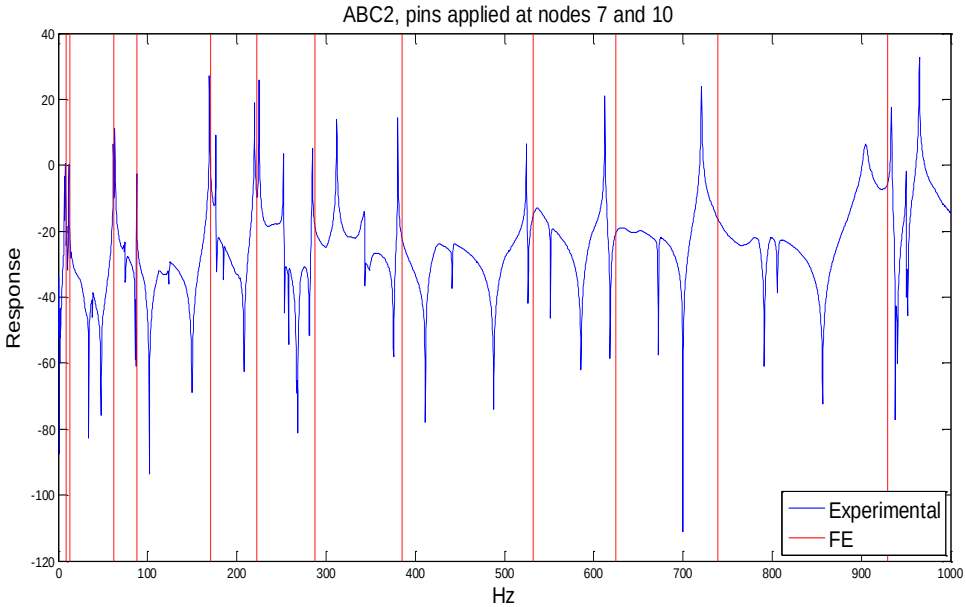

Figure 39. Frequency Response Function for ABC2 with Pins at Nodes 7, 10.

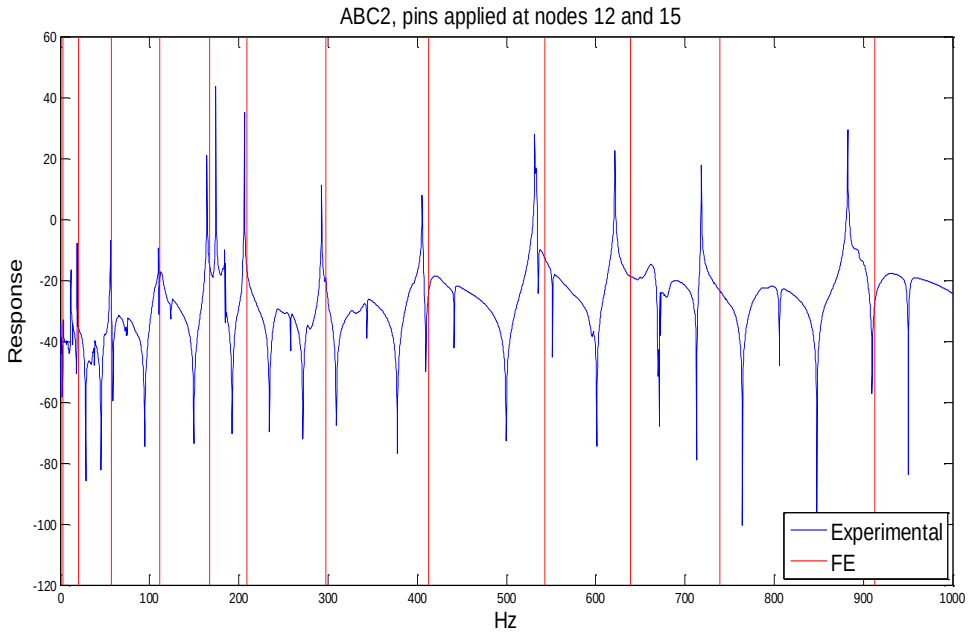

Figure 40. Frequency Response Function for ABC2 with Pins at Nodes 12, 15.

As noted previously, the blue curve is the resulting frequency response function when the synthesis equation, Equation (2.53), is used, and the red lines are the estimated natural frequencies from the finite element model. However, this time the correct peak value for each vibration mode is not as distinct as before. The plot has many discrepancies due to more complicated calculations. At this point, the engineer has to be consistent and use his judgment while he chooses the peak values for each mode.

F. VERIFICATION OF MEASURED, EXTRACTED NATURAL FREQUENCIES

In this research, the eigenvalues of Equation (2.5) are the natural frequencies and mode shapes of the system. As formerly demonstrated, using the synthesis method, the FRF for each different ABC set is created. Then, the researcher can identifies the peak value for each vibration mode and uses the corresponding frequency as the natural frequency. Cauchy's theorem is used to verify that these natural frequencies are in the expected range (bandwidth).

Specifically, the ABC natural frequencies will always interlace the natural frequencies of a higher order system. When one pin (ABC1) is imposed on the baseline system, the free-free beam, the resulting natural frequencies will interlace the natural frequencies of the baseline structure. That is true for every different ABC set. In this research, there are 15 cases for ABC1. After the identification of the natural frequencies for each mode, we plot the results, including the measured natural frequencies of the free-free beam, as Figure 41 shows. These natural frequencies correspond to the experimental data, so a verification of the experimental setup, process, and results is actually performed.

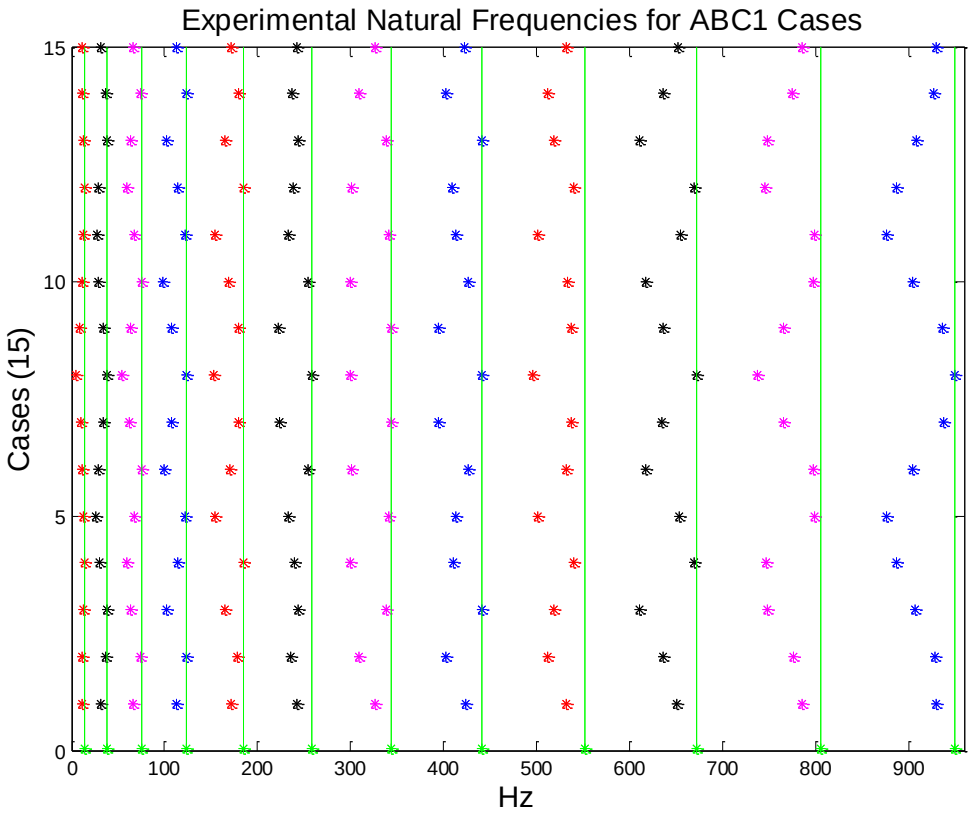

Green stars and lines represent the experimental natural frequencies of the baseline beam. The other stars represent the natural frequencies for a different ABC1 configuration. The way of identifying these natural frequencies is explained in Section E of this chapter.

Figure 41. Interlacing of Experimental Natural Frequencies for ABC1 Sets.

In Figure 41, each row represents the natural frequencies for a different ABC set. The first row, in green color, is the natural frequencies of the baseline structure. The second row has the natural frequencies for ABC1 by imposing the pin on the first node (1). The third row has the natural frequencies for ABC1 by imposing the pin on the second node (2), and so forth. The last row has the natural frequencies for ABC1 by imposing the pin on the last node (15). The natural frequencies for the first mode of each ABC1 set are between (interlace) the natural frequencies of the first and second mode of the baseline structure, as expected. That is the case for each higher mode respectively. This can be validated from Figure 41, which means that the identified natural frequencies are correct.

The same process is performed for the natural frequencies of ABC2 sets. However, this time there are 105 different cases. The results are shown in Figure 42.

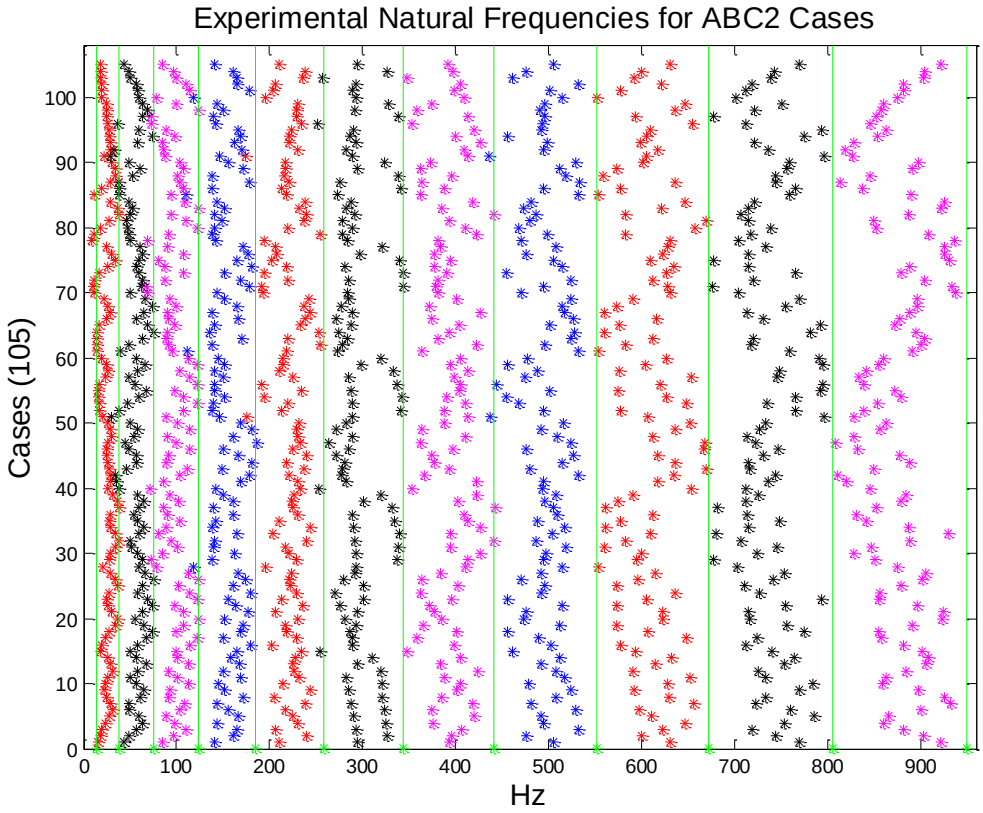

Green stars and lines represent the experimental natural frequencies of the baseline beam. The other stars represent the natural frequencies for a different ABC2 configuration. The way of identifying these natural frequencies is explained in Section E of this chapter.

Figure 42. Interlacing of Experimental Natural Frequencies for ABC2 Sets.

As previously explained, the first row, in green color, contains the values of the natural frequencies of the baseline structure. The second row is the values of the natural frequencies for ABC2 set by imposing the pins at the first (1) and second (2) node. The third row is the values of the natural frequencies for ABC2 set by imposing the pins at the first (1) and third (3) node, and so forth. The last row is the values of the natural frequencies for ABC2 set by imposing the pins at the fourteenth (14) and last (15) node. The expectation of where these values should be is the same as before. However, this time it is obvious that some values are outside of the expected range, especially for lower modes. These values are not used further in the research because they might potentially cause

problems and errors. In Figures 37–40, the FRF of some ABC2 sets was shown. Obviously, the identification of the peak values for some modes is not easy, and that might be one of the reasons that some natural frequencies are not in the expected range.

In conclusion, the natural frequencies calculated using the ABC and synthesis theory have been validated by Cauchy's interlace theorem. These data are further used in the creation of vector $\{\Delta\omega^2\}$, to solve Equation (3.1), as discussed in Section E of this chapter. Some data that are not in the expected range are avoided.

G. SIMULATED ERROR IN EXPERIMENTAL NATURAL FREQUENCIES

The sampling process allows the use of a computer to store and edit a continuous signal. During the vibration experiment, continuous signals are created. However, they have to be discretized or sampled into finite data in order to be stored and edited by a computer. The time step between each sample is called the sample size. The smaller the sample size is, the more accurate the representation of the continuous signal is. The drawback is that it takes more memory to store all these data, and the time to edit or use them is increased. Because of the sampling process, the data between two sampling points are lost. This means that the representation of the experimental data might be inaccurate, especially if the continuous signal changes rapidly with time.

From the measured FRF, the corresponding frequencies to the peak values were used as natural frequencies. Nevertheless, the actual peak value could be anywhere in the sample size range, since these data were lost, as Figure 43 shows.

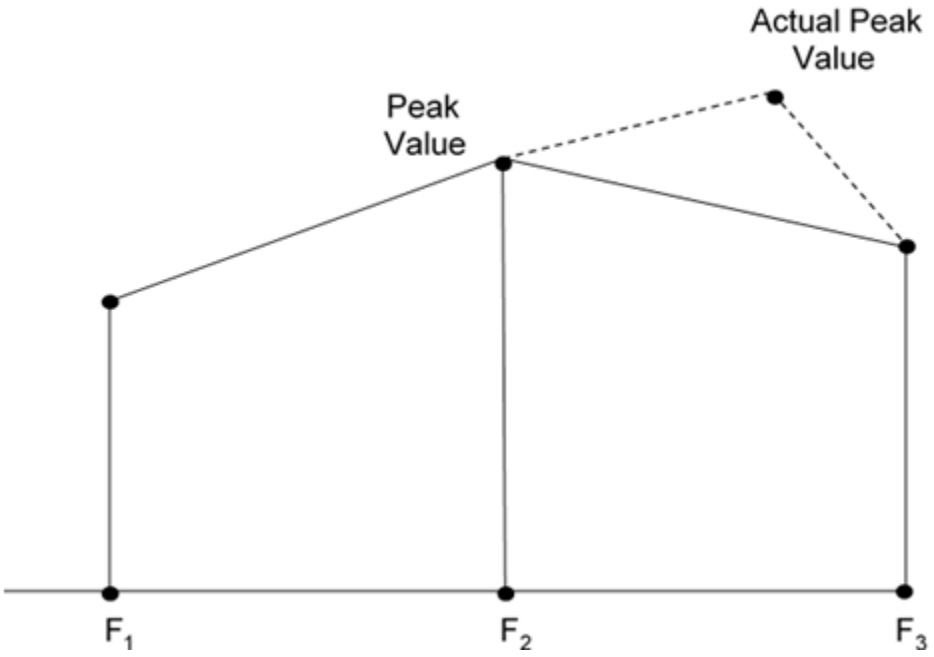

Figure 43. Error Due to Sampling.

Therefore, an investigation to identify the susceptibility of the identified natural frequencies in error due to sampling, must be performed. In this experiment, the sample size has been set to 0.3125Hz. The investigation is performed using the sensitivity matrix $[S_G]$, which has been created from mixed ABC sets and modes. Again, using Equation (3.1), $\{\Delta EI\} = [S_{composite}] \setminus \{\Delta\omega^2\}$,the damage identification process is conducted, and the results are evaluated. This time the value of 0.3124 is added recursively at each experimental natural frequency used to simulate an error due to sampling. Thus, vector $\{\Delta\omega^2\}$ is the same, except for one of its elements, each time, which is changed as follows:

$$\Delta\omega_i^2 = \left[2\pi\left(f_{\exp,i} + 0.3124\right)\right]^2 - \omega_{FE,i}^2 \ , \ i = 1,\ldots,14 \ ,$$

where $f_{\exp,i}$ is the experimental natural frequency to be adjusted, and $\omega_{FE,i}^2$ is the corresponding natural frequency from the finite element model. Initially, the error

is applied at the first element by reducing the stiffness by 10 percent. Figures 44–57 show the results of the damage identification process for the first element, by perturbing recursively each element of the vector $\{\Delta\omega^2\}$.

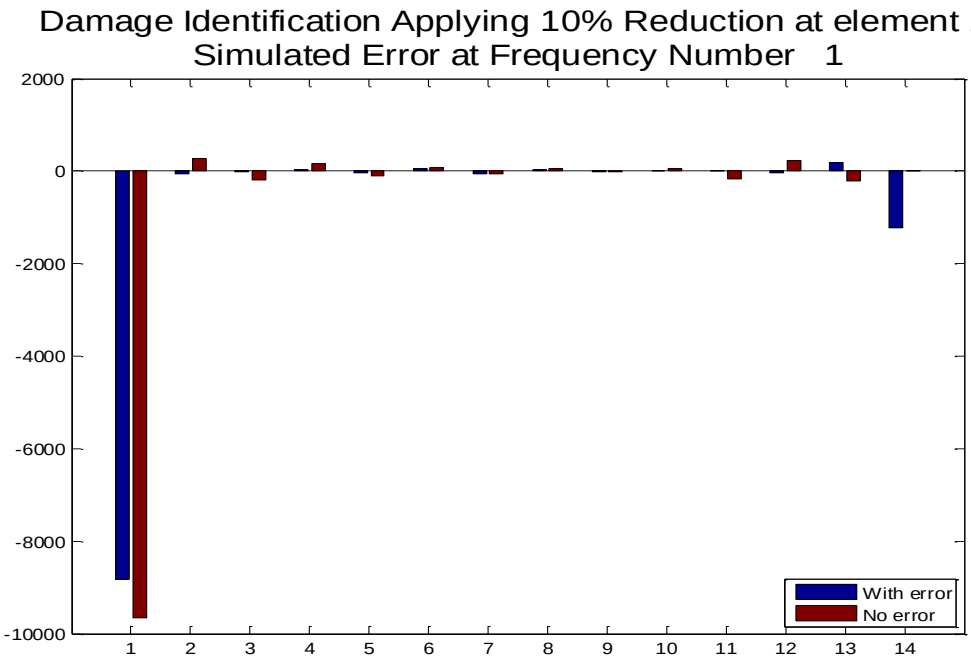

Figure 44. Damage Identification for Element 1, Perturbing the First Frequency.

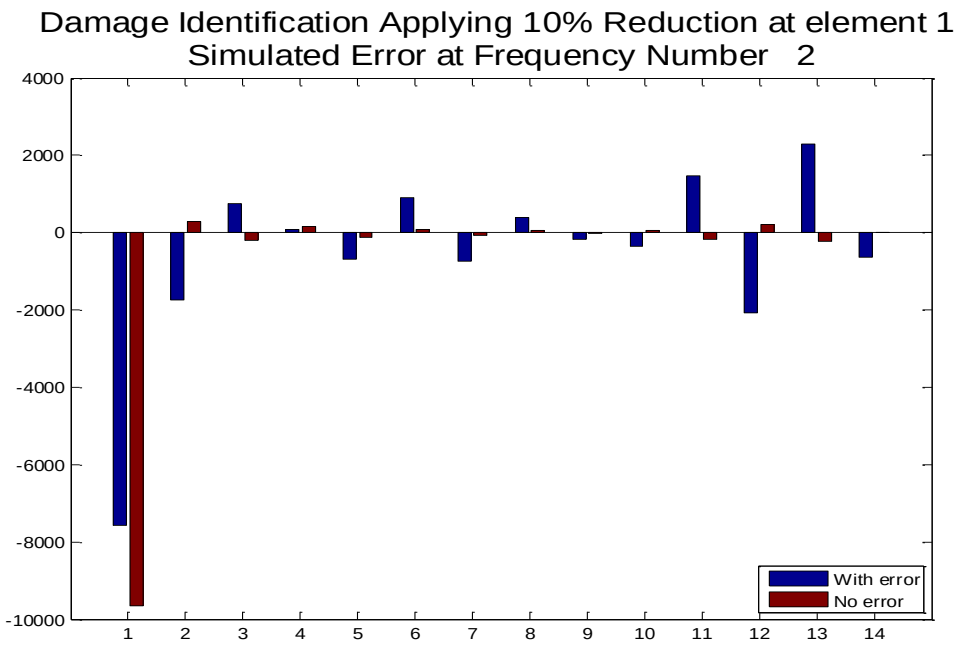

Figure 45. Damage Identification for Element 1, Perturbing the Second Frequency.

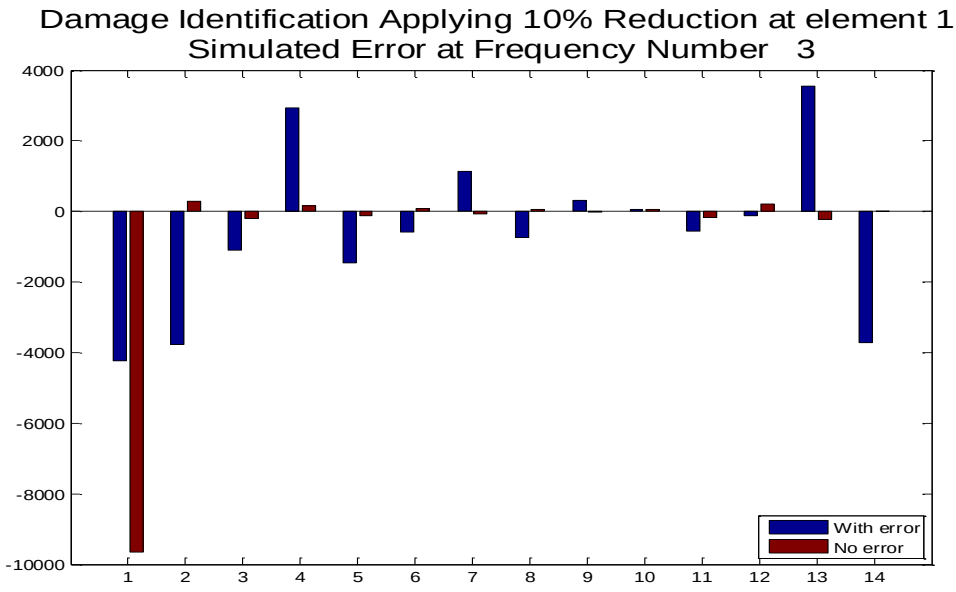

Figure 46. Damage Identification for Element 1, Perturbing the Third Frequency.

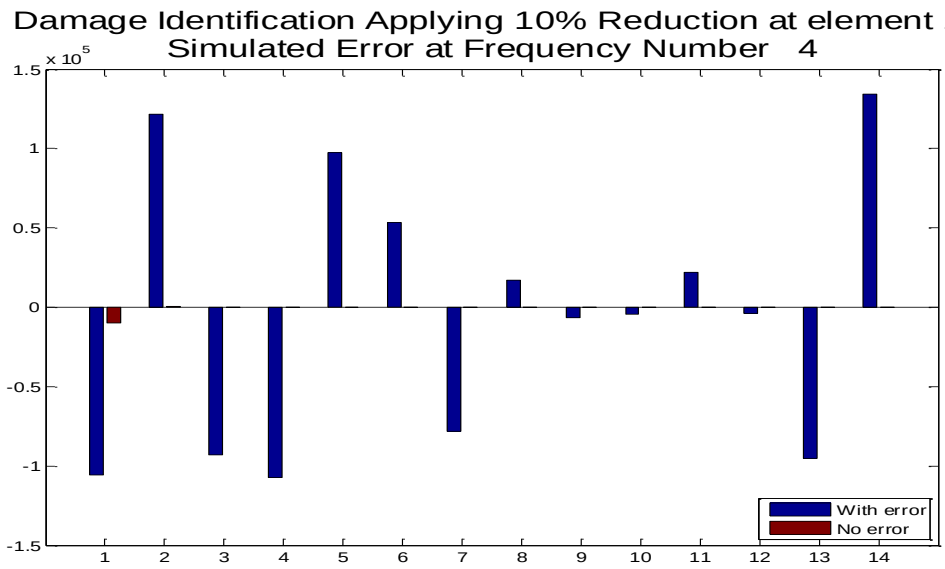

Figure 47. Damage Identification for Element 1, Perturbing the Fourth Frequency.

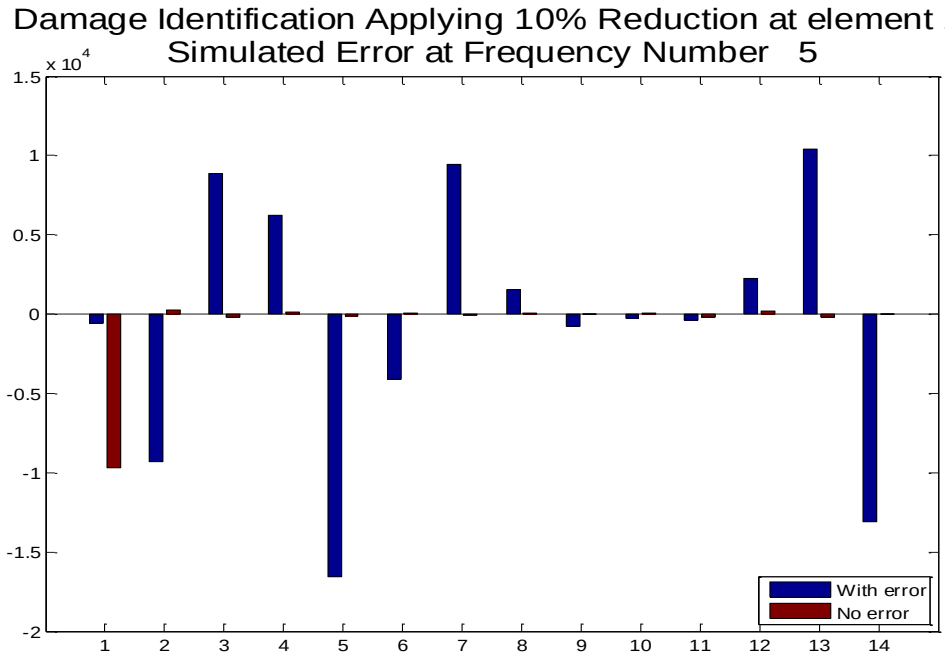

Figure 48. Damage Identification for Element 1, Perturbing the Fifth Frequency.

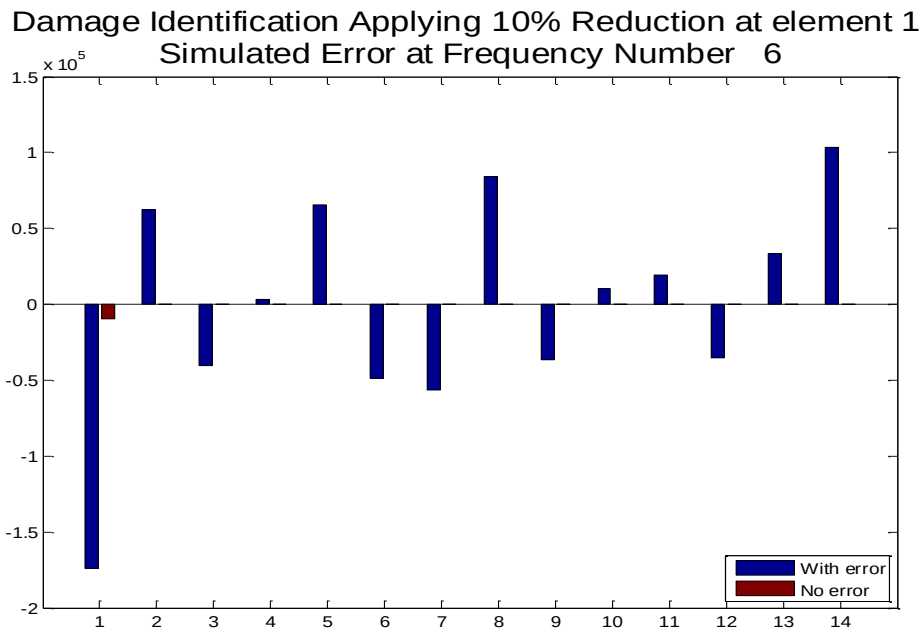

Figure 49. Damage Identification for Element 1, Perturbing the Sixth Frequency.

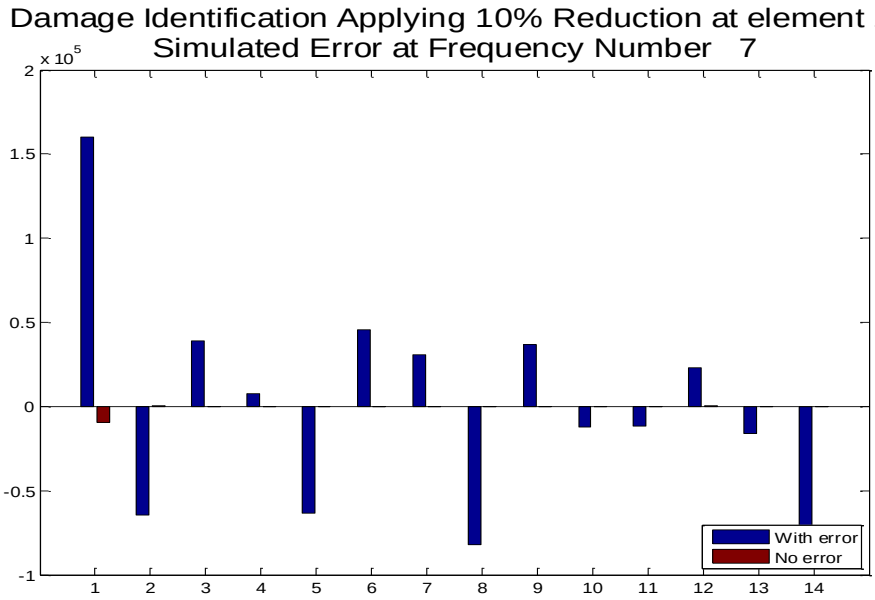

Figure 50. Damage Identification for Element 1, Perturbing the Seventh Frequency.

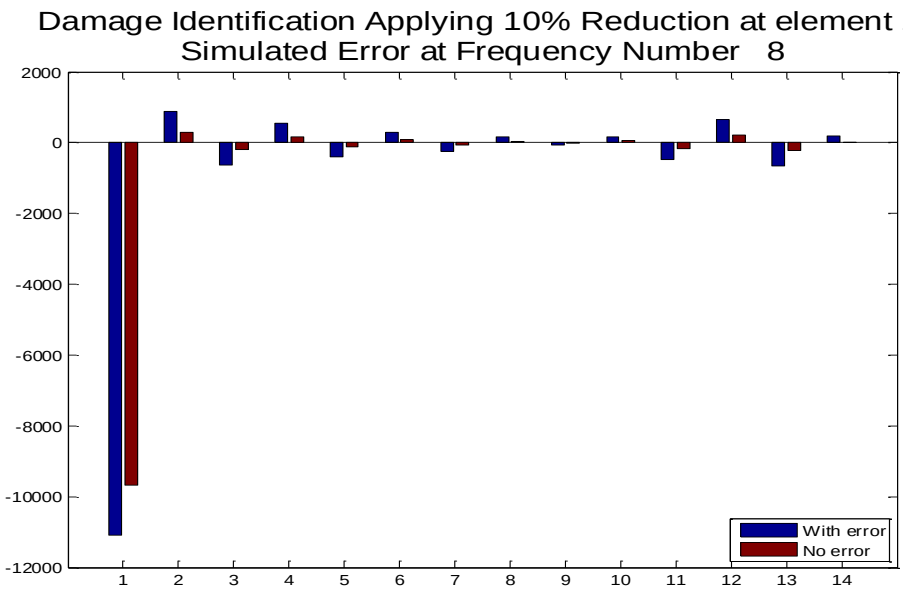

Figure 51. Damage Identification for Element 1, Perturbing the Eighth Frequency.

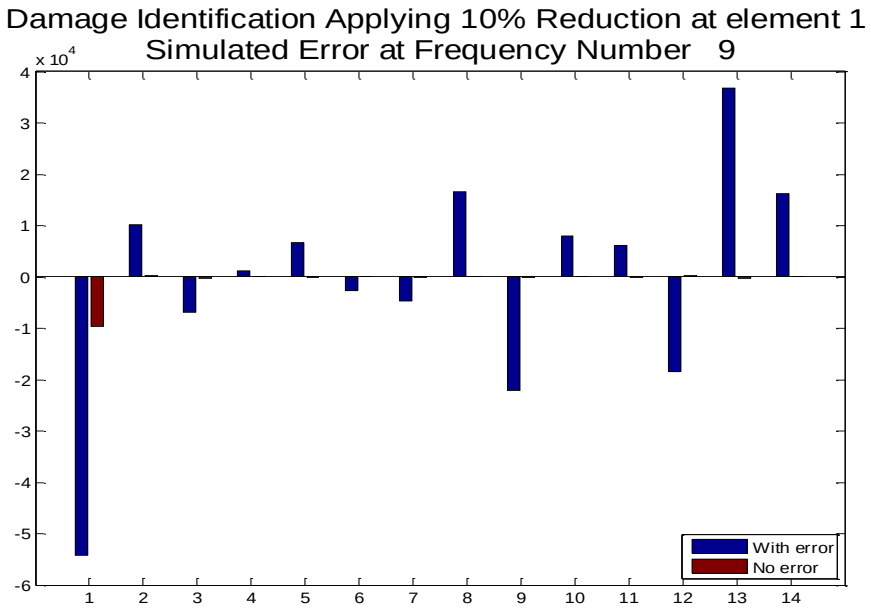

Figure 52. Damage Identification for Element 1, Perturbing the Ninth Frequency.

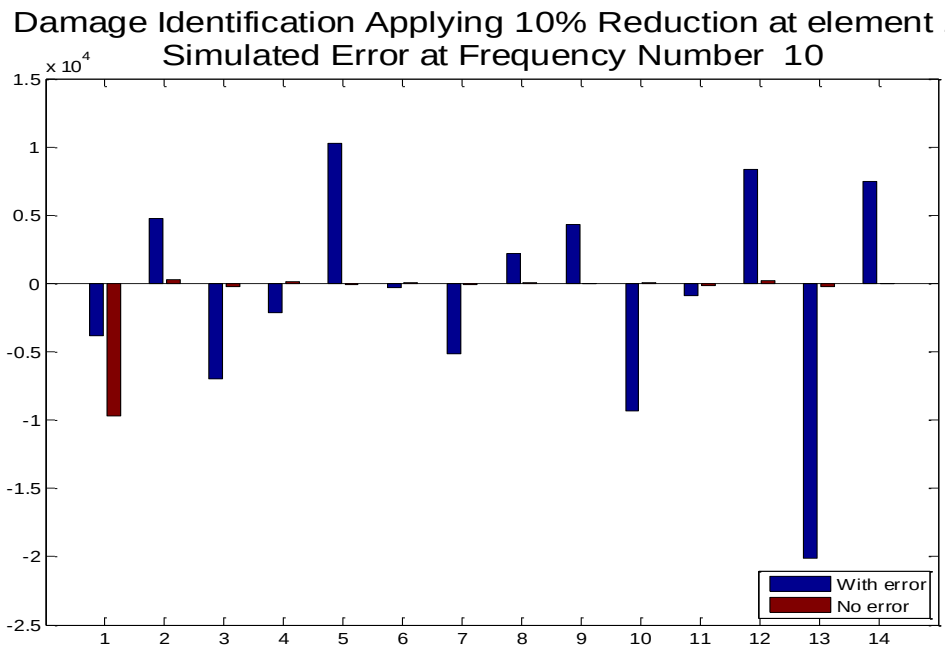

Figure 53. Damage Identification for Element 1, Perturbing the Tenth Frequency.

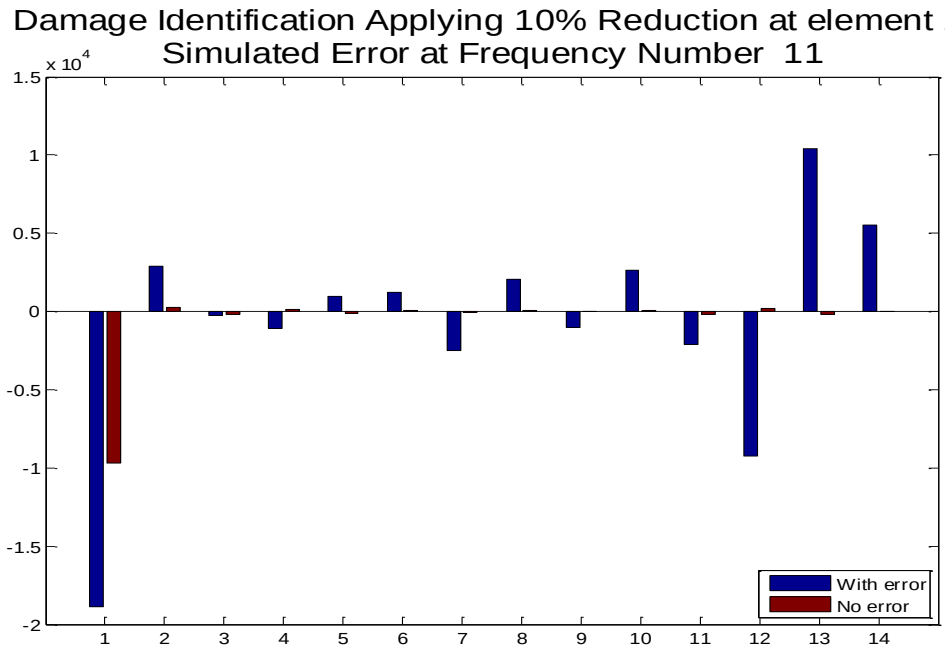

Figure 54. Damage Identification for Element 1, Perturbing the Eleventh Frequency.

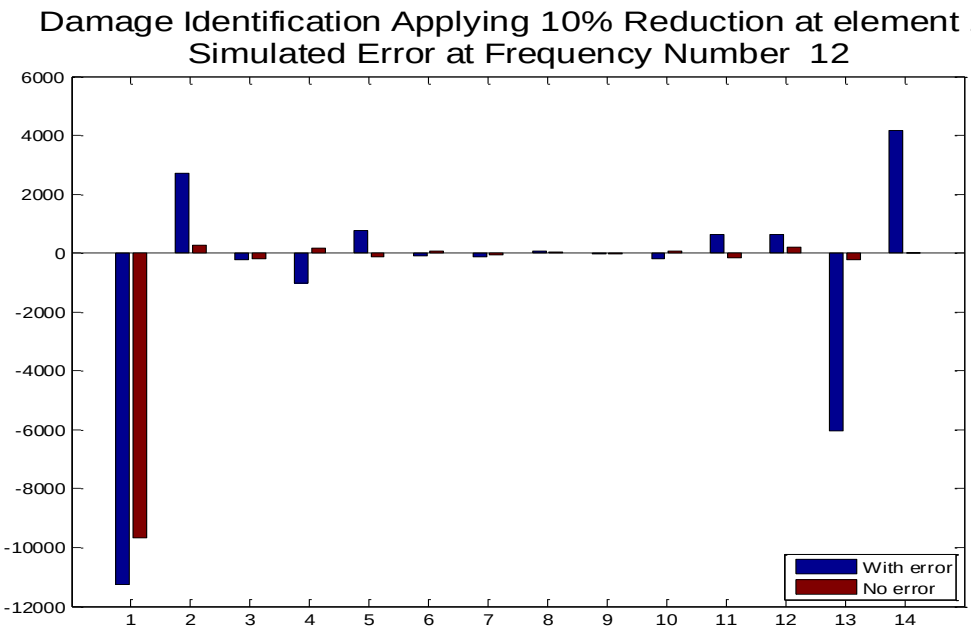

Figure 55. Damage Identification for Element 1, Perturbing the Twelfth Frequency.

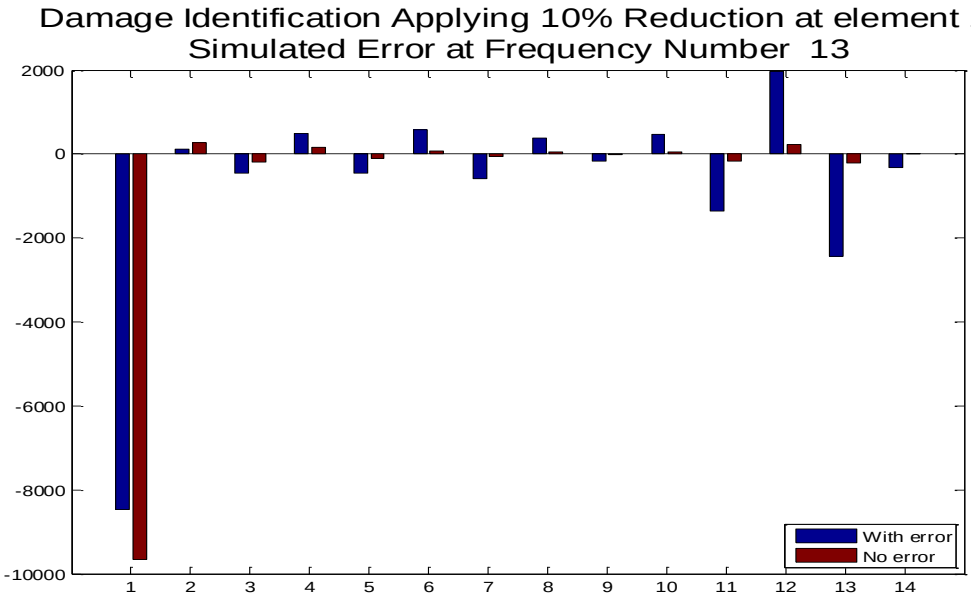

Figure 56. Damage Identification for Element 1, Perturbing the Thirteenth Frequency.

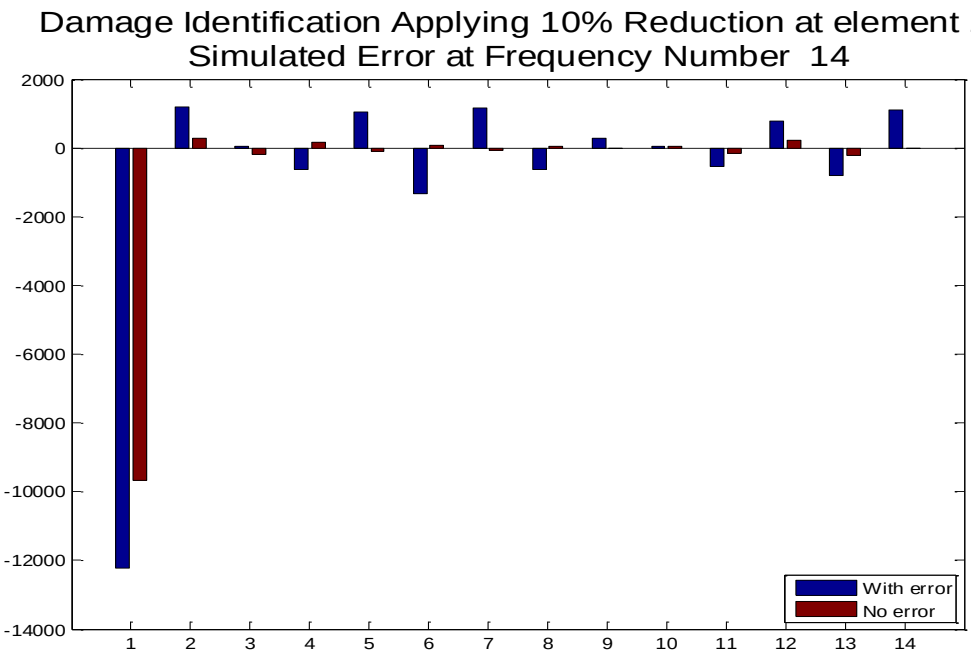

Figure 57. Damage Identification for Element 1, Perturbing the Fourteenth Frequency.

In each figure, the red bars are the results from the damage identification process, applying damage at the first element, with no change at the natural frequency vector. Thus, the red bars are the same as the first plot of Figure 12. The blue bars are the result of the damage identification process at the same finite element, with perturbation at one natural frequency. In some cases (1, 8, 14), the damage identification process can still identify the damaged element, even if the “experimental error” has been added in the corresponding natural frequency. The natural frequencies in these cases are the frequencies of the ninth, eighth, and seventh mode. Then, in some cases (2, 13), the damage identification process cannot be conducted easily, since it is not obvious which is the damaged element. The natural frequencies that have been changed in these cases are the frequencies of the fifth and sixth mode, respectively. Finally, in all the other cases the damage identification process cannot be conducted. The natural frequencies that have been changed in these cases are frequencies of lower modes (first through fourth).

The same process is conducted for each finite element, and the results are provided in Table 8 using a color code. The green color means that the damage identification can easily be conducted, the yellow color means that there are some discrepancies in the results that make the damage identification process difficult, and the red color means that the damage identification process cannot be conducted.

Table 8. Results of Damage Identification for Each Finite Element, by Perturbing Each Used Natural Frequency.

Perturbed Element of Vector $\{\Delta\omega^2\}$	**Mode Used for the Creation of the Corresponding Element of Vector** $\{\Delta\omega^2\}$	**Damaged Element**													
		1	**2**	**3**	**4**	**5**	**6**	**7**	**8**	**9**	**10**	**11**	**12**	**13**	**14**
1	9														
2	5														
3	4														
4	1														
5	2														
6	1														
7	1														
8	8														
9	2														
10	2														
11	2														
12	4														
13	6														
14	7														

The green boxes indicate that the damage identification process can be easily performed at the corresponding element. The yellow boxes indicate that the damage identification process cannot be performed with accuracy at the corresponding element. The red boxes indicate that the damage identification process cannot be performed at the corresponding element.

From Table 8, it is obvious that the natural frequencies of eighth mode and higher are not susceptible to experimental error for the specific sample size that has been used. That is happening because the relative error is small in comparison to the error using lower modes. In this experiment, the sample size is 0.3125Hz, so the perturbation used is 0.3124Hz, and the experimental natural frequency of the eighth mode is 447.2Hz. Therefore, the relative error is:

$$\left| \frac{f_{\exp} - f_{error}}{f_{\exp}} \right| = 0.00069 = 0.069\% .$$

Thus, if the relative error is smaller than 0.069 percent, the natural frequency is not susceptible to error due to sampling for this specific experiment and for the specific sample size. Again, the use of higher modes is better.

THIS PAGE INTENTIONALLY LEFT BLANK

IV. MODEL UPDATE USING EXPERIMENTAL DATA

A. INTRODUCTION

Taking into consideration the analysis of Chapter III, we find the use of natural frequencies of higher modes generally is better than lower modes, due to smaller relative errors in relation to the frequency spacing. To update the initial finite element model, Equation (3.1) is used. This time the vector $\{\Delta\omega^2\}$ is created using the measured natural frequencies from the experiment and the estimated natural frequencies from the finite element model.

Moreover, the composite sensitivity matrix $[S_H]$, is used. This matrix was created using frequencies of higher modes, except from the thirteenth element, as described in Chapter III, Section D, where the following row is used: $S^{ABC_1}_{4,14}$. This row is created from the higher available frequency and can identify damage at the thirteenth finite element based on QR decomposition.

Then Equation (3.1) is solved again, and the results are shown in Figure 58.

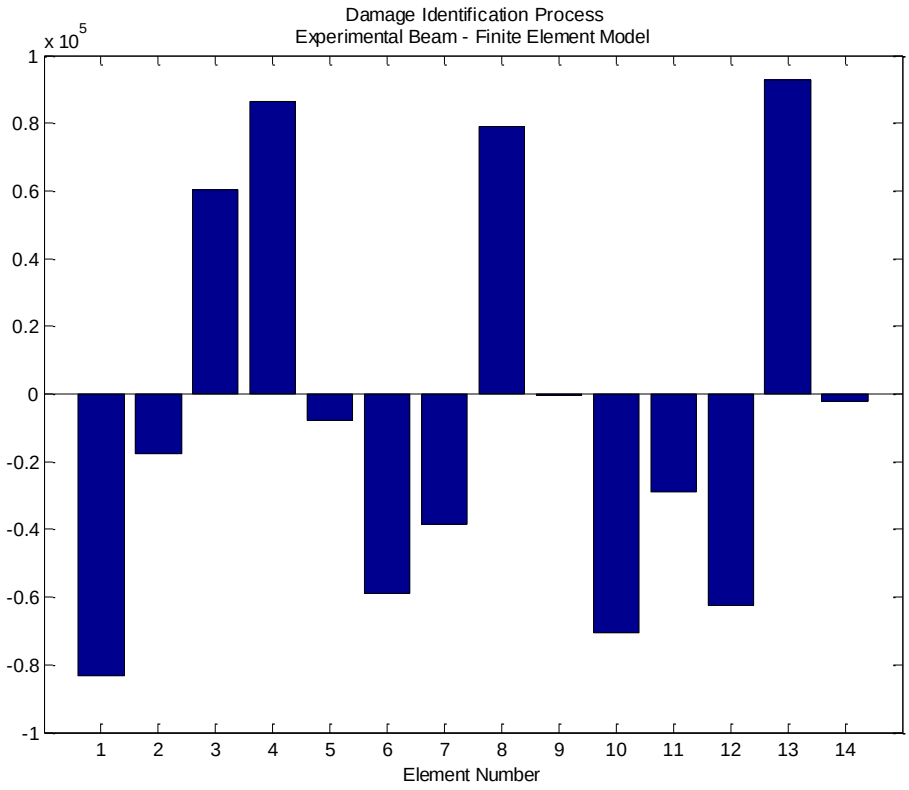

Figure 58. Damage Identification Process, Experimental Beam—Finite Element Model.

The results shown in Figure 58 actually represent the change of the stiffness value (EI), which has to be applied at each element in order for the natural frequencies of the finite element model to match the natural frequencies of the beam. Thus, by applying those changes, we would expect the finite element model to more accurately represent the real structure. Next, this investigation is performed.

B. MODEL UPDATE USING THE ACTUAL VALUES OF STIFFNESS

After applying these changes at the finite element model, the evaluation of its natural frequencies is conducted again, as Figure 59 shows.

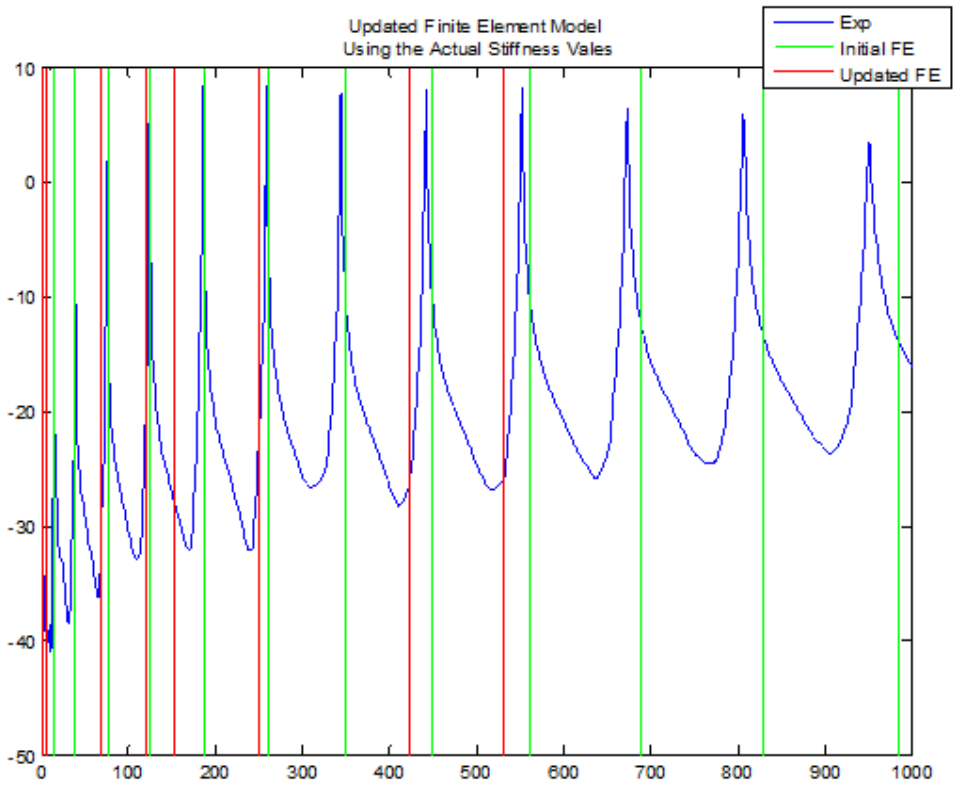

Figure 59. Resonant Frequencies of Updated Finite Element Model, Using the Actual Values of Stiffness.

In Figure 59, the blue curve is the FRF of the experimental beam, the green lines are the estimated natural frequencies of the initial finite element model, and the red lines are the natural frequencies of the updated finite element model. The expectation was that the red lines would match the peaks of the FRF curve. Not only is that not the case, but the updated model is even worse than the initial one.

Going back to Figure 58, we observe that the changes that have to be applied to the finite element model are not logical. The stiffness value of the beam (EI) is 232.34 $N*m^2$ (80961 $lbm*in^2$). The changes that have to be applied at most of the elements are of the same order of magnitude. Imagining that these changes are applied to a uniform beam, we can conclude that the updated structure will not be a uniform beam anymore. In other words, physically realistic updating changes made to the beam should preserve its uniformity.

C. MODEL UPDATE USING THE MEAN VALUE OF STIFFNESS

Instead, a more reasonable approach seems to be the use of the mean value of the stiffness changes, which has to be applied at each element. That idea is demonstrated using the three different composite sensitivity matrices.

1. Model Update Using the Composite Sensitivity Matrix $[S_H]$

The mean value is shown in Figure 60 with a green line, and its value is –10.57 N*m^2 (3686 lbm*in^2). This change is applied at each element. Thus, a constant value across the finite element model is added (or subtracted). The resulting structure will still be a uniform beam, with smaller stiffness value in this case, because the mean value is negative.

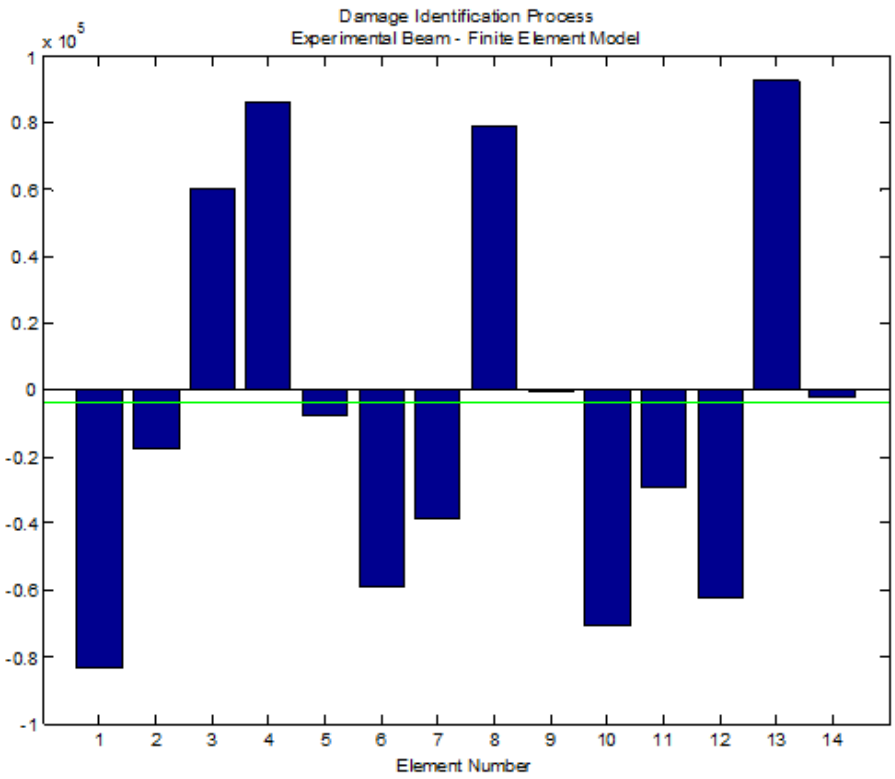

The green horizontal line is the mean value of the stiffness changes of each element.

Figure 60. Mean Value of Stiffness Changes Using $[S_H]$.

The natural frequencies of the updated finite element model are shown in Figure 61.

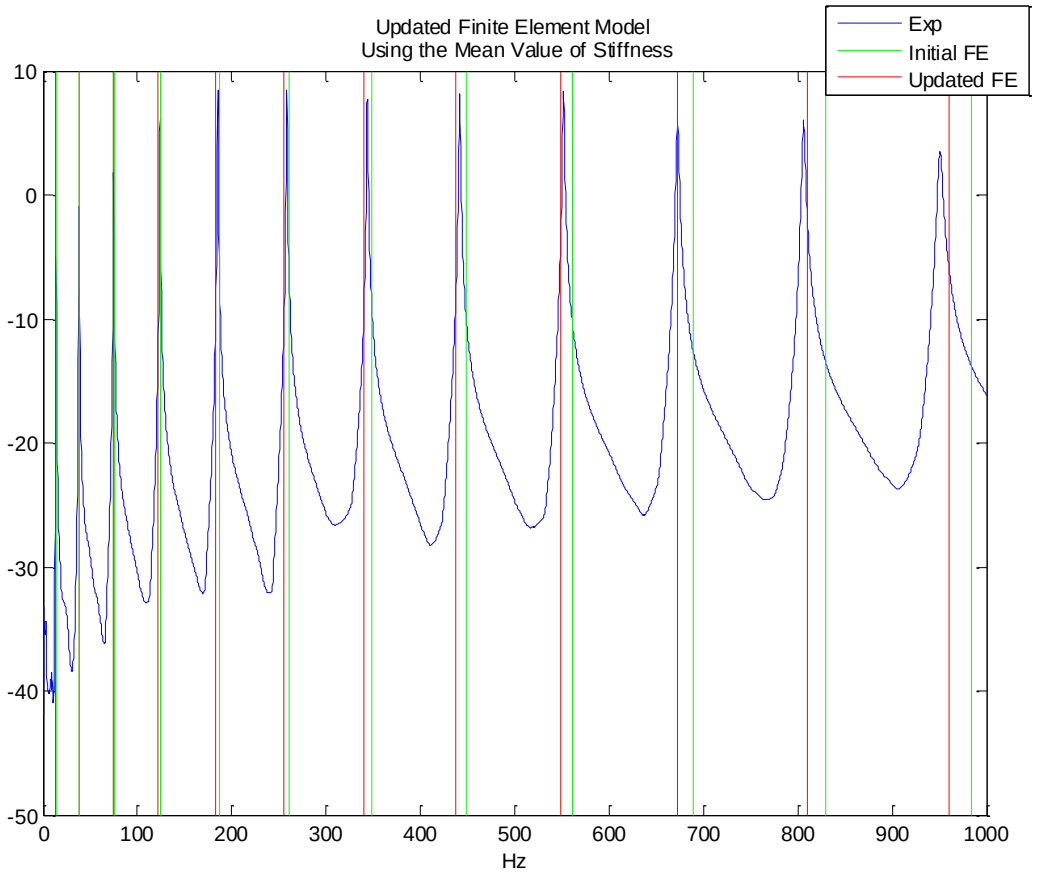

Figure 61. Resonant Frequencies of the Updated Finite Element Model, Using the Mean Value of Stiffness and $[S_H]$.

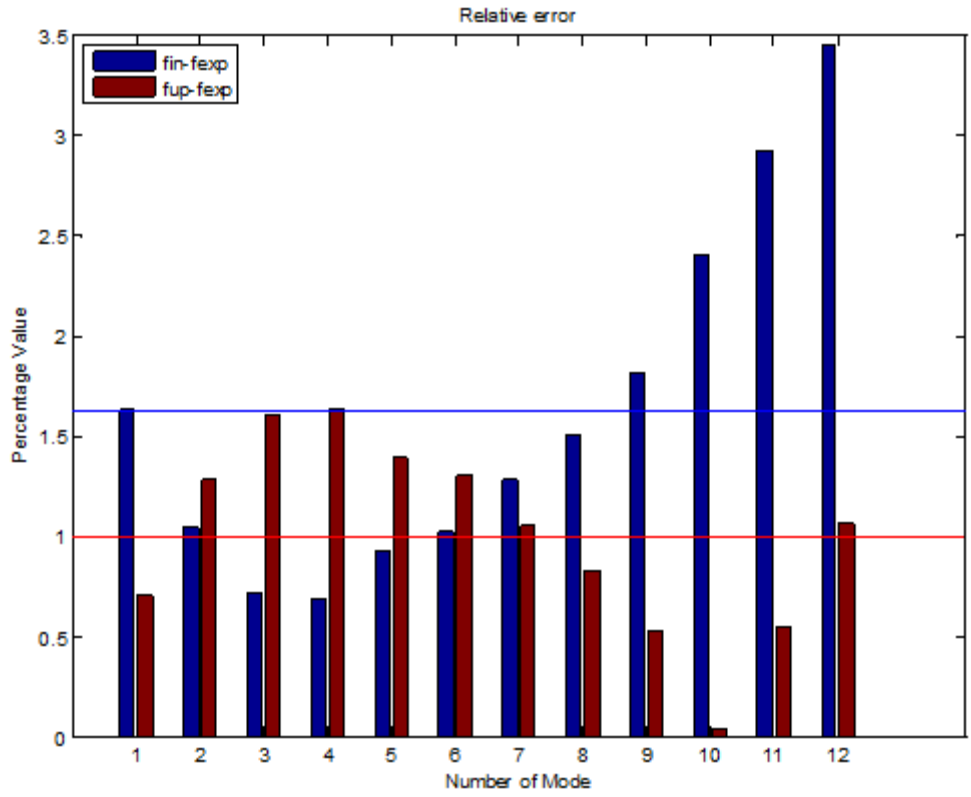

The red horizontal line is the mean value of the error between the updated finite element model and the experimental natural frequencies. The blue horizontal line is the mean value of the error between the initial finite element model and the experimental natural frequencies.

Figure 62. Relative Errors Between Experimental, Initial FE, Updated FE Natural Frequencies.

In Figure 62, the blue columns represent the relative error between the estimated natural frequencies of the initial FE model and the measured natural frequencies. The red columns represent the relative error between the estimated natural frequencies of the updated FE model and the measured natural frequencies. The horizontal lines are the mean value of the error for each case. It is obvious that the updated model better represents the real beam. Moreover, the accuracy of the higher modes, which are better to use based on the analysis so far, has been greatly improved.

Yet the estimated natural frequencies are not an exact match with the experimental data. Thus, using Equation (3.1) again causes new values of

stiffness changes for each element to arise. Again, the expectation is that the mean value will be used to further update the model. However, this time the mean value is close to zero, as shown in Figure 63; thus, the model cannot be updated further using this procedure. The remaining stiffness values are called residual stiffness errors.

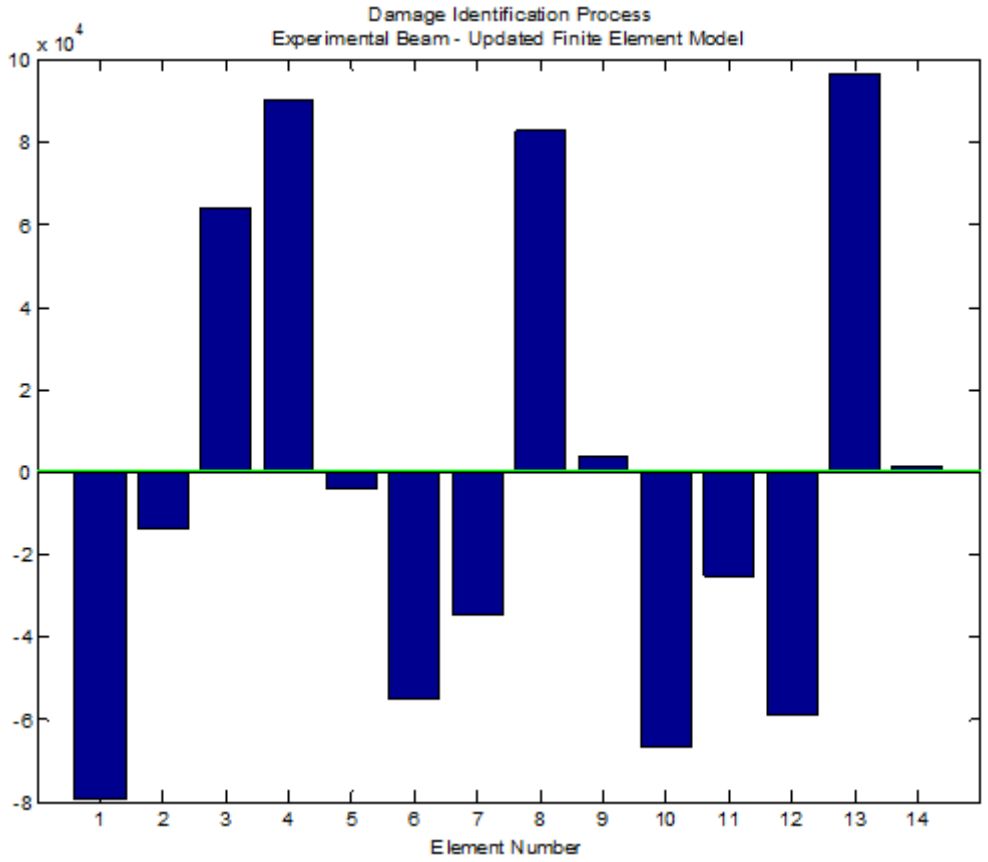

Figure 63. Mean Value of Stiffness Changes After the First Update.

2. Model Update Using the Composite Sensitivity Matrix $[S_L]$

The update of the finite element model using the composite sensitivity matrix $[S_H]$, which was created using higher modes, has been successfully performed. Next, the ability of the composite sensitivity matrix $[S_L]$, which was created using lower modes, to update the finite element model is investigated.

The results of the solution of Equation (3.1) by using the sensitivity matrix $[S_L]$ are presented in Figure 64. The mean value of the stiffness changes that must be applied at each element is -4563 N*m^2 (1.59*10^6 lbm*in^2). The stiffness value of the beam is 232.34 N*m^2 (80961 lbm*in^2). Thus, this mean value cannot be applied in order to update the finite element model. Consequently, the composite sensitivity matrix created by lower modes, $[S_L]$, cannot be used for updating purposes. For demonstration purposes only, the finite element model has been updated using the incorrect mean value, and the results are provided in Figure 65.

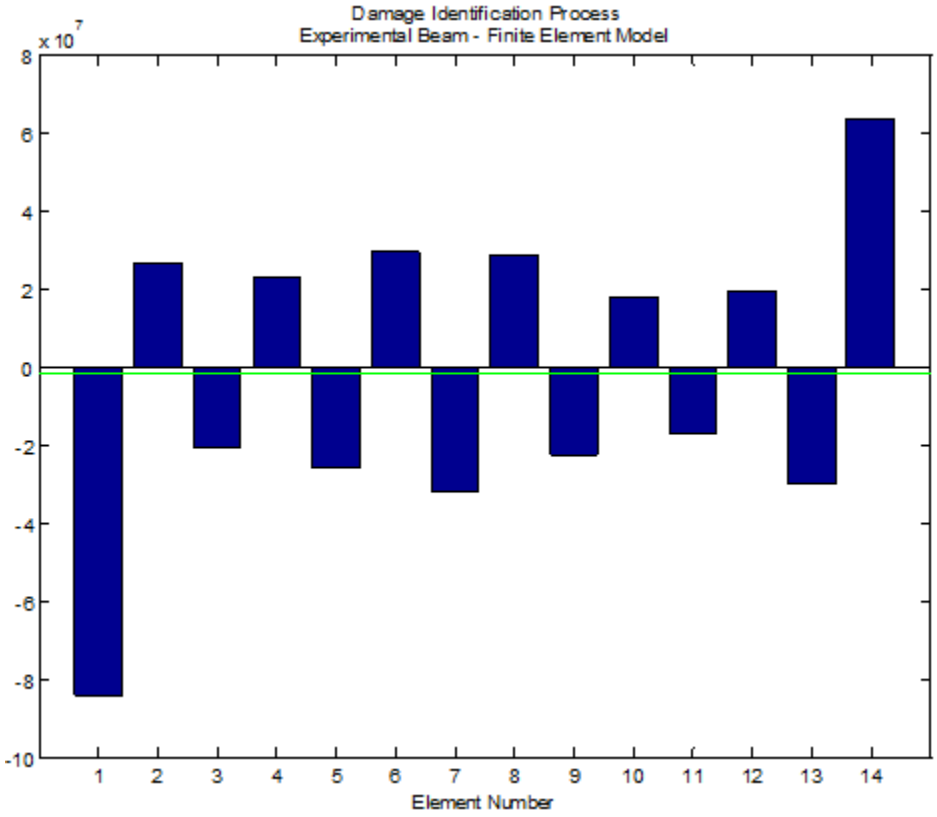

Figure 64. Mean Value of Stiffness Changes Using $[S_L]$ Sensitivity Matrix.

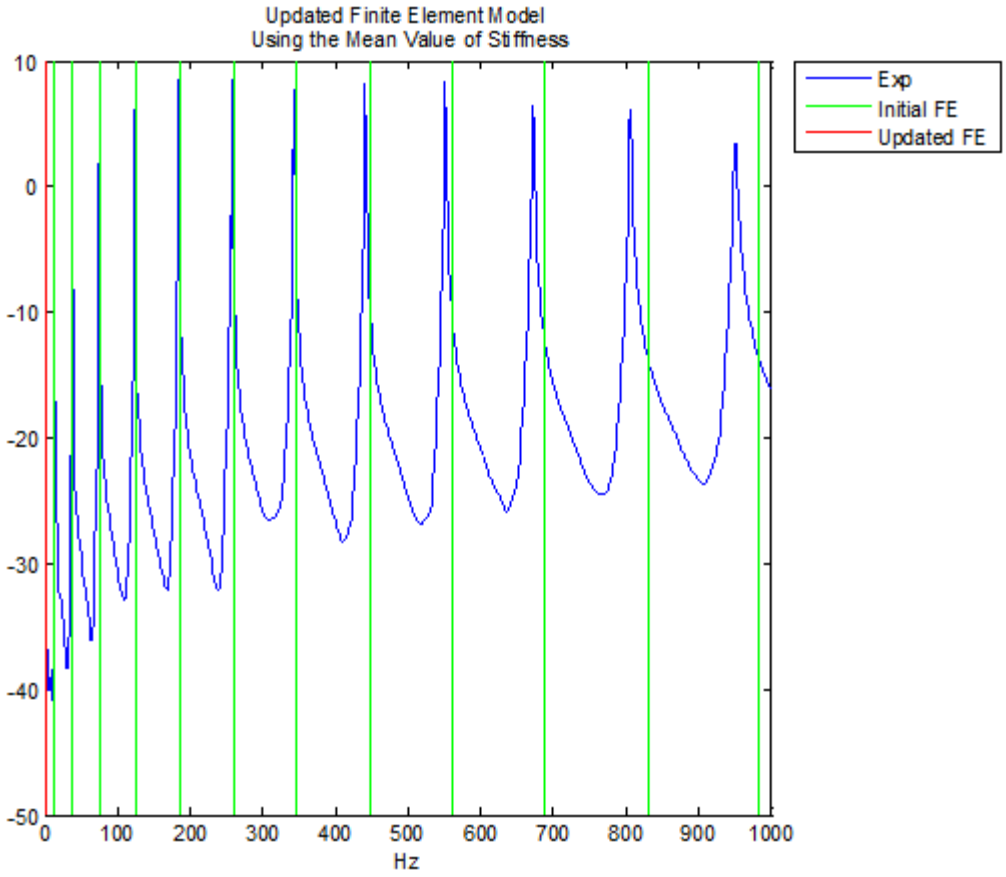

Figure 65. Resonant Frequencies of the Updated Finite Element Model, Using the Mean Value of Stiffness and $[S_L]$ Sensitivity Matrix.

It is obvious from Figure 65 that all the resonant frequencies of the updated finite element model are zeros since there is no beam. Thus, a sensitivity matrix created by lower modes is not able to update the model.

3. Model Update Using the Composite Sensitivity Matrix $[S_G]$

Finally, the composite sensitivity matrix $[S_G]$, which was created by mixed ABC sets and modes, is used to update the finite element model. Again, using the composite sensitivity matrix $[S_G]$ and solving Equation (3.1), we get the changes of stiffness at each element as shown in Figure 66. The mean value of stiffness changes this time is 1256.98 N*m^2 (4.38*10^5 lbm*in^2). It is a positive value; however, the order of magnitude compared to the stiffness of the beam is

higher. Again, it does not seem reasonable to add this value in order to update the finite element model. The resonant frequencies of the updated finite element model, using the composite sensitivity matrix $[S_G]$, are provided in Figure 67.

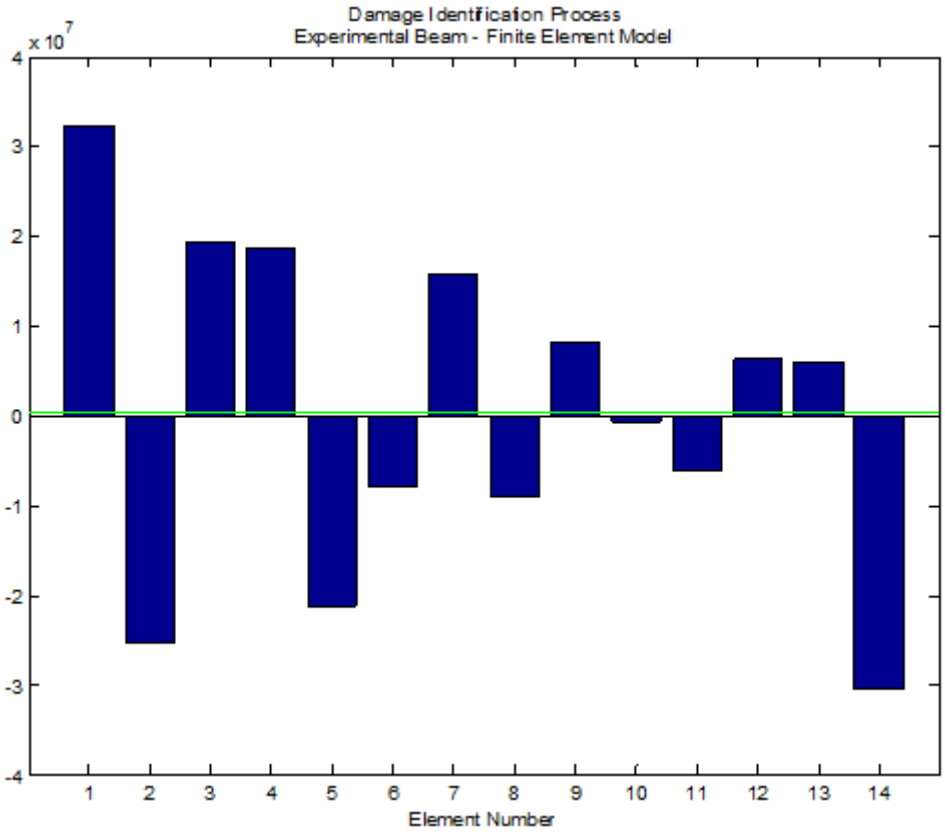

Figure 66. Mean Value of Stiffness Changes Using $[S_G]$ Sensitivity Matrix.

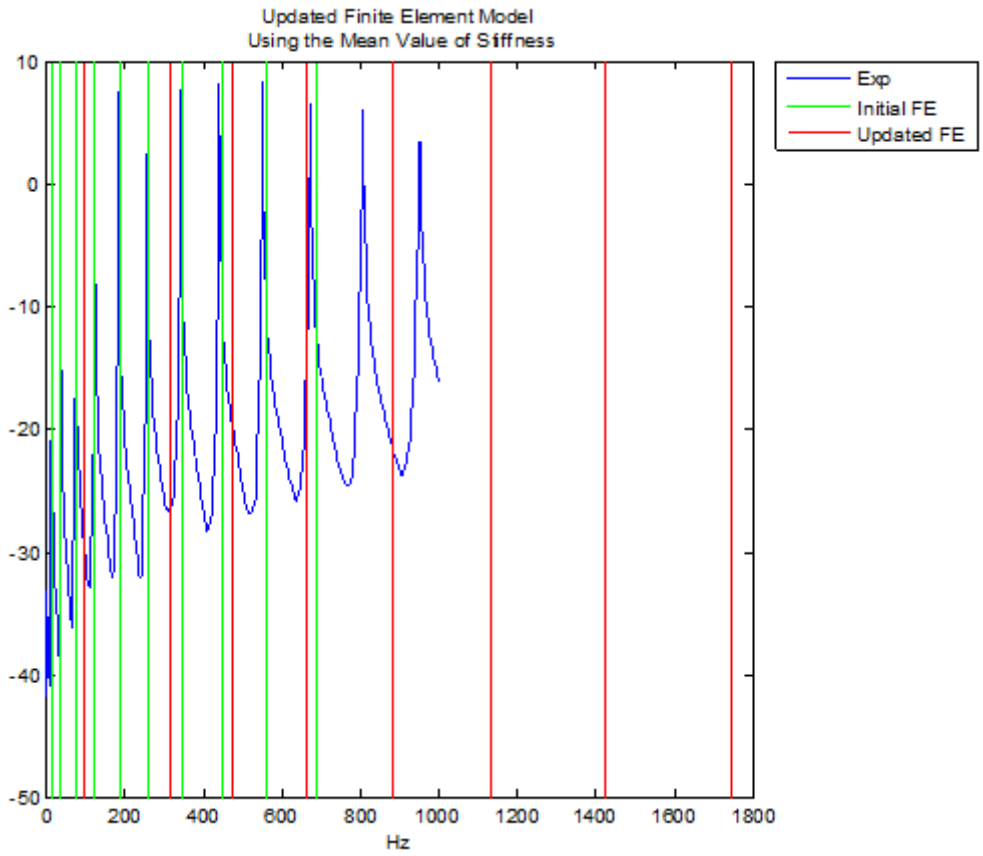

Figure 67. Resonant Frequencies of the Updated Finite Element Model, Using the Mean Value of Stiffness and $[S_G]$ Sensitivity Matrix.

The resonant frequencies of the updated finite element model are not even close to the measured natural frequencies of the beam due to the large value of the mean stiffness, which was added at each element. Thus, the composite sensitivity matrix $[S_G]$ cannot be used to update the finite element model.

For the rest research the finite element model updated using the composite sensitivity matrix created by higher modes, $[S_H]$, is used.

D. CONCLUDING REMARKS

In this chapter the finite element model update was performed. It was demonstrated that when the actual value of stiffness changes is applied at each

element, the model update process fails. A new concept for model update was introduced, in which the mean value of stiffness changes is applied at every element.

The update process has been successfully performed using a composite sensitivity matrix made by higher modes. The use of other sensitivity matrices made from lower modes or mixed modes could not update the finite element model. It is worth mentioning that the sensitivity matrix $[S_G]$ has the best performance in damage identification using simulated data, as shown in Chapter III; however, it cannot be used for updating purposes.

Even if the finite element model was updated, the estimated natural frequencies still would not exactly correspond with the measured natural frequencies. The error of the higher natural frequencies between the FE model and the experimental data has been significantly decreased. However, after the update of the finite element model, because of the mismatch of the natural frequencies, we still find some changes of stiffness value at each element using Equation (3.1) again. These values are called residual stiffness errors. In this research, the model cannot be updated further using the mean stiffness value technique.

Using the mean stiffness to update the finite element model, we find the sensitivity matrices of the different ABC sets remain the same. Therefore, there is no need to recalculate a sensitivity matrix for future purposes if its calculation has already been done. That decreases the required computational time.

V. DAMAGE IDENTIFICATION PROCESS

A. INTRODUCTION

One purpose of finite element model updating is to provide a baseline finite element model with which to conduct health monitoring of a real structure in the future. By measuring the dynamic behavior of the structure in the future and comparing the results with the updated finite element model, we can identify and locate potential damage on the structure. This is the main reason that a finite element model has to represent as accurately as possible the real structure.

To measure the dynamic behavior of the structure in the future, a vibration experiment must be conducted again. If the dynamic characteristics are the same as in the initial one, then the structure is intact. If there are some mismatches at any dynamic characteristic (for example at the natural frequencies) that means the structure might have been damaged.

B. DAMAGE IDENTIFICATION

From the analysis of the previous chapter, it is known that the updated finite element model does not have the same exact dynamic behavior as the structure. Thus, using Equation (3.1) results in some residual stiffness errors, $\{\Delta EI_{RES}\}$.

The damage identification process is conducted using Equation (3.1), $\{\Delta EI\} = [S] \backslash \{\Delta\omega^2\}$, which in this case has the form:

$$\{\Delta EI_{RES}\} = [S_H] \backslash \{\omega^2{}_{\exp} - \omega^2_{upd}\}, \tag{5.1}$$

where $\omega^2{}_{\exp}$ are the experimental natural frequencies of the structure, ω^2_{upd} are the calculated natural frequencies of the finite element model, $[S_H]$ is the composite sensitivity matrix created using the higher modes, and $\{\Delta EI_{RES}\}$ is the

vector with the residual stiffness errors. Since the update of the finite element model has been conducted, any composite sensitivity matrix can be used for the damage identification process. As will be explained later in this research, due to the way that the finite element model has been updated (using the mean stiffness value), the sensitivity matrices do not change.

In actuality, the beam would be damaged, but for practical reasons, the real beam was not damaged in this case. For the purposes of this research, we introduced damage to the updated FEM to simulate damage on the beam.

Then, the composite sensitivity matrix of the updated finite element model has to be calculated again. However, because at each element the same amount of stiffness changes (mean value) was applied, any sensitivity matrix remains the same. Thus, there is no need to recalculate any sensitivity matrix that has already been calculated. In this case, the composite sensitivity matrix $\left[\mathrm{S}_H\right]$ is used again. The damage is simulated by decreasing the stiffness value of the corresponding element. Initially, a 0.1 percent decrease of stiffness is applied at the fifth element. This time Equation (3.1) has the form:

$$\left\{\Delta EI_1\right\} = [S_H] \backslash \left\{\omega^2{}_{\exp} - \omega^2_{upd\_Dam}\right\}, \tag{5.2}$$

where $\omega^2_{upd\_Dam}$ are the calculated natural frequencies of the damaged updated finite element model. The results of the damage identification process, i.e., vector $\left\{\Delta EI_1\right\}$, are provided in Figure 68.

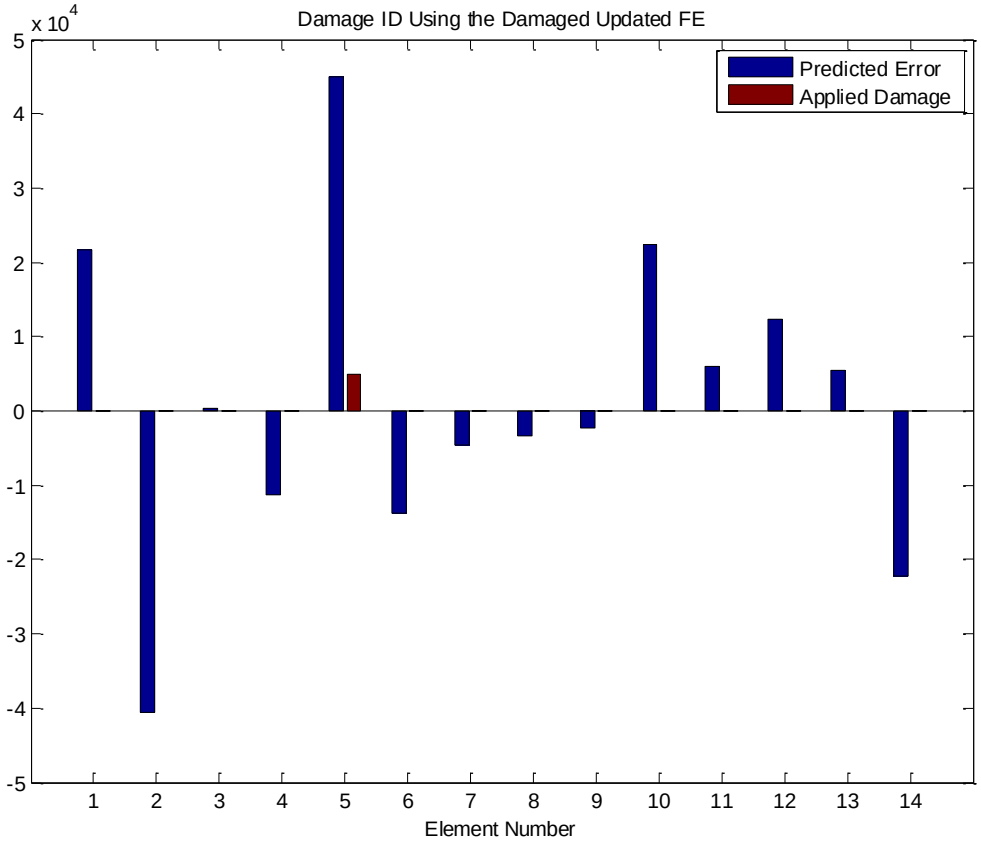

Figure 68. Damage Identification Process, Using the Damaged Updated FE Model.

It is obvious that the damage identification process cannot identify the damaged element. The same case applies for each element.

C. DAMAGE IDENTIFICATION USING COMPARISON

It was shown that using the updated model, the damage identification process cannot be conducted. To overcome this problem, a new idea is introduced: the comparison of stiffness values. This method is investigated using all the composite sensitivity matrices.

1. Comparison of Stiffness Values Using the Composite Sensitivity Matrix $[S_H]$

Writing again Equations (5.1) and (5.2) results in:

$$\left\{\omega^2_{\exp} - \omega^2_{upd}\right\} = [S_H]\left\{\Delta EI_{RES}\right\}, \tag{5.1}$$

$$\left\{\omega^2_{\exp} - \omega^2_{upd\_Dam}\right\} = [S_H]\left\{\Delta EI_1\right\}. \tag{5.2}$$

By subtracting Equations 5.1 and 5.2 yields:

$$\left\{\omega^2_{upd} - \omega^2_{upd\_Dam}\right\} = [S_H]\left\{\Delta EI_1 - \Delta EI_{RES}\right\}. \tag{5.3}$$

Solving for the stiffness value results in:

$$\left\{\Delta EI_1 - \Delta EI_{RES}\right\} = [S_H] \setminus \left\{\omega^2_{upd} - \omega^2_{upd\_Dam}\right\}. \tag{5.4}$$

This is actually a comparison of the initial results from the damage identification process (residual stiffness) and the results from the damage identification process of the damaged updated finite element model. Therefore, Equation (5.4) is actually used to perform damage identification. The investigation of the damage identification process is then conducted by applying 0.1 percent decrease of stiffness recursively at each element of the updated finite element model. The results of the damage identification process using comparison are provided in Figures 69–82.

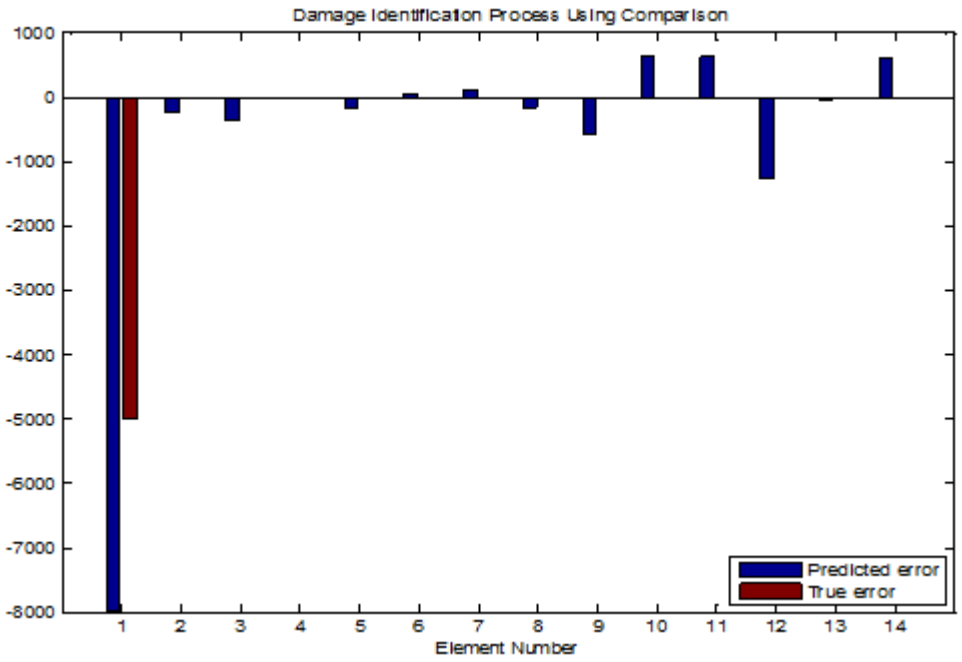

Figure 69. Damage Identification Using Comparison and the Sensitivity Matrix $[S_H]$, Applying 0.1% Damage at Element Number 1.

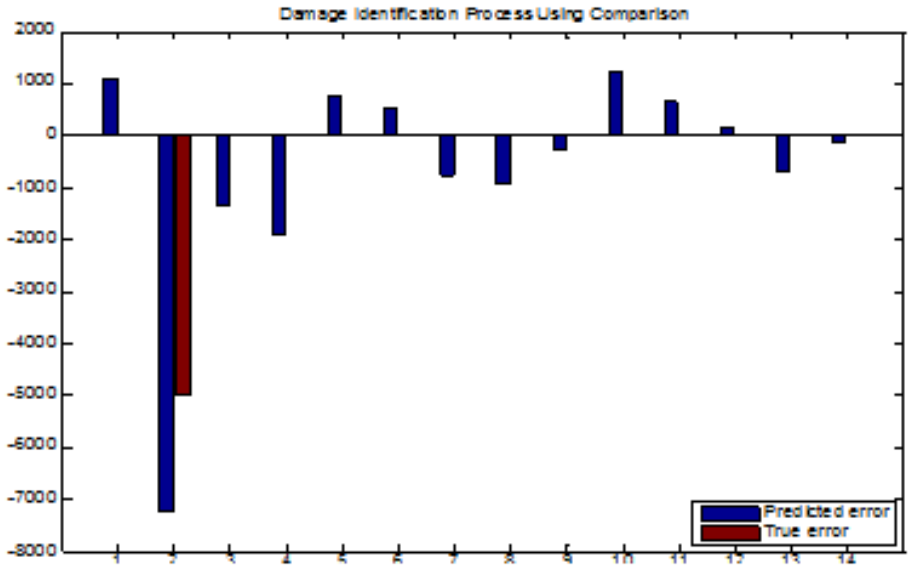

Figure 70. Damage Identification Using Comparison and the Sensitivity Matrix $[S_H]$, Applying 0.1% Damage at Element Number 2.

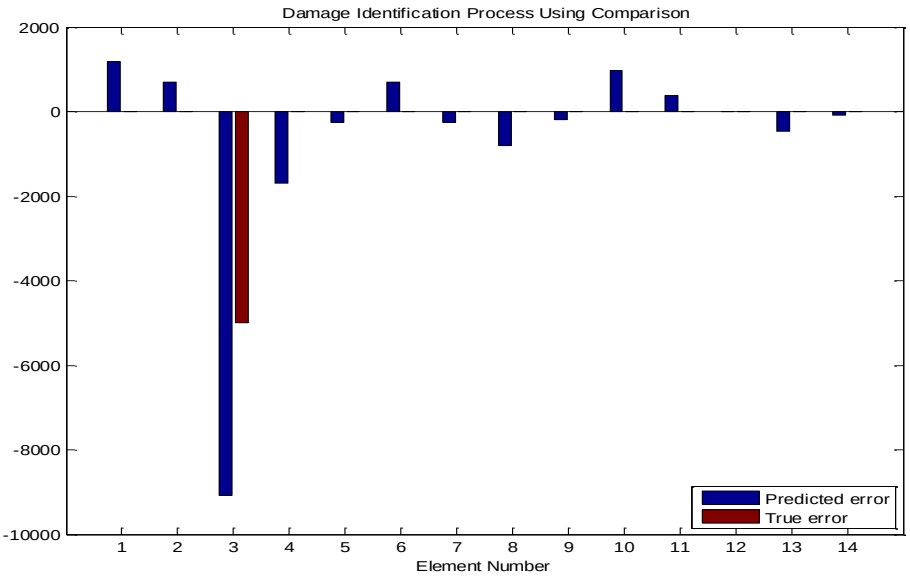

Figure 71. Damage Identification Using Comparison and the Sensitivity Matrix $[S_H]$, Applying 0.1% Damage at Element Number 3.

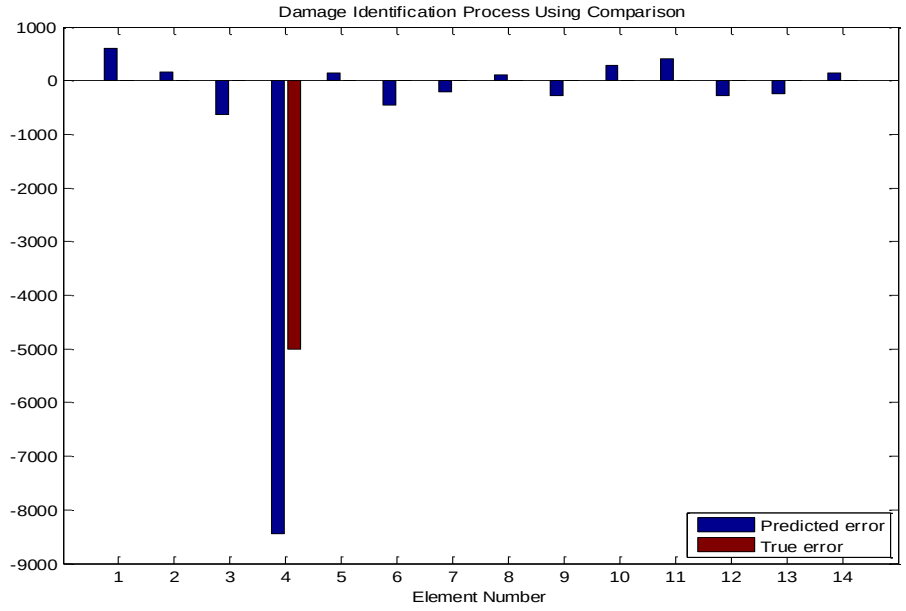

Figure 72. Damage Identification Using Comparison and the Sensitivity Matrix $[S_H]$, Applying 0.1% Damage at Element Number 4.

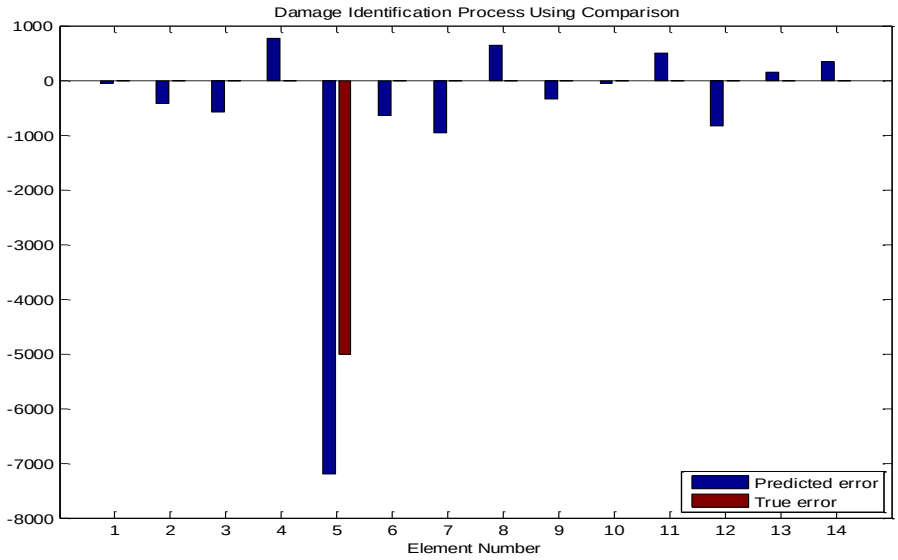

Figure 73. Damage Identification Using Comparison and the Sensitivity Matrix $[S_H]$, Applying 0.1% Damage at Element Number 5.

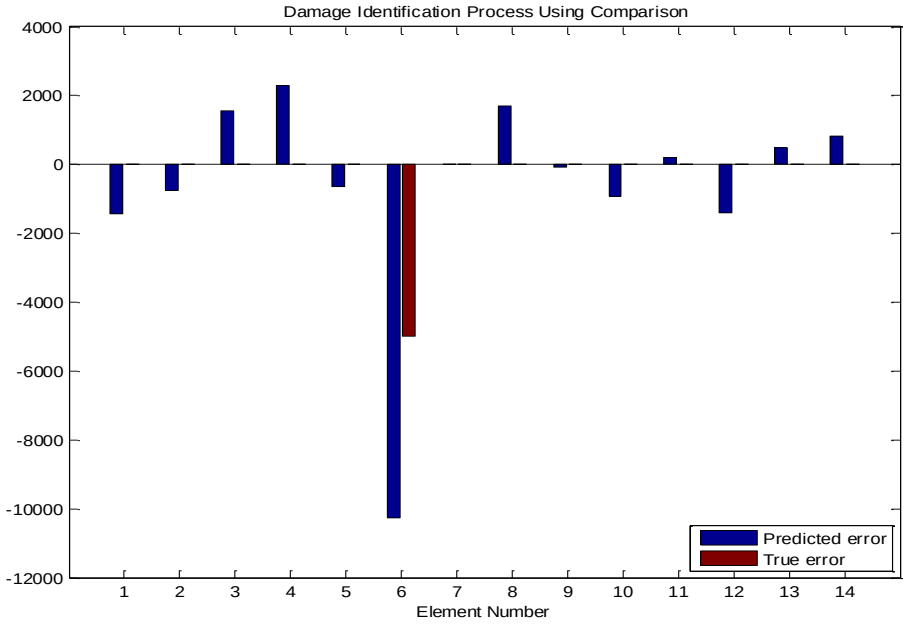

Figure 74. Damage Identification Using Comparison and the Sensitivity Matrix $[S_H]$, Applying 0.1% Damage at Element Number 6.

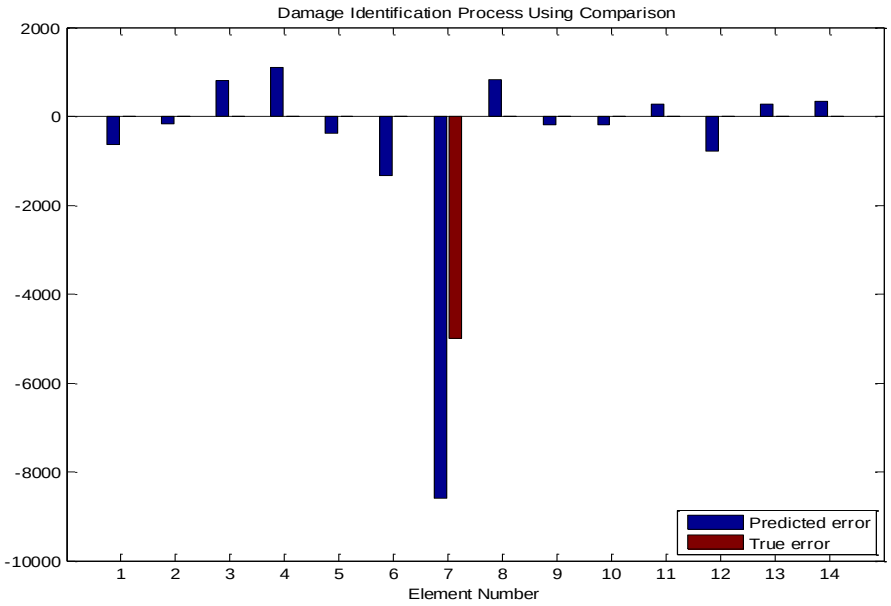

Figure 75. Damage Identification Using Comparison and the Sensitivity Matrix $[S_H]$, Applying 0.1% Damage at Element Number 7.

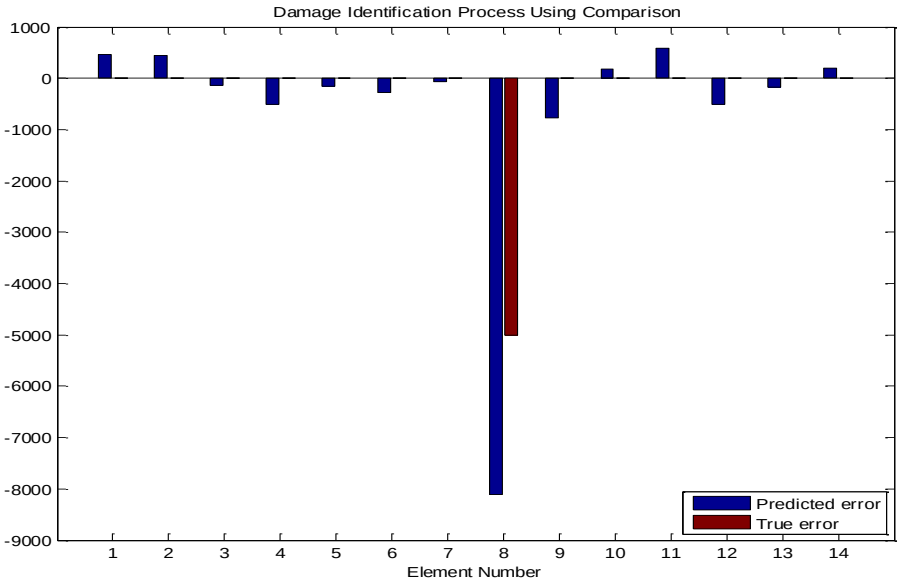

Figure 76. Damage Identification Using Comparison and the Sensitivity Matrix $[S_H]$, Applying 0.1% Damage at Element Number 8.

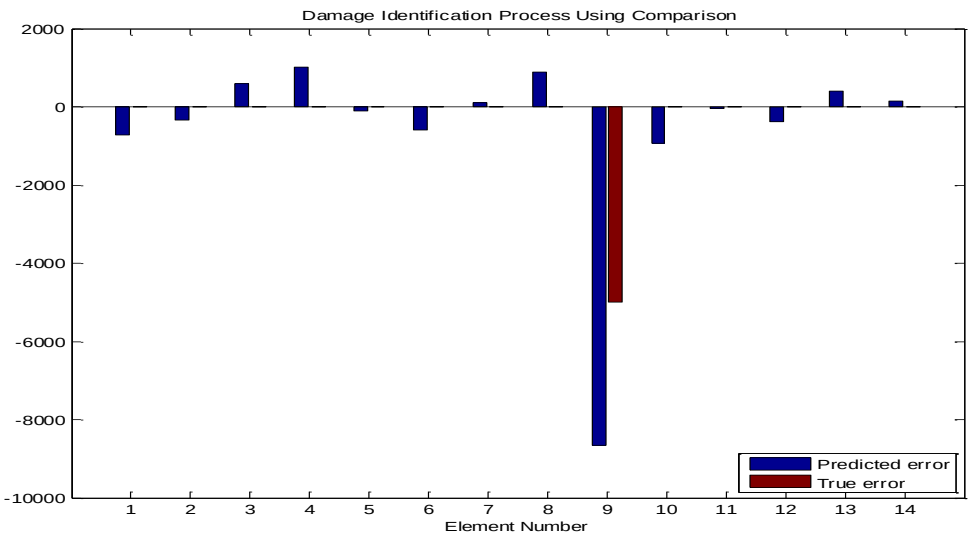

Figure 77. Damage Identification Using Comparison and the Sensitivity Matrix $[S_H]$, Applying 0.1% Damage at Element Number 9.

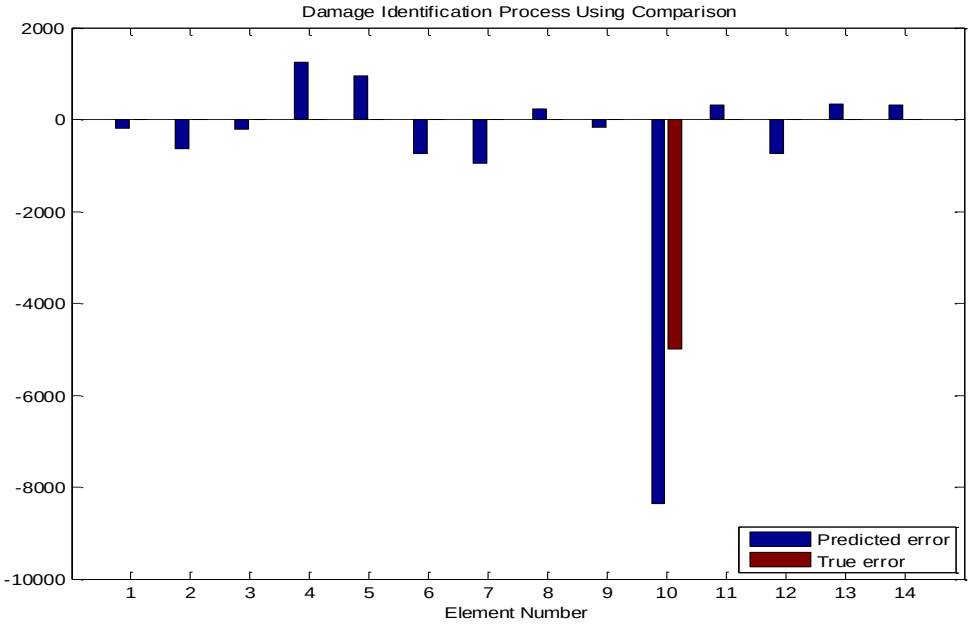

Figure 78. Damage Identification Using Comparison and the Sensitivity Matrix $[S_H]$, Applying 0.1% Damage at Element Number 10.

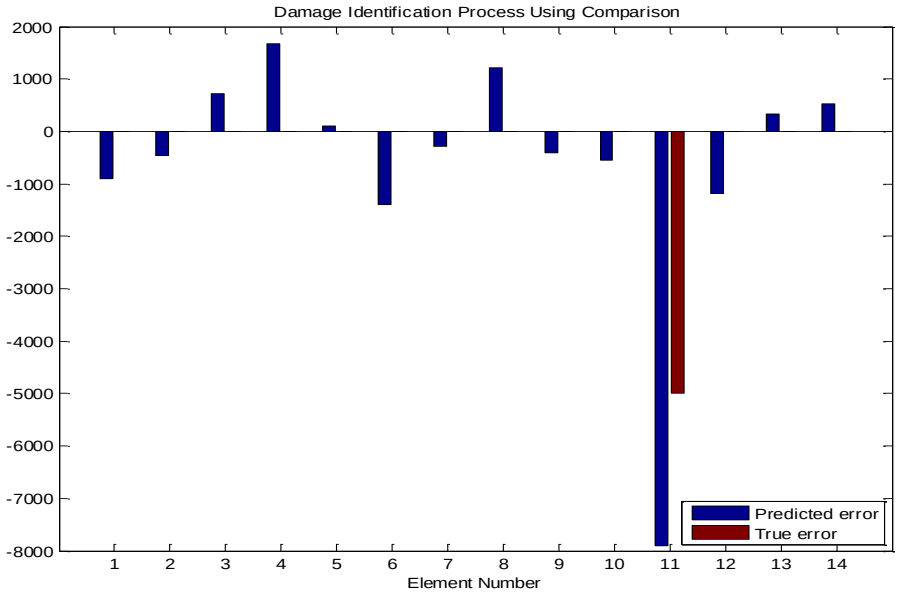

Figure 79. Damage Identification Using Comparison and the Sensitivity Matrix $[S_H]$, Applying 0.1% Damage at Element Number 11.

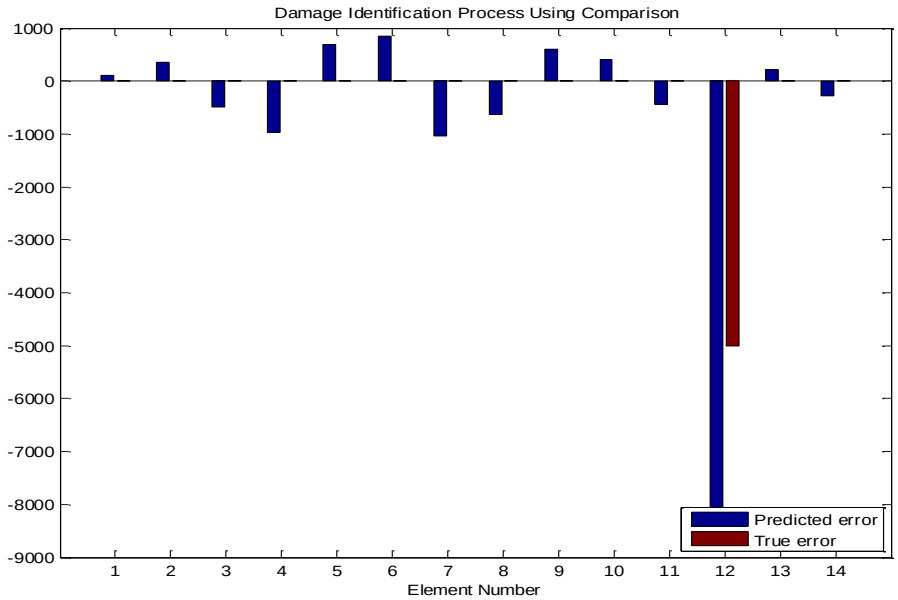

Figure 80. Damage Identification Using Comparison and the Sensitivity Matrix $[S_H]$, Applying 0.1% Damage at Element Number 12.

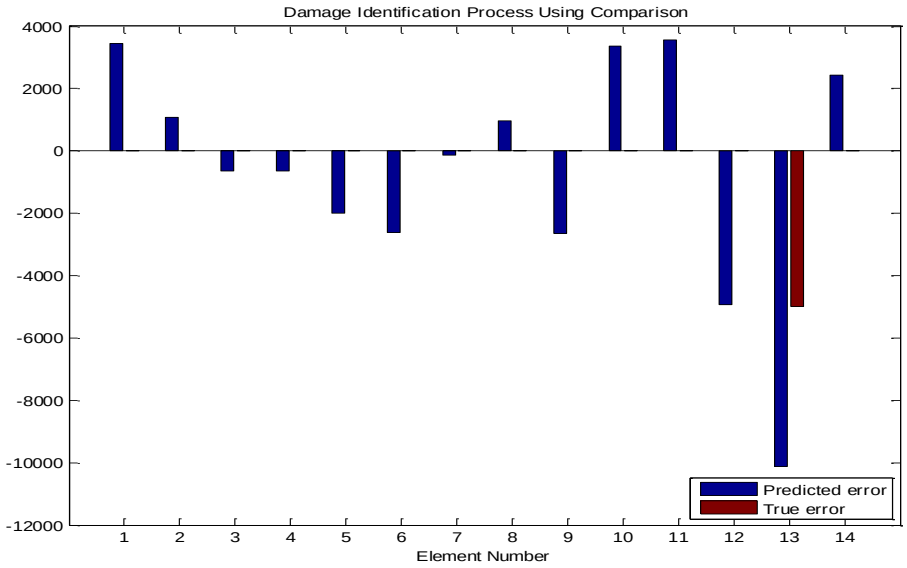

Figure 81. Damage Identification Using Comparison and the Sensitivity Matrix $[S_H]$, Applying 0.1% Damage at Element Number 13.

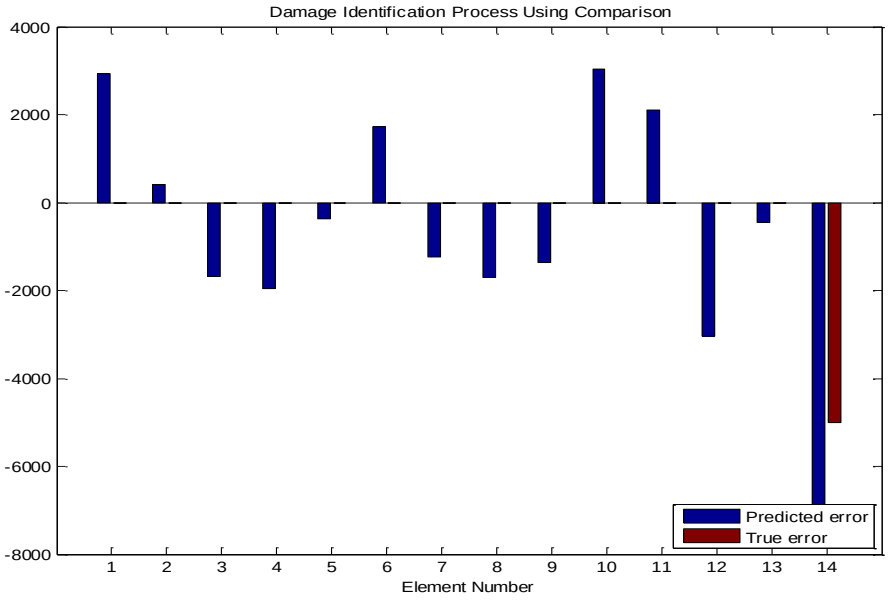

Figure 82. Damage Identification Using Comparison and the Sensitivity Matrix $[S_H]$, Applying 0.1% Damage at Element Number 14.

Generally speaking, the damage identification process can be easily conducted at elements 1–12; although for elements 13 and 14 the damaged element cannot be identified. Thus, by comparing the residual stiffness errors of the updated finite element model and the stiffness values of the updated damaged finite element model, we can identify potential damage at the first 12 elements. In Equation (5.4) the left hand side ($\{\Delta EI_1 - \Delta EI_{RES}\}$), has been created from Equations (5.2) and (5.1), respectively, where experimental data have been used. Because of the experimental data that have been used, there are more discrepancies in the results of the damage identification process when compared to the use of simulated data only. The use of the sensitivity matrix $[S_H]$ cannot identify damage at the last two elements.

2. Comparison of Stiffness Values Using the Composite Sensitivity Matrix $[S_L]$

Next, the use of the sensitivity matrix $[S_L]$ for damage identification by comparison is investigated. Equation (5.4) becomes:

$$\{\Delta EI_2 - \Delta EI_{RES}\} = [S_L] \backslash \{\omega_{upd}^2 - \omega_{upd\_Dam}^2\} . \tag{5.5}$$

Again, the damage is simulated by decreasing the stiffness value of the element. A decrease of 0.1 percent of stiffness is applied recursively at each element. The results of the damage identification by comparison are shown in Figures 83–96.

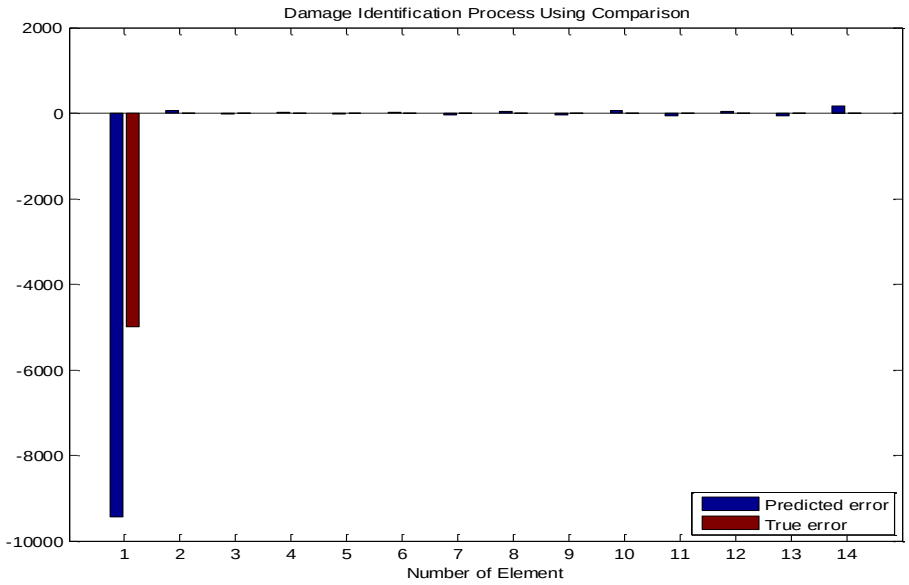

Figure 83. Damage Identification Using Comparison and the Sensitivity Matrix $[S_L]$, Applying 0.1% Damage at Element Number 1.

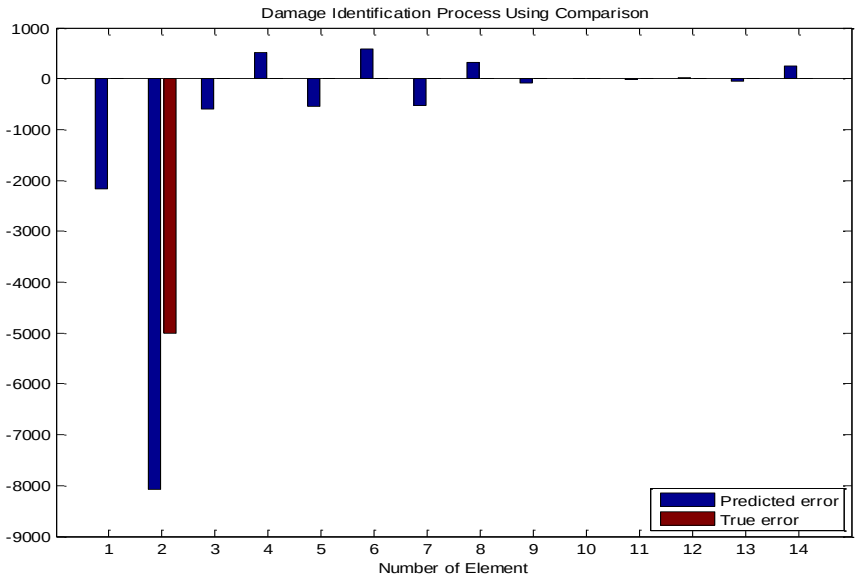

Figure 84. Damage Identification Using Comparison and the Sensitivity Matrix $[S_L]$, Applying 0.1% Damage at Element Number 2.

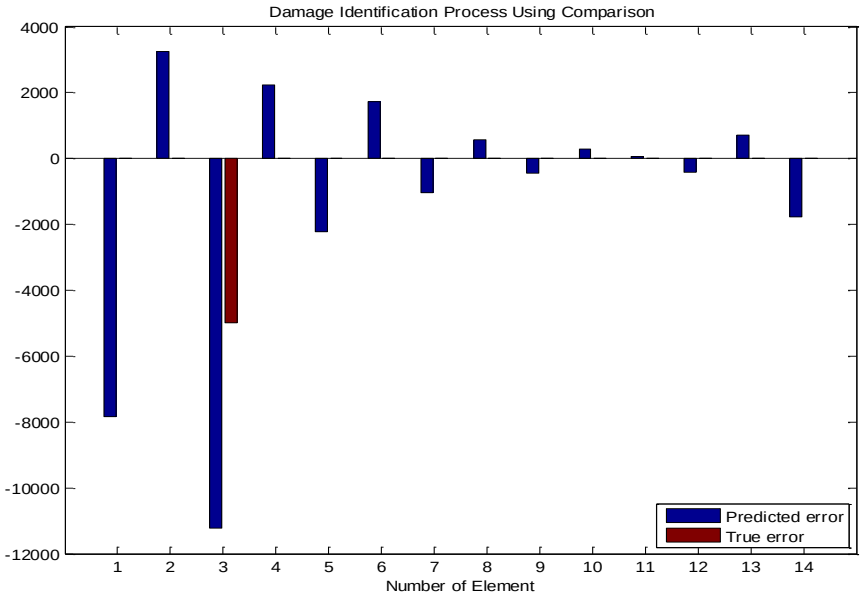

Figure 85. Damage Identification Using Comparison and the Sensitivity Matrix $[S_L]$, Applying 0.1% Damage at Element Number 3.

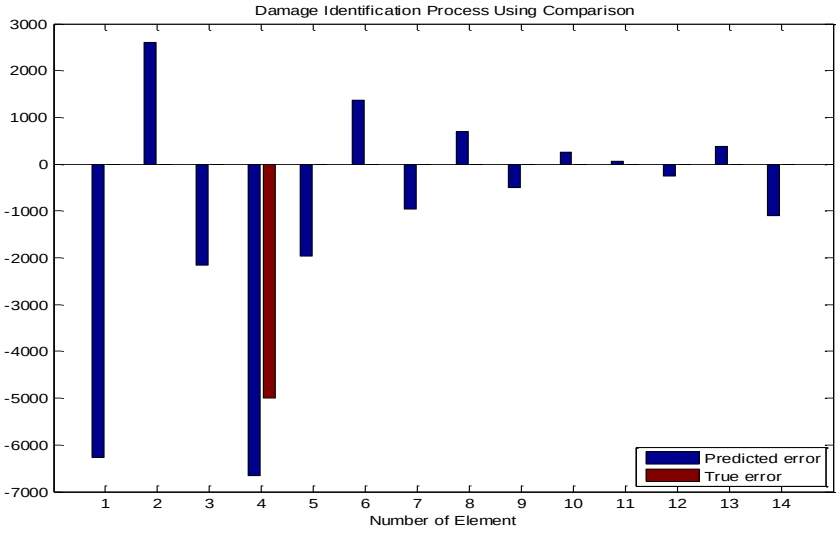

Figure 86. Damage Identification Using Comparison and the Sensitivity Matrix $[S_L]$, Applying 0.1% Damage at Element Number 4.

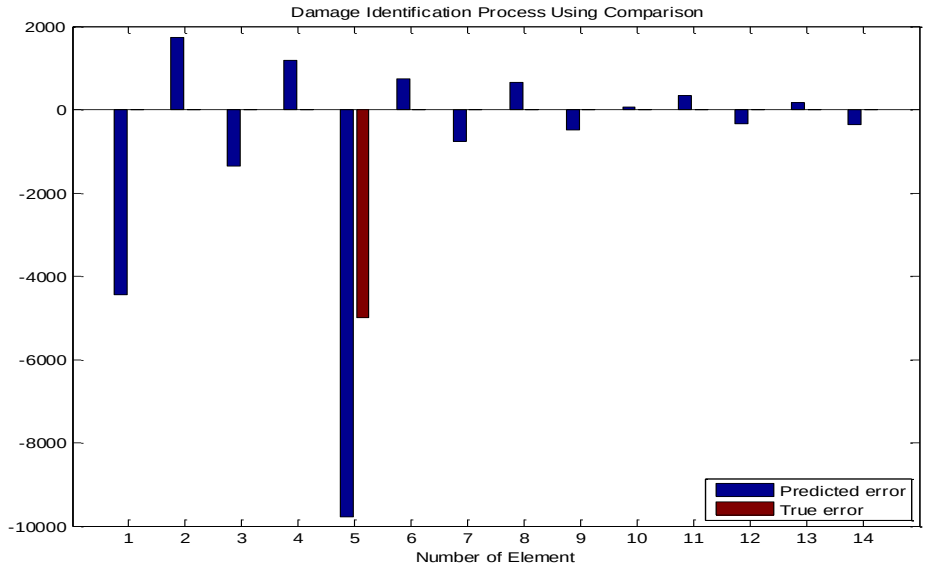

Figure 87. Damage Identification Using Comparison and the Sensitivity Matrix $[S_L]$, Applying 0.1% Damage at Element Number 5.

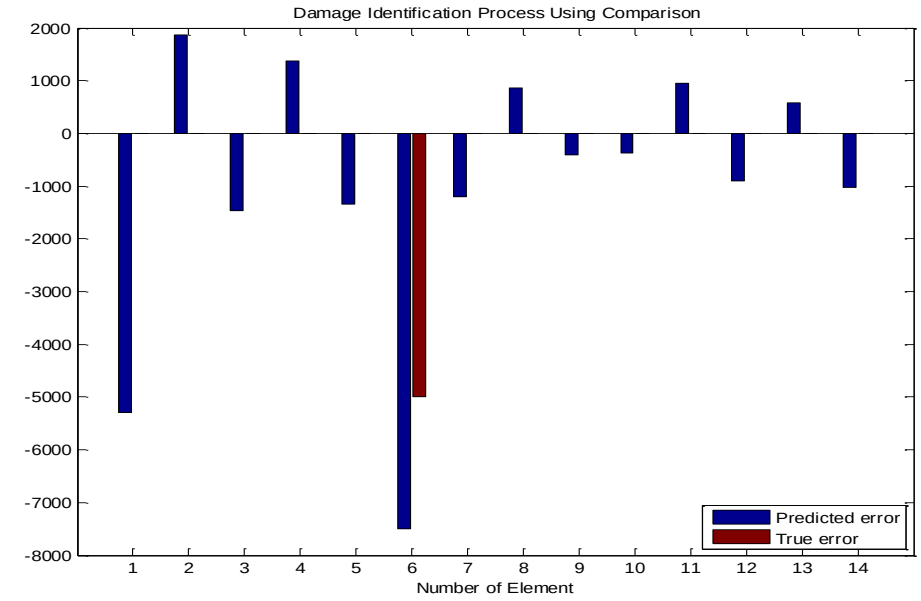

Figure 88. Damage Identification Using Comparison and the Sensitivity Matrix $[S_L]$, Applying 0.1% Damage at Element Number 6.

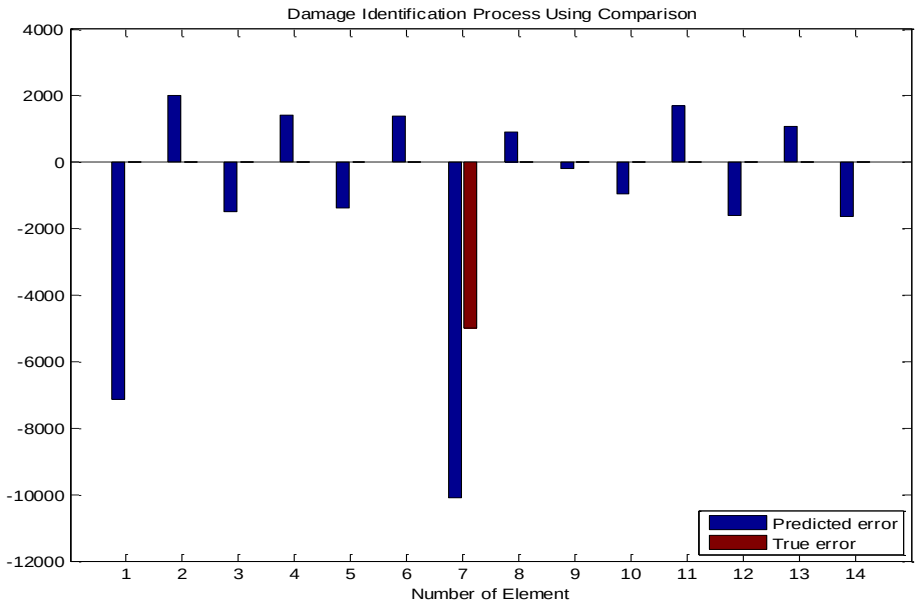

Figure 89. Damage Identification Using Comparison and the Sensitivity Matrix $[S_L]$, Applying 0.1% Damage at Element Number 7.

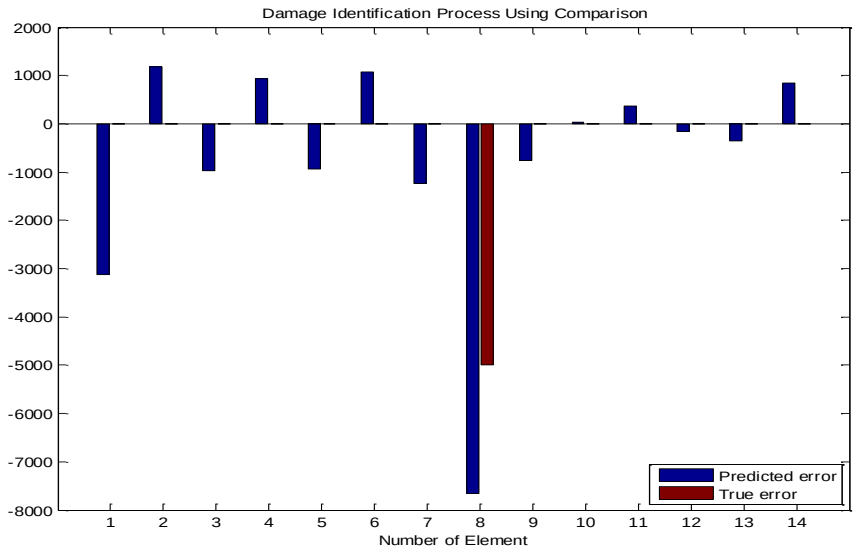

Figure 90. Damage Identification Using Comparison and the Sensitivity Matrix $[S_L]$, Applying 0.1% Damage at Element Number 8.

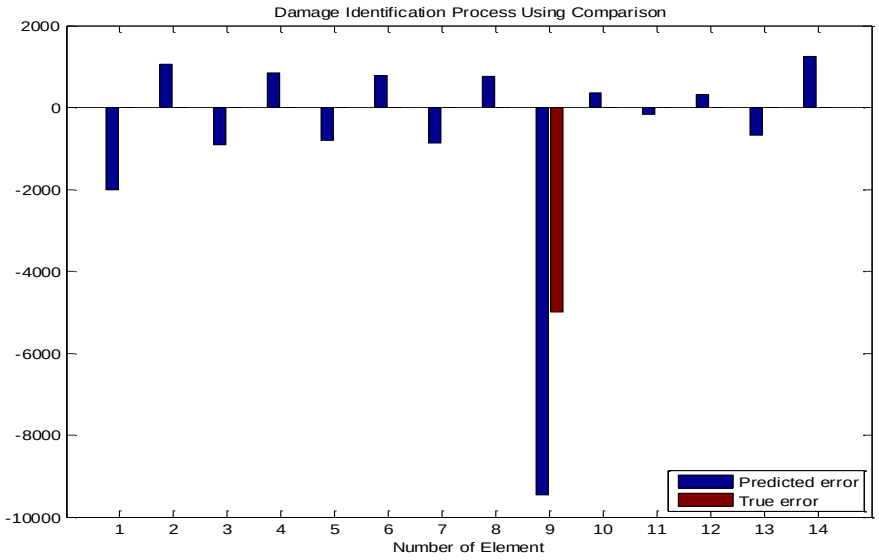

Figure 91. Damage Identification Using Comparison and the Sensitivity Matrix $[S_L]$, Applying 0.1% Damage at Element Number 9.

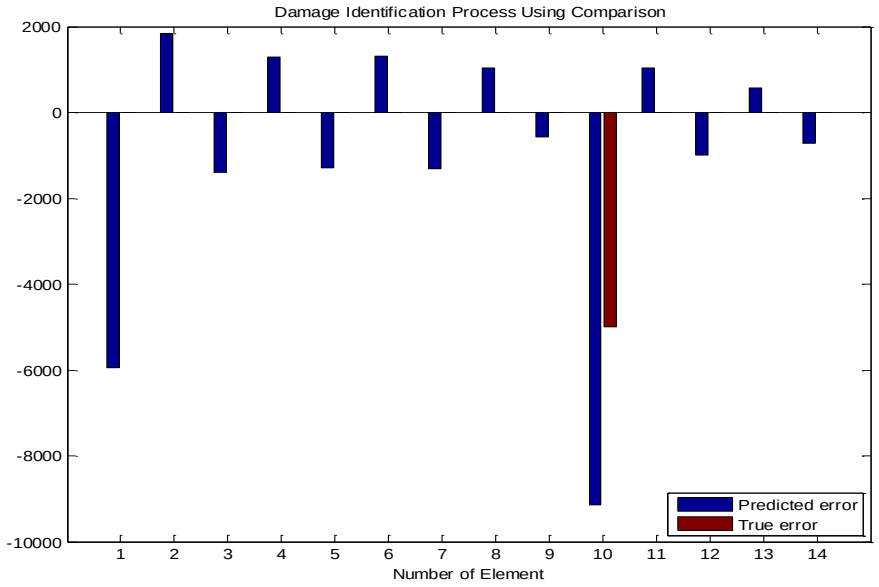

Figure 92. Damage Identification Using Comparison and the Sensitivity Matrix $[S_L]$, Applying 0.1% Damage at Element Number 10.

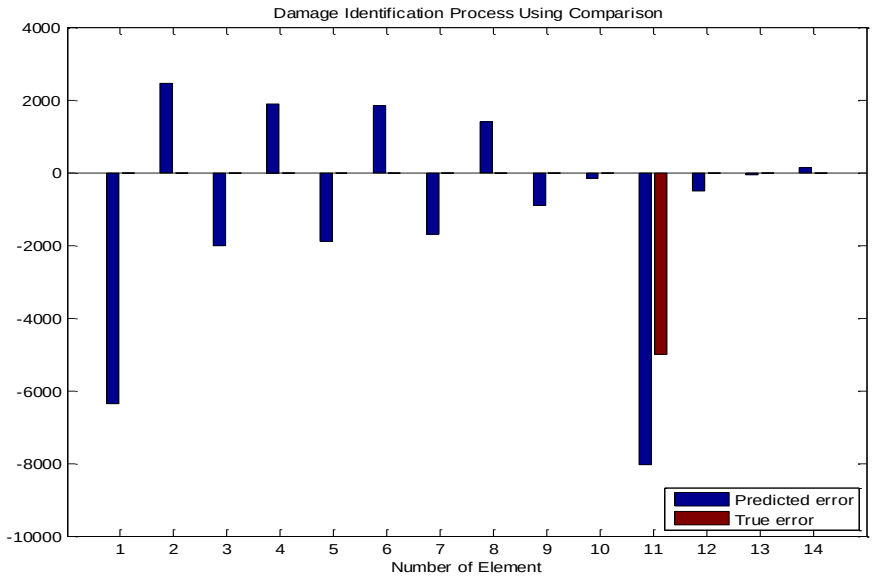

Figure 93. Damage Identification Using Comparison and the Sensitivity Matrix $[S_L]$, Applying 0.1% Damage at Element Number 11.

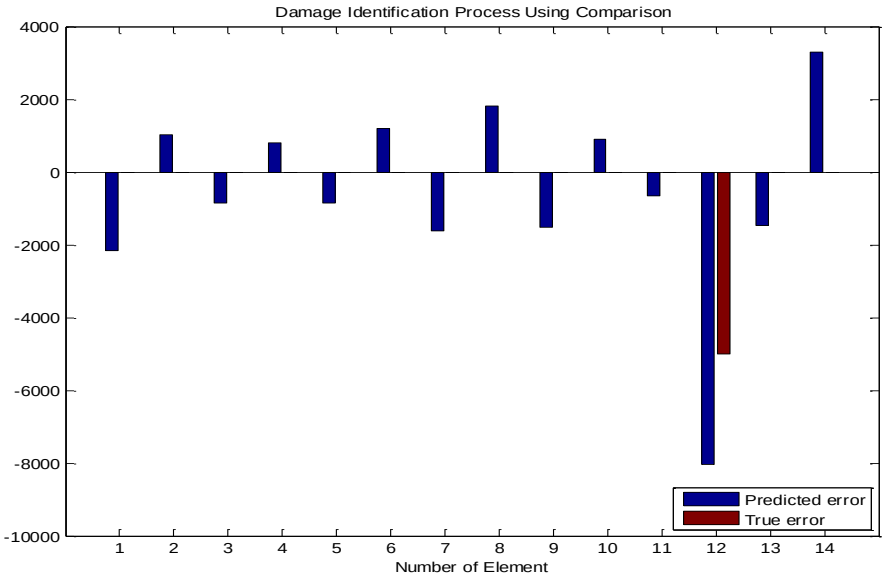

Figure 94. Damage Identification Using Comparison and the Sensitivity Matrix $[S_L]$, Applying 0.1% Damage at Element Number 12.

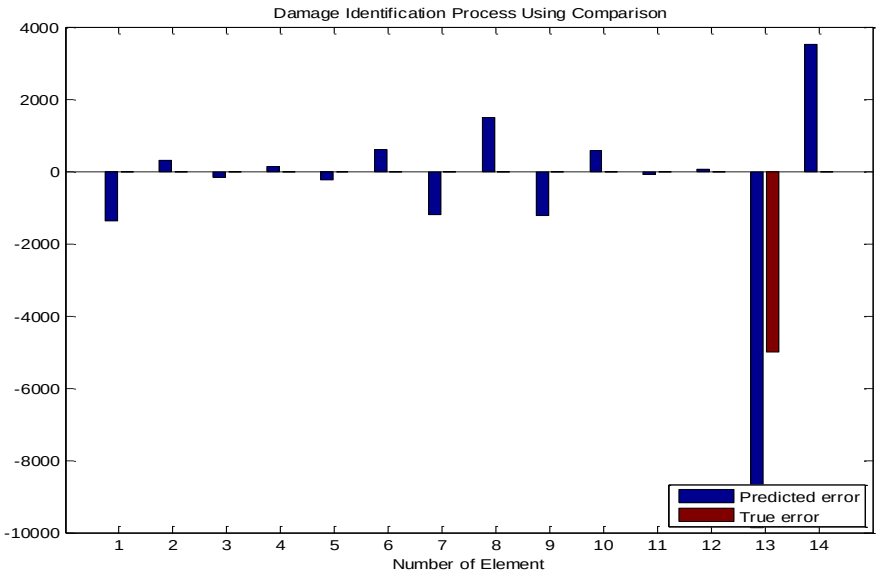

Figure 95. Damage Identification Using Comparison and the Sensitivity Matrix $[S_L]$, Applying 0.1% Damage at Element Number 13.

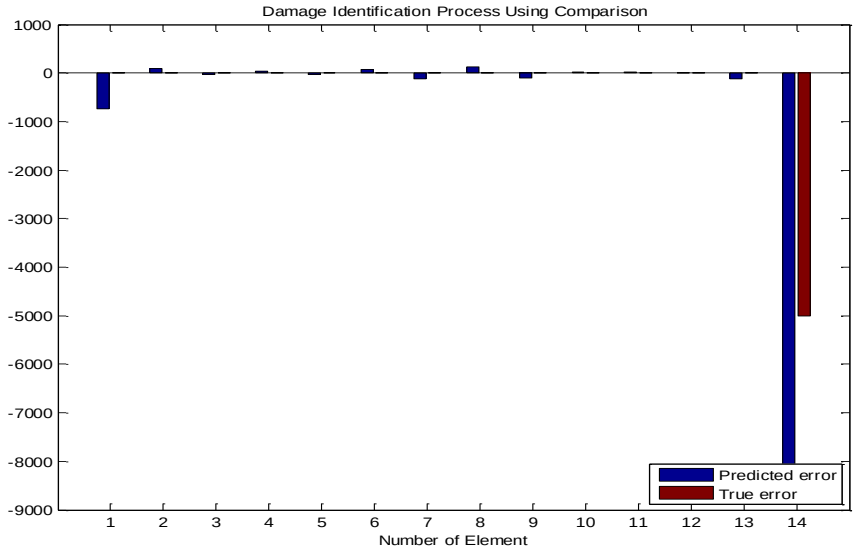

Figure 96. Damage Identification Using Comparison and the Sensitivity Matrix $[S_L]$, Applying 0.1% Damage at Element Number 14.

A conclusion that can be reached by inspecting Figures 83–96 is that the damage identification process cannot be successfully conducted at the most of the elements. Thus, the use of a composite sensitivity matrix made by lower modes will not yield correct results.

3. Comparison of Stiffness Values Using the Composite Sensitivity Matrix $[S_G]$

Finally, the composite sensitivity matrix $[S_G]$, which was created by mixed artificial boundary condition sets and modes, is tested. It is worth remembering that this sensitivity matrix had the best performance in damage identification using simulated data only. This time Equation (5.4) becomes:

$$\{\Delta EI_3 - \Delta EI_{RES}\} = [S_G] \setminus \{\omega_{upd}^2 - \omega_{upd\_Dam}^2\}. \tag{5.6}$$

As before, the damage is simulated by decreasing the stiffness value of the element. A decrease of 0.1 percent of stiffness is applied recursively at each element of the updated finite element model. The results of the damage identification process by comparison are provided in Figures 97–110.

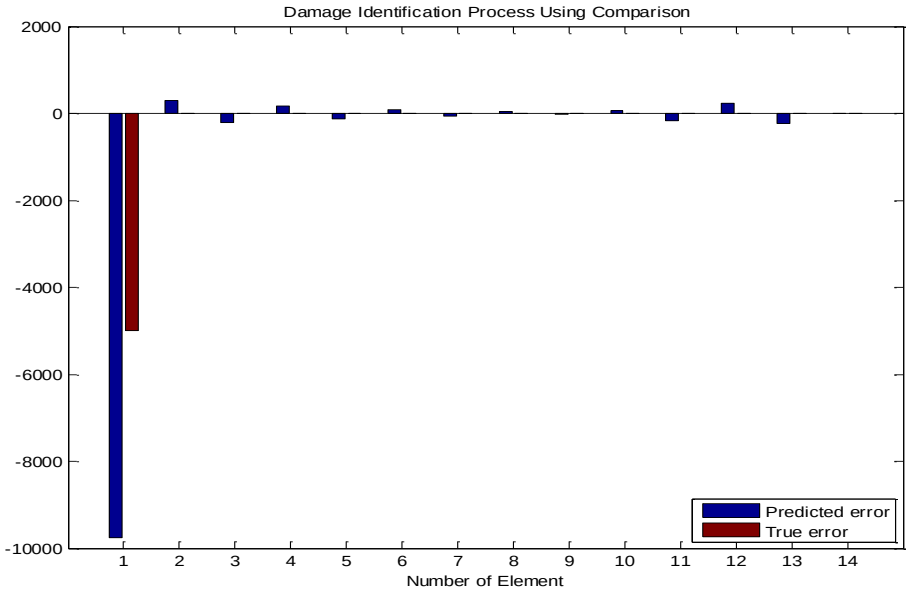

Figure 97. Damage Identification Using Comparison and the Sensitivity Matrix $[S_G]$, Applying 0.1% Damage at Element Number 1.

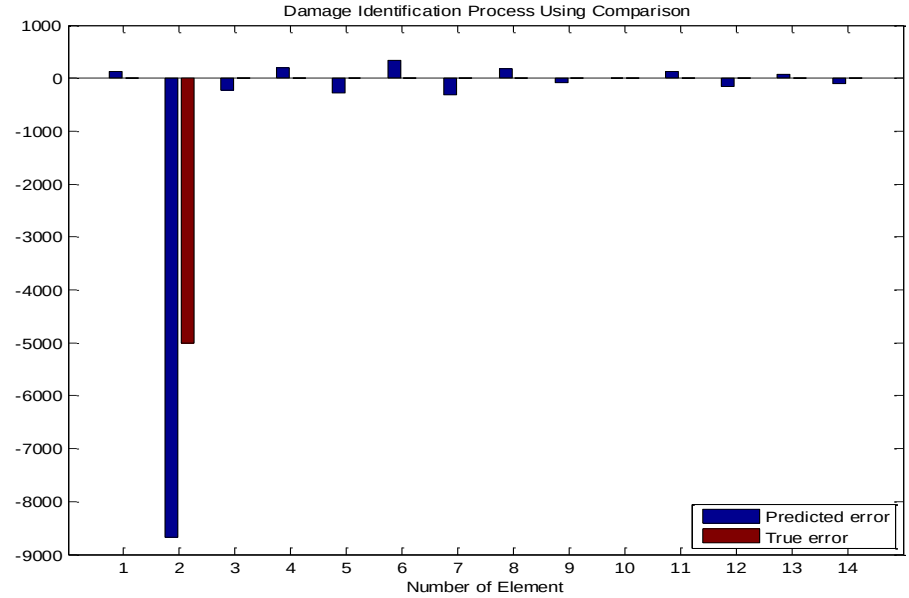

Figure 98. Damage Identification Using Comparison and the Sensitivity Matrix $[S_G]$, Applying 0.1% Damage at Element Number 2.

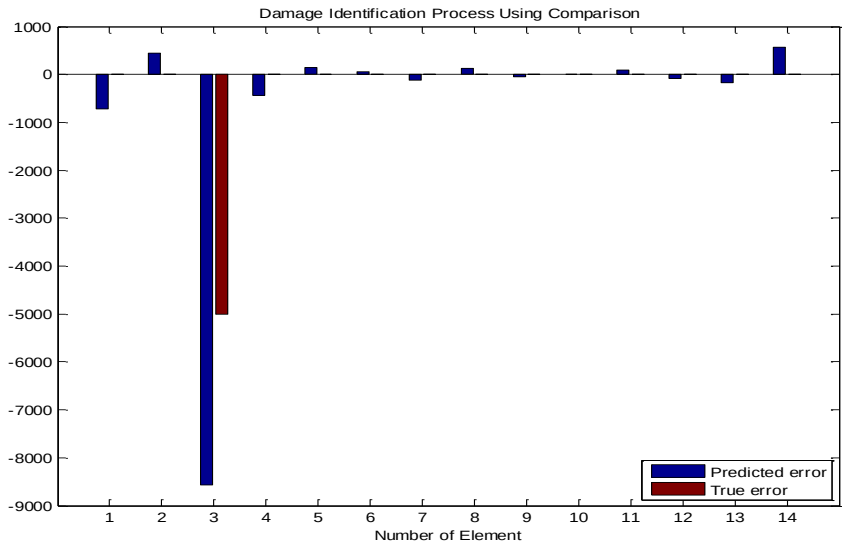

Figure 99. Damage Identification Using Comparison and the Sensitivity Matrix $[S_G]$, Applying 0.1% Damage at Element Number 3.

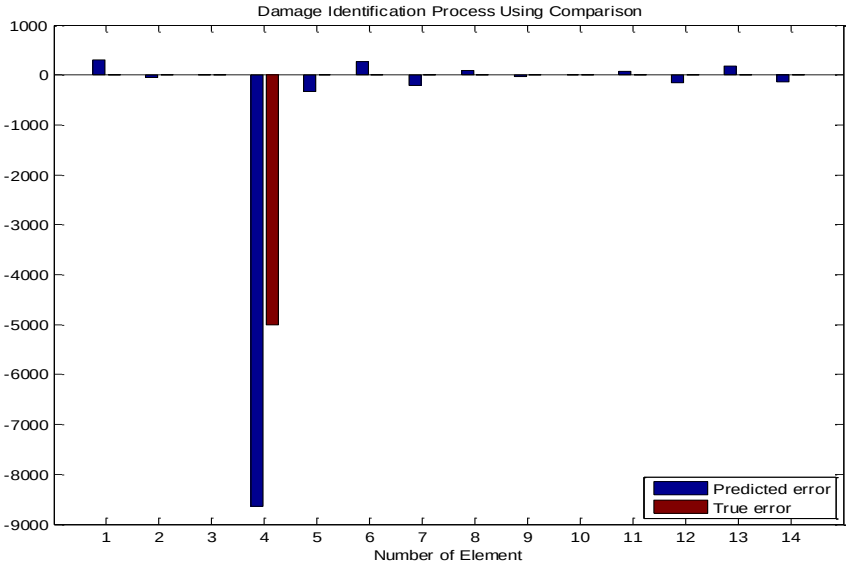

Figure 100. Damage Identification Using Comparison and the Sensitivity Matrix $[S_G]$, Applying 0.1% Damage at Element Number 4.

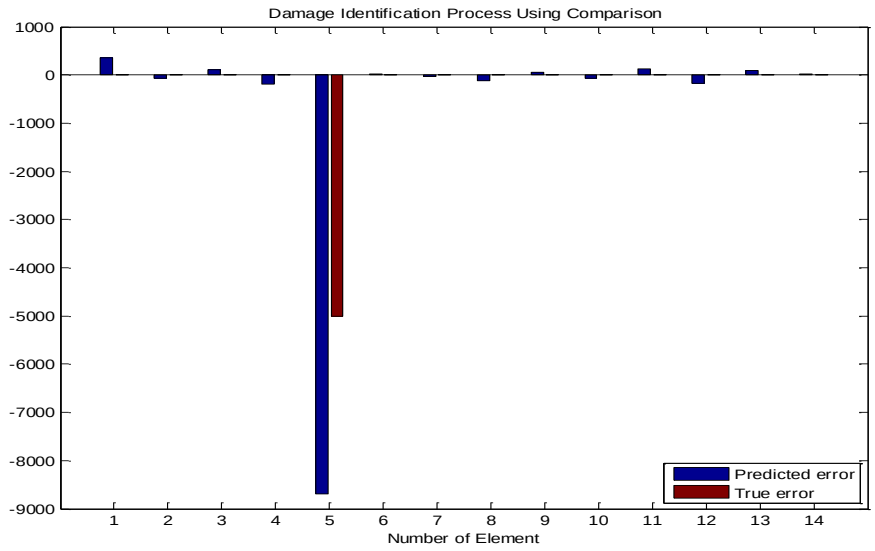

Figure 101. Damage Identification Using Comparison and the Sensitivity Matrix $[S_G]$, Applying 0.1% Damage at Element Number 5.

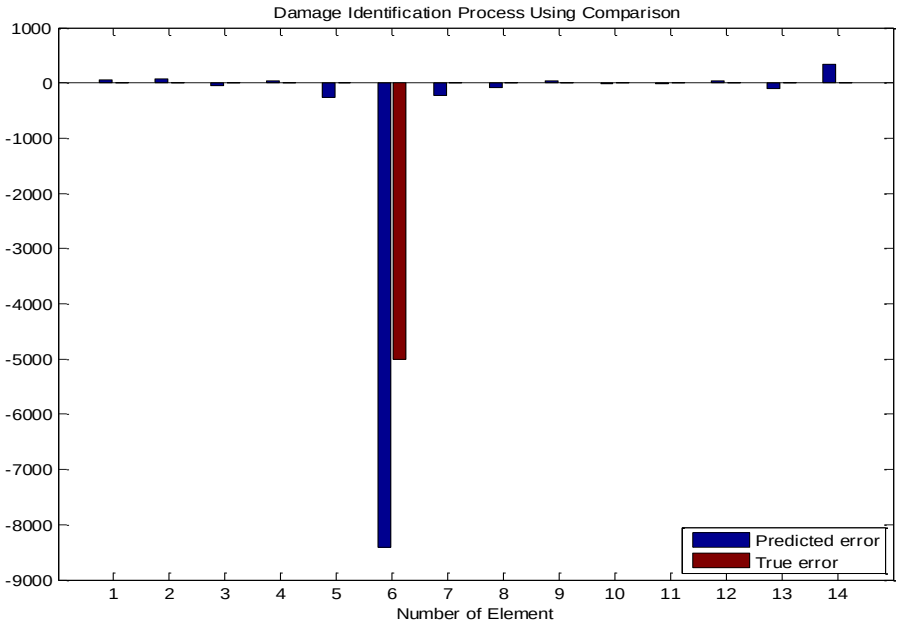

Figure 102. Damage Identification Using Comparison and the Sensitivity Matrix $[S_G]$, Applying 0.1% Damage at Element Number 6.

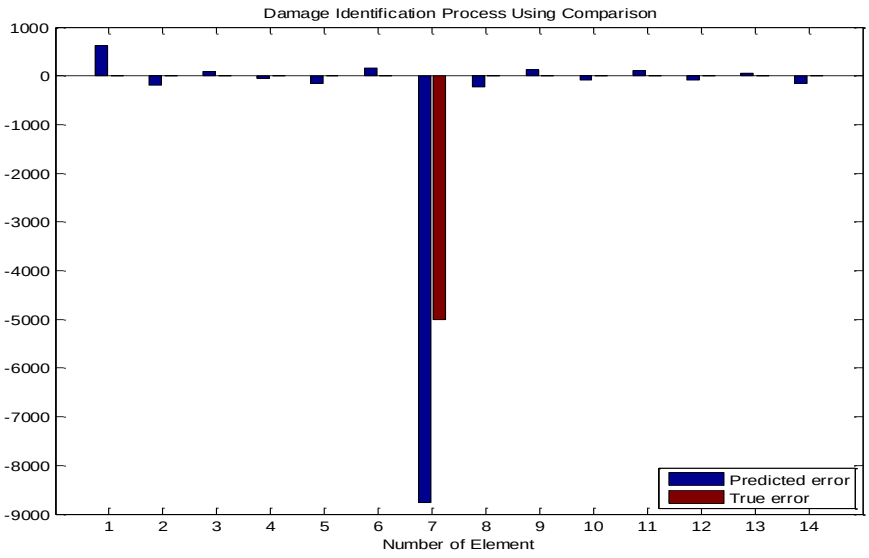

Figure 103. Damage Identification Using Comparison and the Sensitivity Matrix $[S_G]$, Applying 0.1% Damage at Element Number 7.

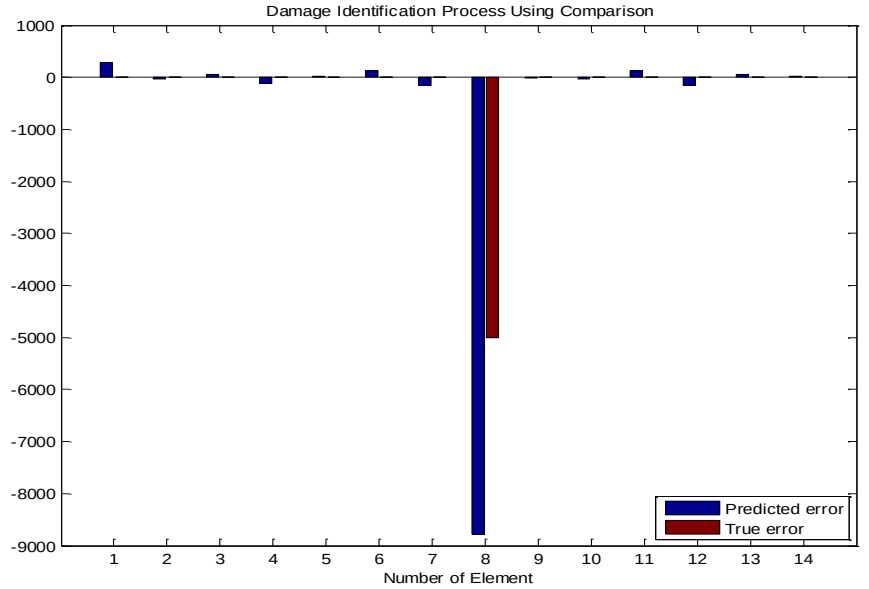

Figure 104. Damage Identification Using Comparison and the Sensitivity Matrix $[S_G]$, Applying 0.1% Damage at Element Number 8.

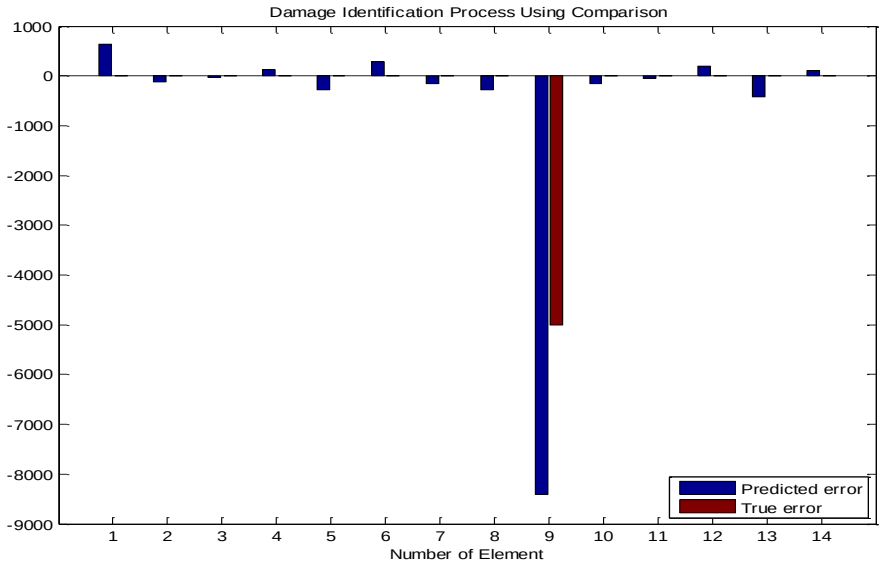

Figure 105. Damage Identification Using Comparison and the Sensitivity Matrix $[S_G]$, Applying 0.1% Damage at Element Number 9.

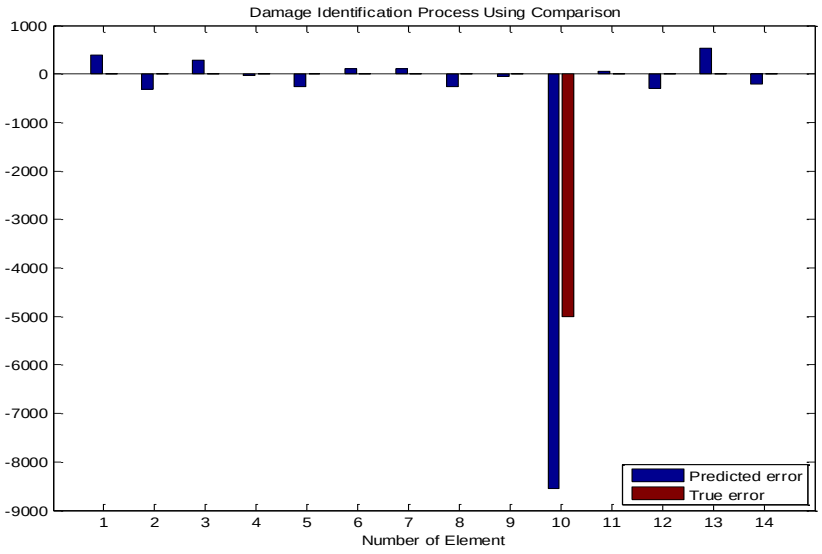

Figure 106. Damage Identification Using Comparison and the Sensitivity Matrix $[S_G]$, Applying 0.1% Damage at Element Number 10.

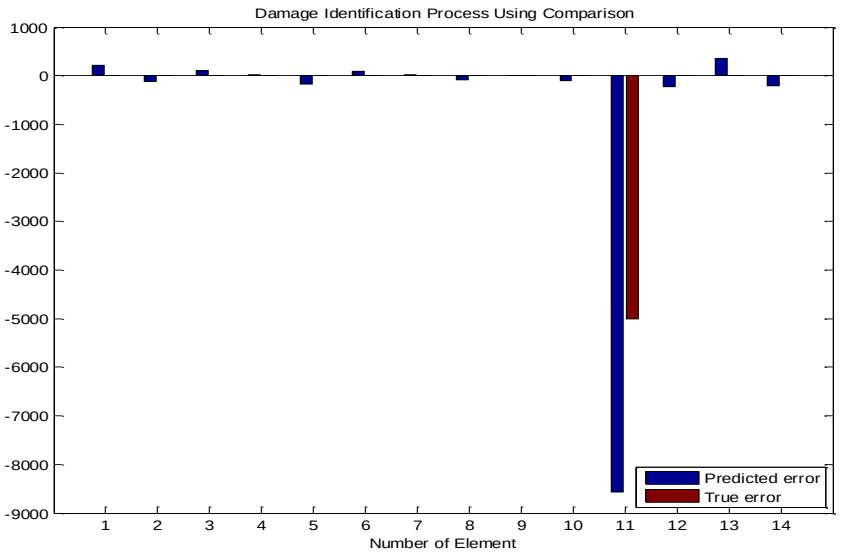

Figure 107. Damage Identification Using Comparison and the Sensitivity Matrix $[S_G]$, Applying 0.1% Damage at Element Number 11.

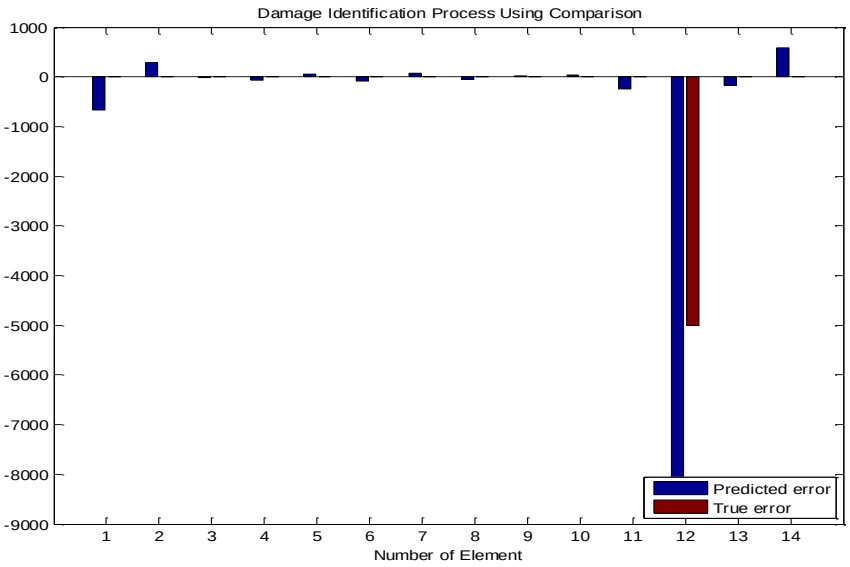

Figure 108. Damage Identification Using Comparison and the Sensitivity Matrix $[S_G]$, Applying 0.1% Damage at Element Number 12.

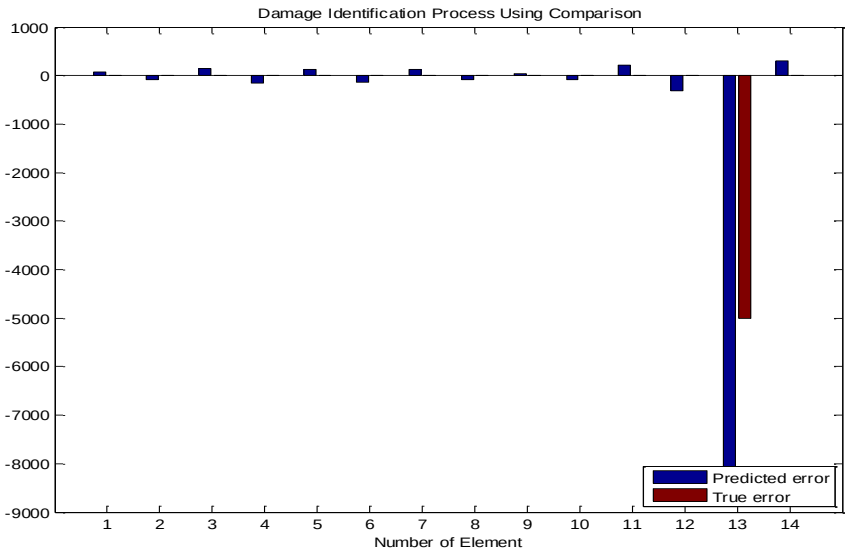

Figure 109. Damage Identification Using Comparison and the Sensitivity Matrix $[S_G]$, Applying 0.1% Damage at Element Number 13.

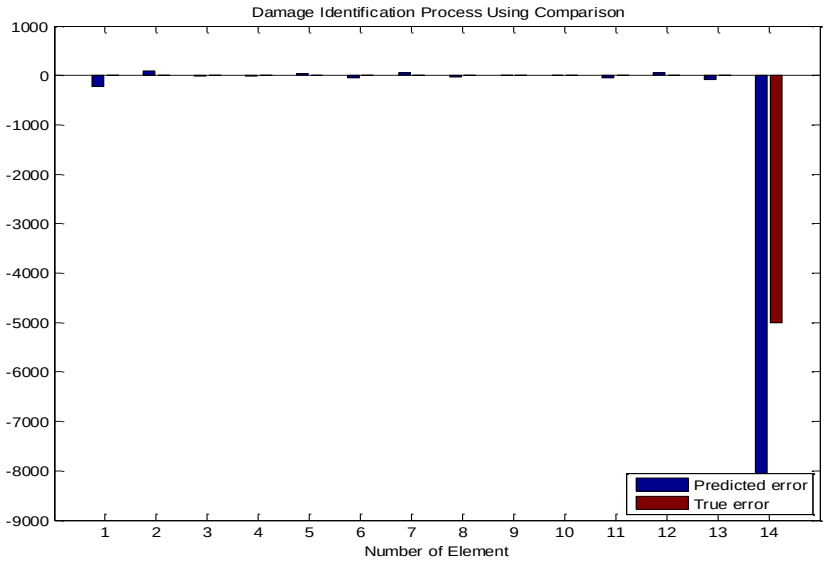

Figure 110. Damage Identification Using Comparison and the Sensitivity Matrix $[S_G]$, Applying 0.1% Damage at Element Number 14.

It is obvious that the damaged element can always be identified accurately. Thus, this sensitivity matrix has the best performance in damage identification by comparison.

D. MULTIPLE DAMAGE IDENTIFICATION BY COMPARISON

So far, it was possible to identify damage at a single element using the damage identification by comparison method. The best sensitivity matrix for this purpose has been shown to be the $[S_G]$, followed by the $[S_H]$, which could not identify the damage at the last two elements.

Next, the ability of these matrices to identify multiple damages is investigated. In this investigation, three elements are modeled as damaged each time. Again, a decrease of the stiffness by 0.1 percent is applied at the corresponding elements. There are many possible combinations; nevertheless, in order to be consistent and reach a conclusion, each time three consecutive elements are damaged. The sensitivity matrix $[S_L]$ is not examined because the damage identification process by comparison using that matrix could not identify the damage at a single element.

1. Multiple Damage Identification by Comparison, Using the Composite Sensitivity Matrix $[S_G]$

The result of the damage identification process using comparison is provided in Figures 111–122.

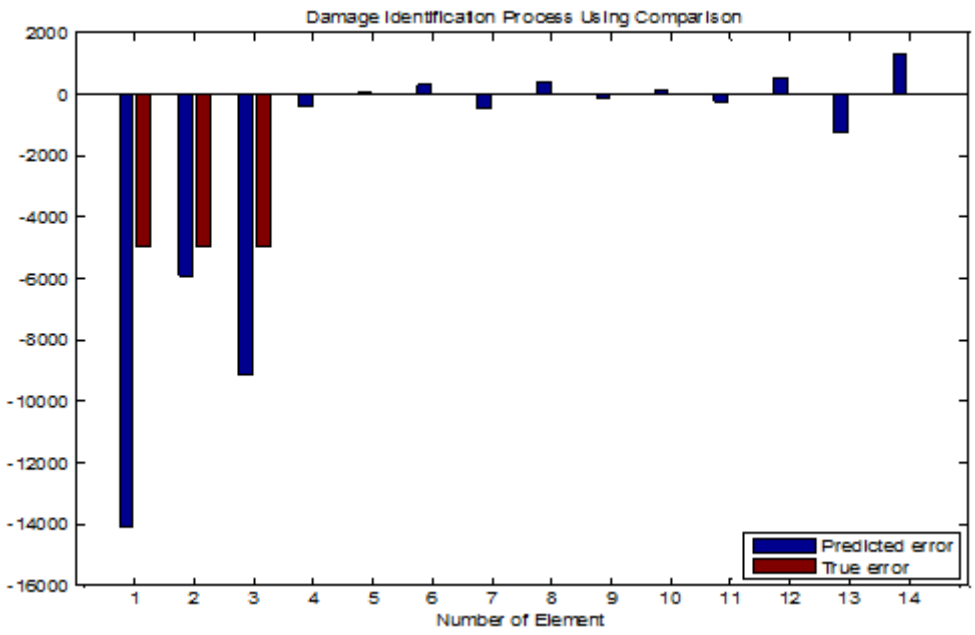

Figure 111. Multiple Damage Identification Using Comparison and the Sensitivity Matrix $[S_G]$, Applying 0.1% Damage at Elements 1, 2, 3.

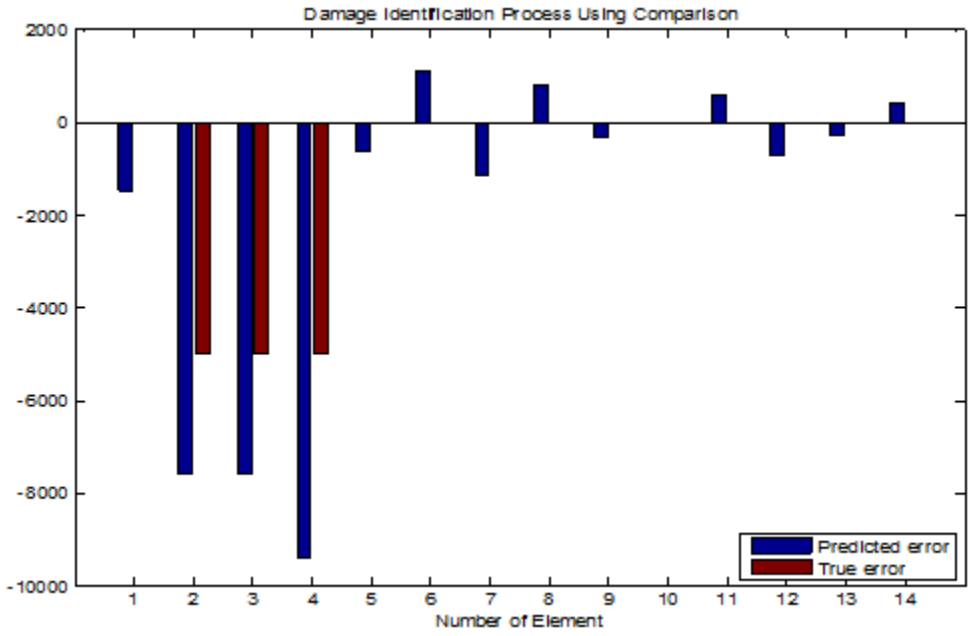

Figure 112. Multiple Damage Identification Using Comparison and the Sensitivity Matrix $[S_G]$, Applying 0.1% Damage at Elements 2, 3, 4.

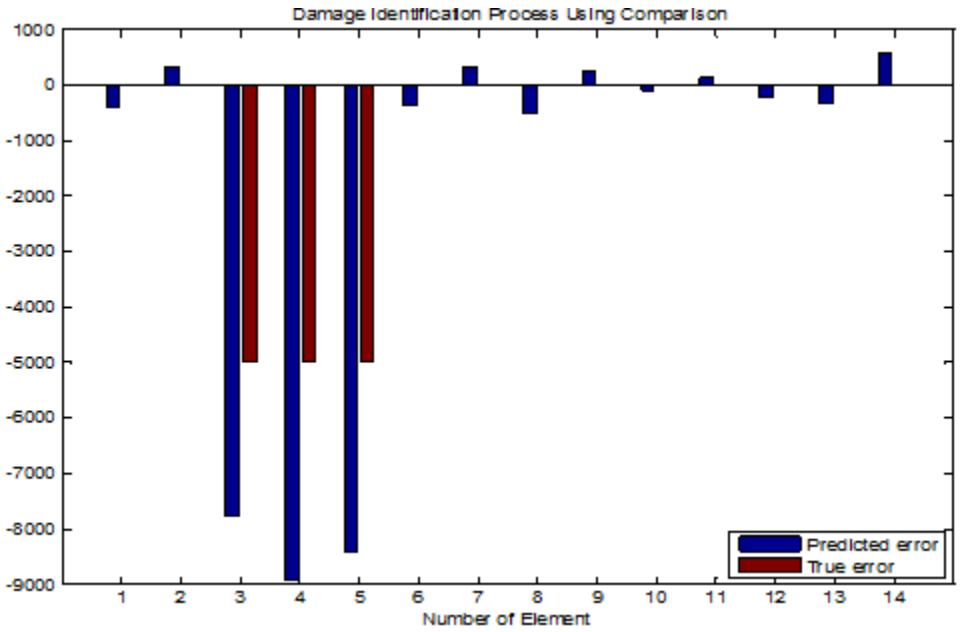

Figure 113. Multiple Damage Identification Using Comparison and the Sensitivity Matrix $[S_G]$, Applying 0.1% Damage at Elements 3, 4, 5.

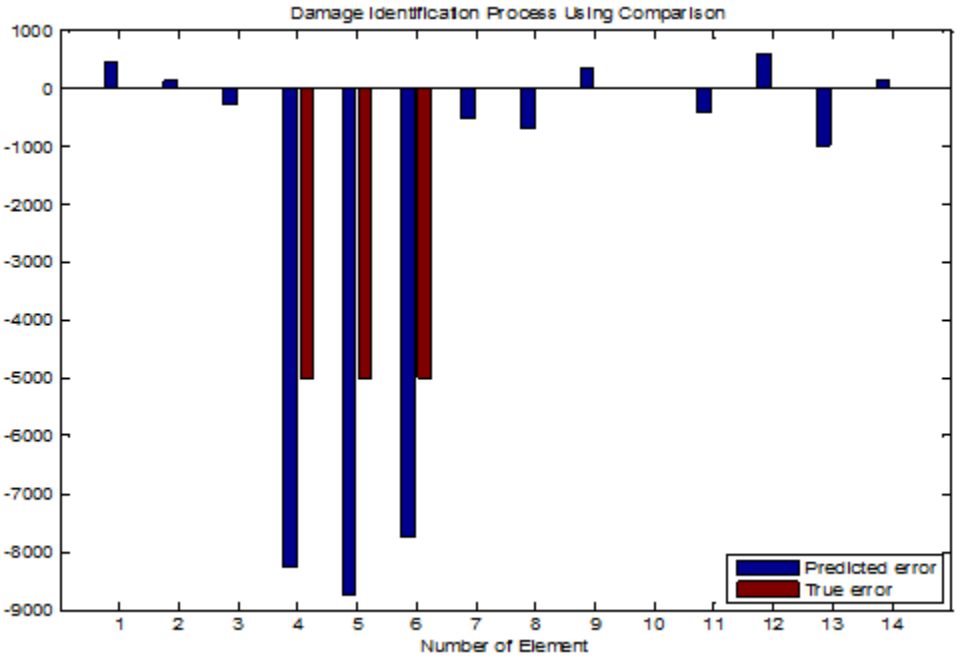

Figure 114. Multiple Damage Identification Using Comparison and the Sensitivity Matrix $[S_G]$, Applying 0.1% Damage at Elements 4, 5, 6.

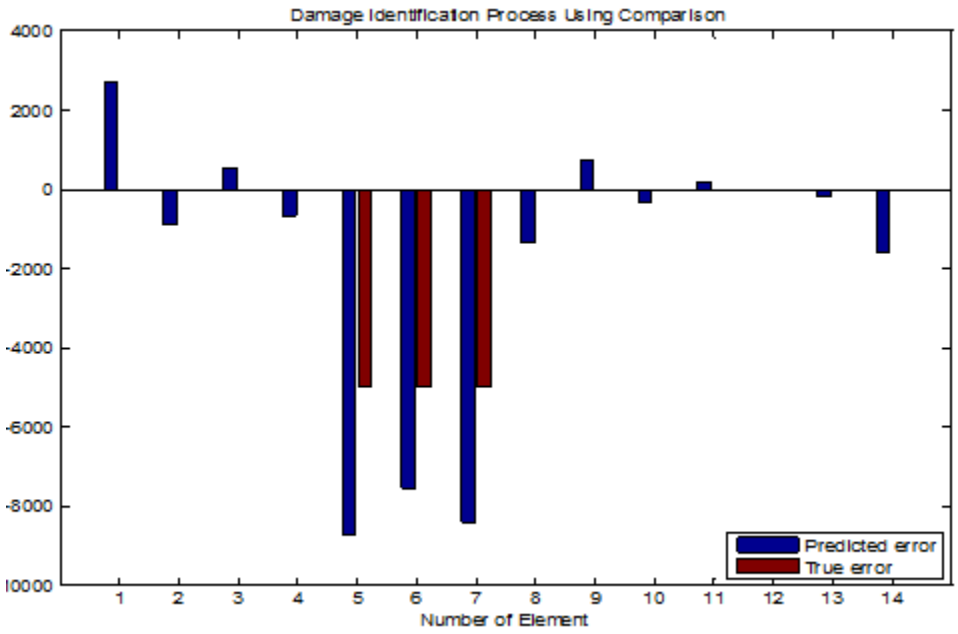

Figure 115. Multiple Damage Identification Using Comparison and the Sensitivity Matrix $[S_G]$, Applying 0.1% Damage at Elements 5, 6, 7.

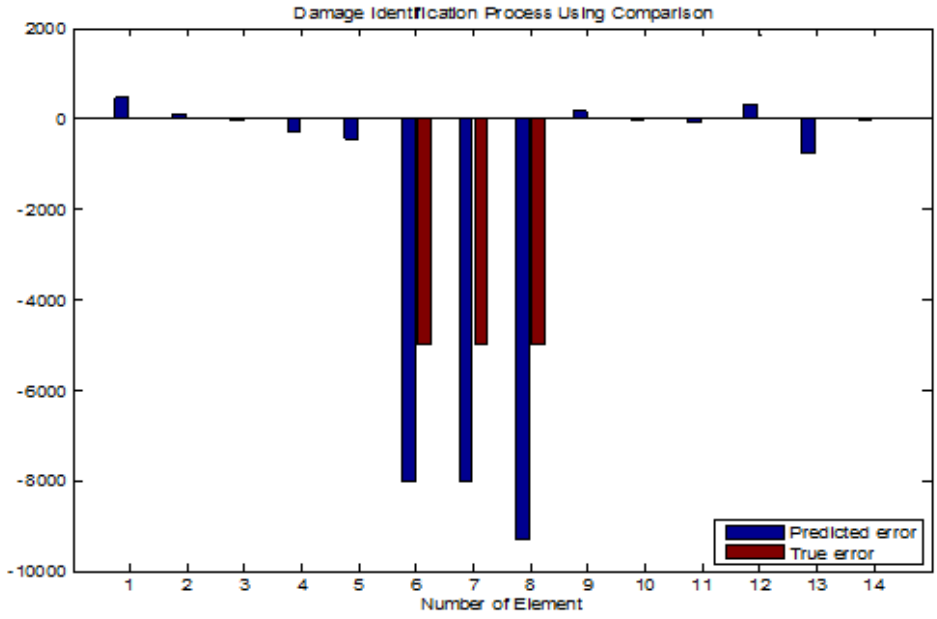

Figure 116. Multiple Damage Identification Using Comparison and the Sensitivity Matrix $[S_G]$, Applying 0.1% Damage at Elements 6, 7, 8.

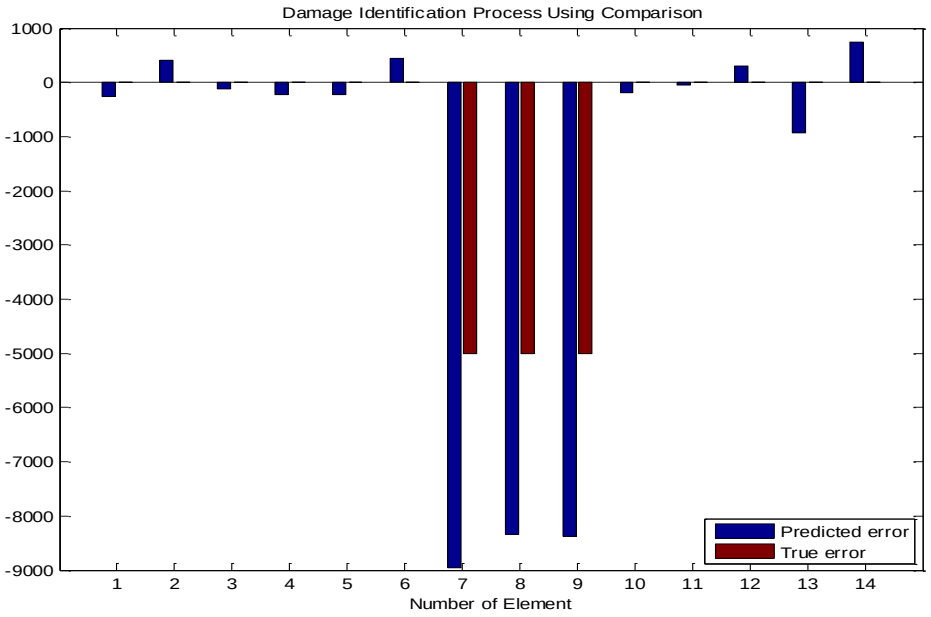

Figure 117. Multiple Damage Identification Using Comparison and the Sensitivity Matrix $[S_G]$, Applying 0.1% Damage at Elements 7, 8, 9.

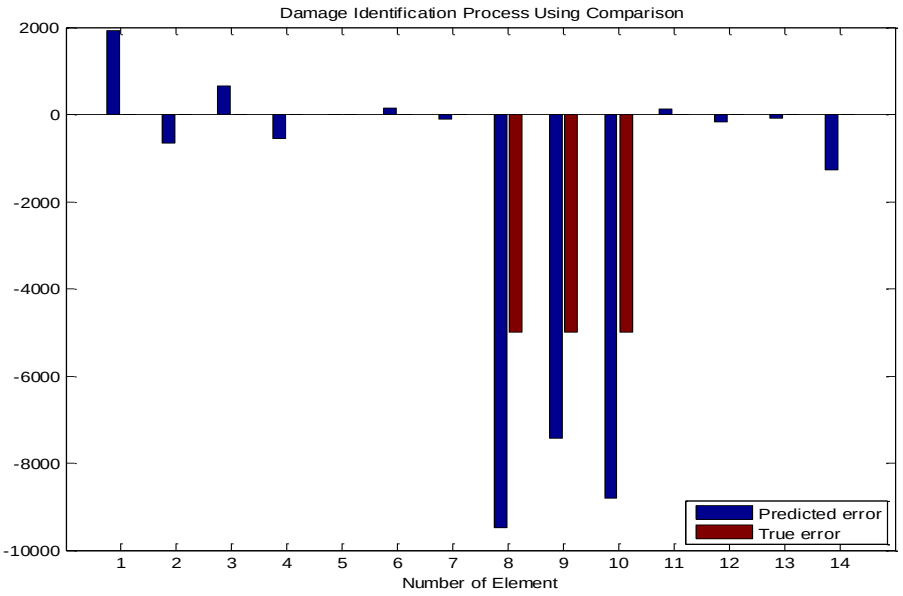

Figure 118. Multiple Damage Identification Using Comparison and the Sensitivity Matrix $[S_G]$, Applying 0.1% Damage at Elements 8, 9, 10.

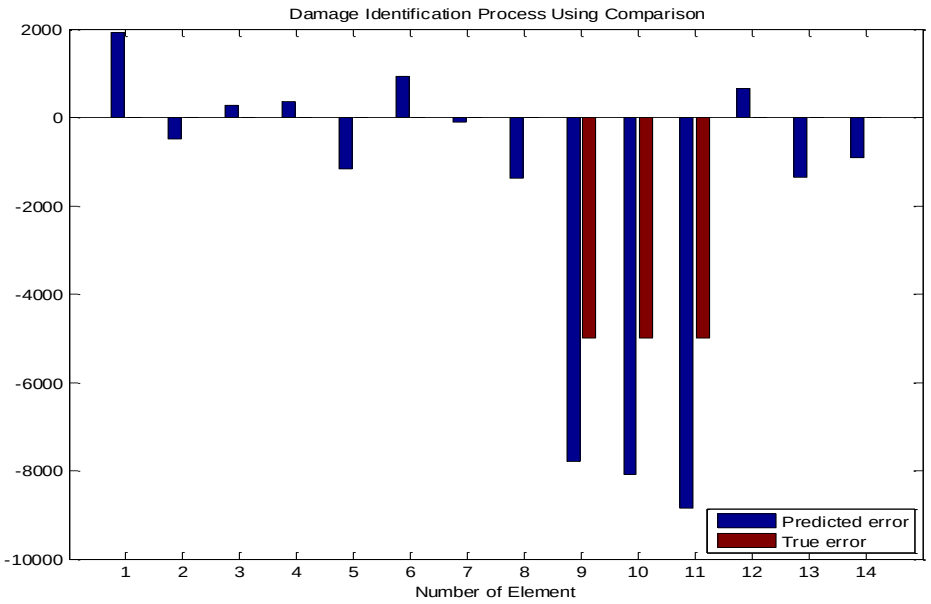

Figure 119. Multiple Damage Identification Using Comparison and the Sensitivity Matrix $[S_G]$, Applying 0.1% Damage at Elements 9, 10, 11.

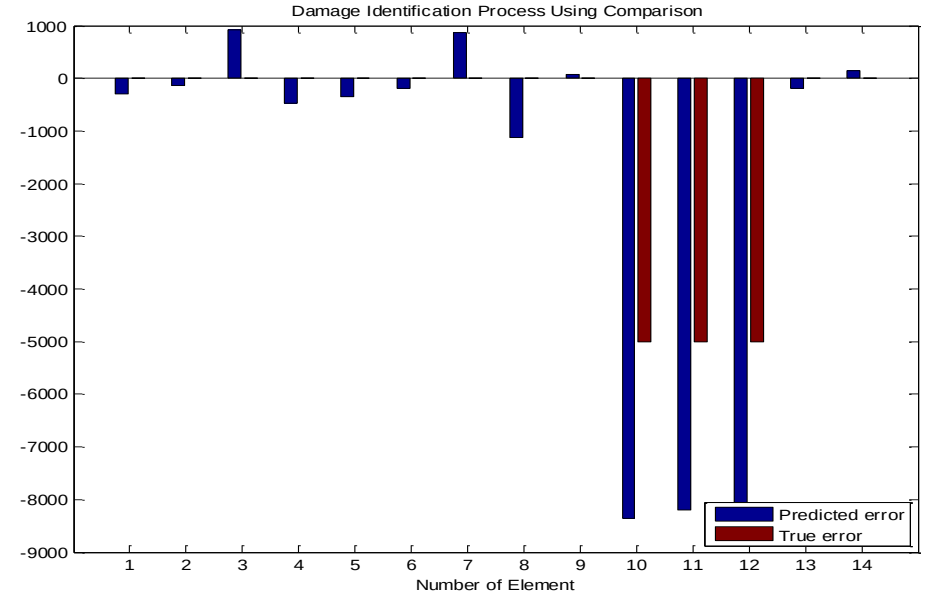

Figure 120. Multiple Damage Identification Using Comparison and the Sensitivity Matrix $[S_G]$, Applying 0.1% Damage at Elements 10, 11, 12.

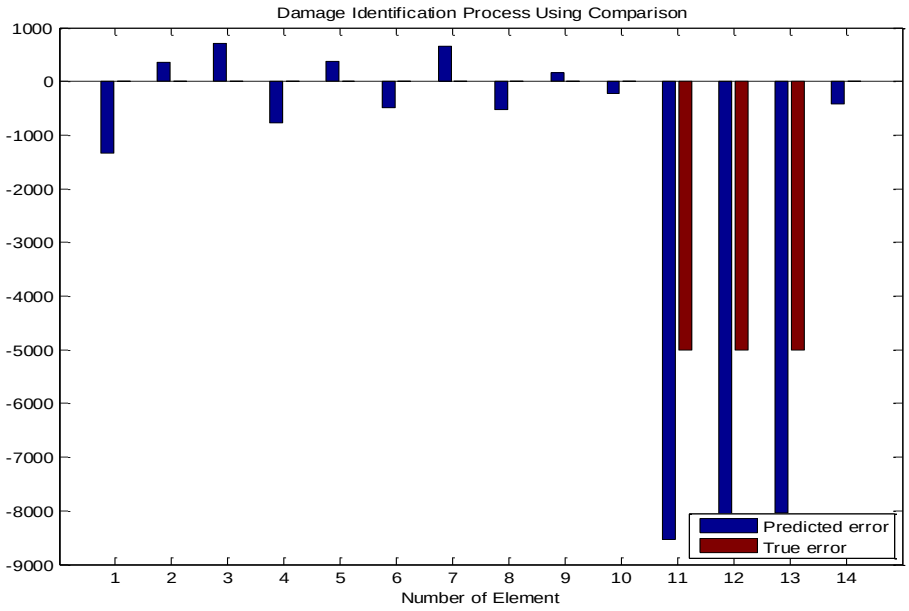

Figure 121. Multiple Damage Identification Using Comparison and the Sensitivity Matrix $[S_G]$, Applying 0.1% Damage at Elements 11, 12, 13.

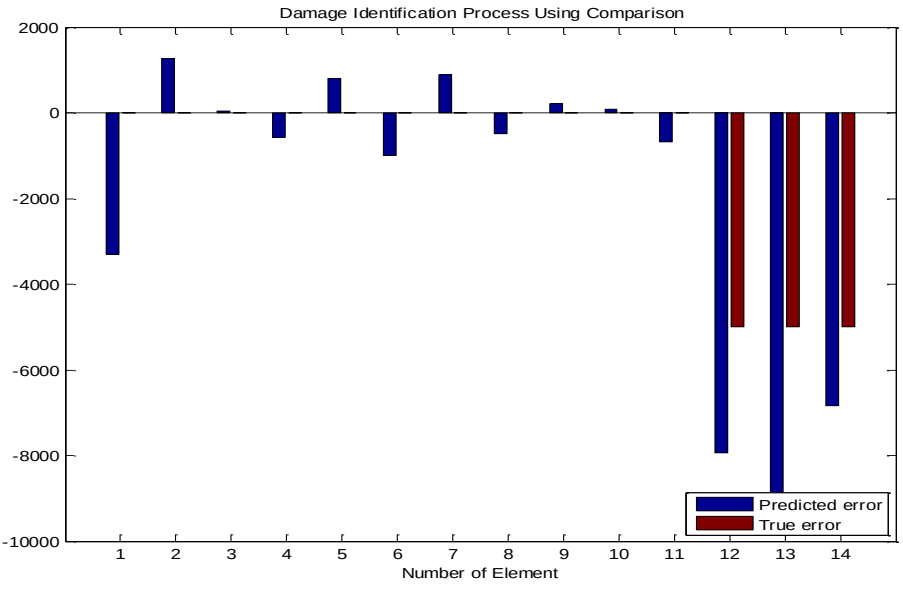

Figure 122. Multiple Damage Identification Using Comparison and the Sensitivity Matrix $[S_G]$, Applying 0.1% Damage at Elements 12, 13, 14.

Generally speaking, the localization of the damage can be performed accurately in most cases. In this investigation, the damage is extended to three elements, which amounts to 21 percent of the beam's length. Thus, large damage is simulated. This is the reason that the results are not as accurate as before.

2. Multiple Damage Identification by Comparison, Using the Composite Sensitivity Matrix $[S_H]$

Finally, the ability of the $[S_H]$ matrix to identify multiple damages is investigated. As previously, three elements are modeled as damaged by applying a decrease of stiffness by 0.1 percent at the corresponding elements. The results of the damage identification process by comparison are provided in Figures 123–134.

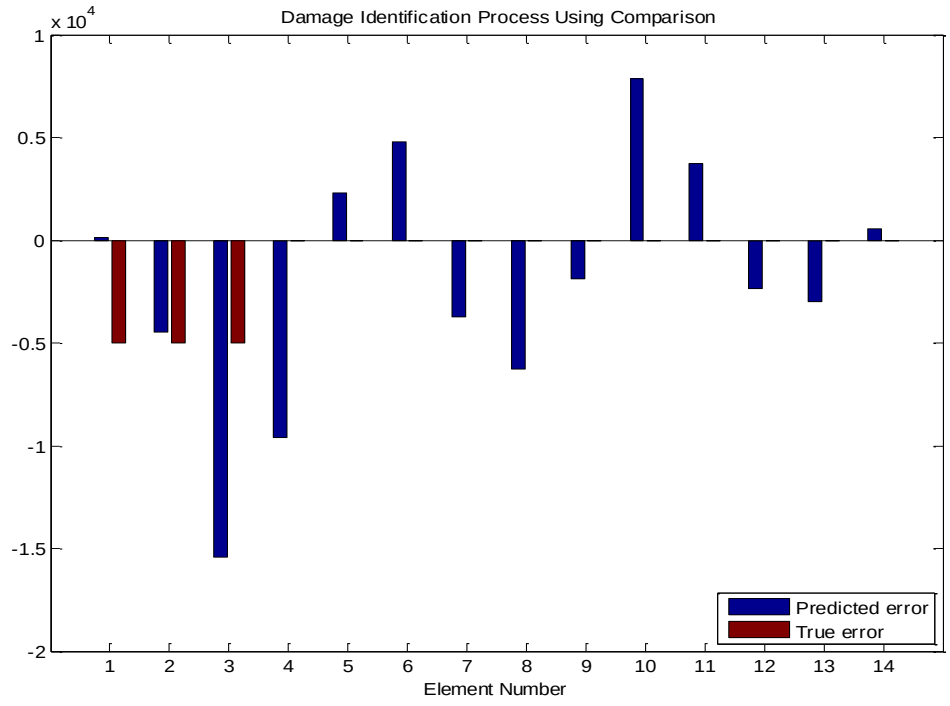

Figure 123. Multiple Damage Identification Using Comparison and the Sensitivity Matrix $[S_H]$, Applying 0.1% Damage at Elements 1, 2, 3.

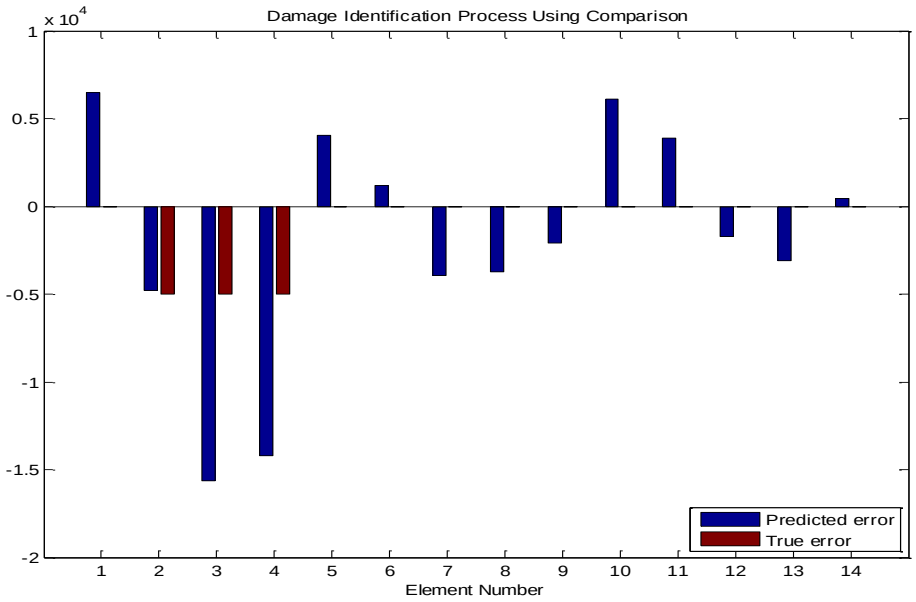

Figure 124. Multiple Damage Identification Using Comparison and the Sensitivity Matrix $[S_H]$, Applying 0.1% Damage at Elements 2, 3, 4.

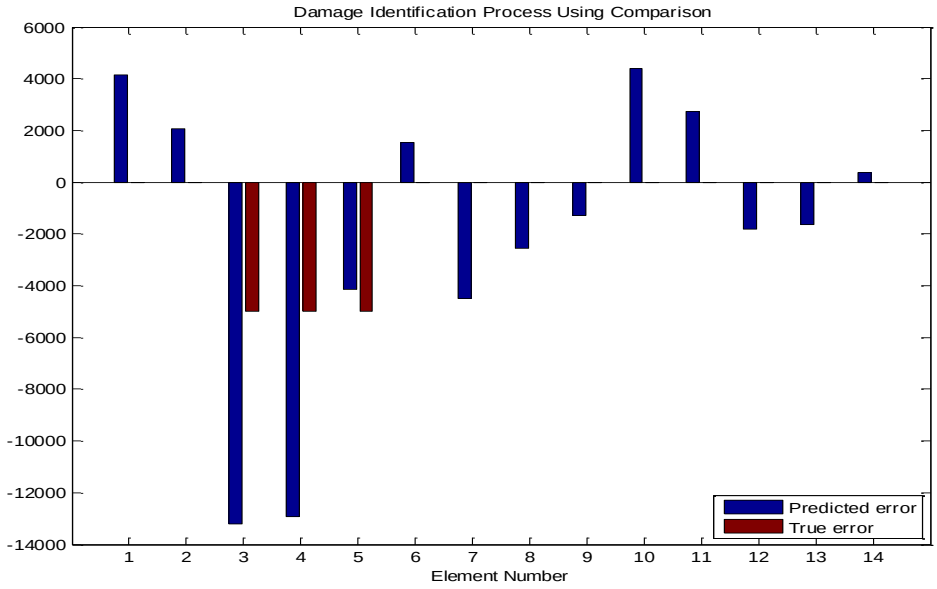

Figure 125. Multiple Damage Identification Using Comparison and the Sensitivity Matrix $[S_H]$, Applying 0.1% Damage at Elements 3, 4, 5.

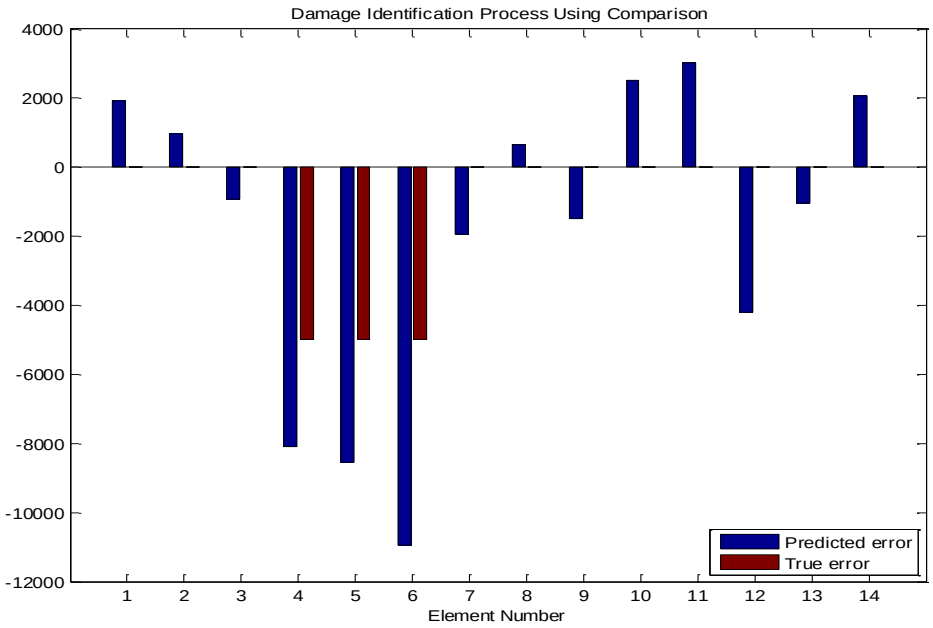

Figure 126. Multiple Damage Identification Using Comparison and the Sensitivity Matrix $[S_H]$, Applying 0.1% Damage at Elements 4, 5, 6.

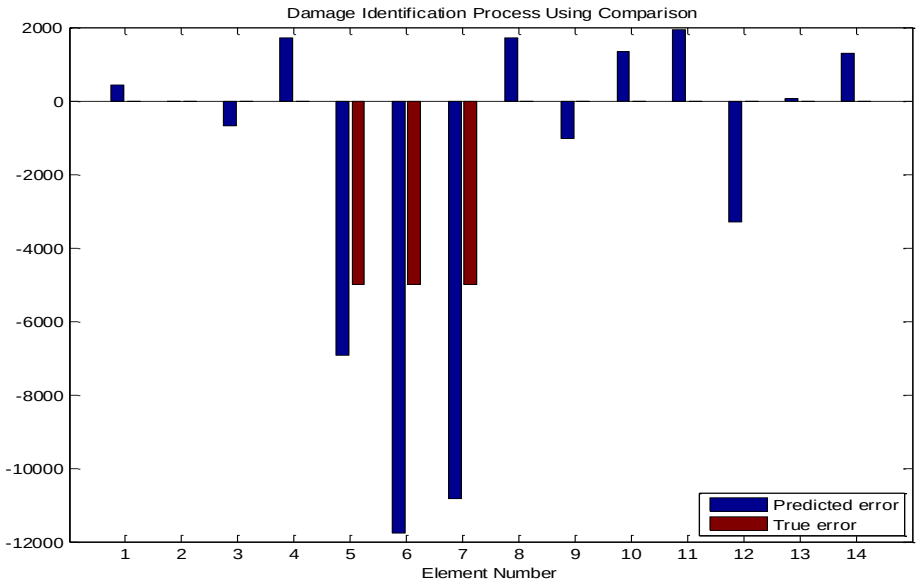

Figure 127. Multiple Damage Identification Using Comparison and the Sensitivity Matrix $[S_H]$, Applying 0.1% Damage at Elements 5, 6, 7.

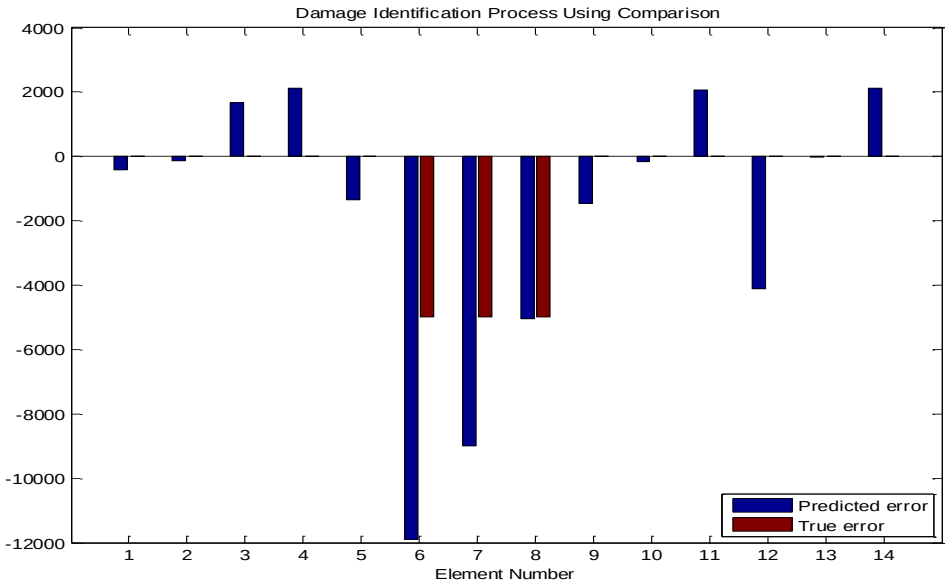

Figure 128. Multiple Damage Identification Using Comparison and the Sensitivity Matrix $[S_H]$, Applying 0.1% Damage at Elements 6, 7, 8.

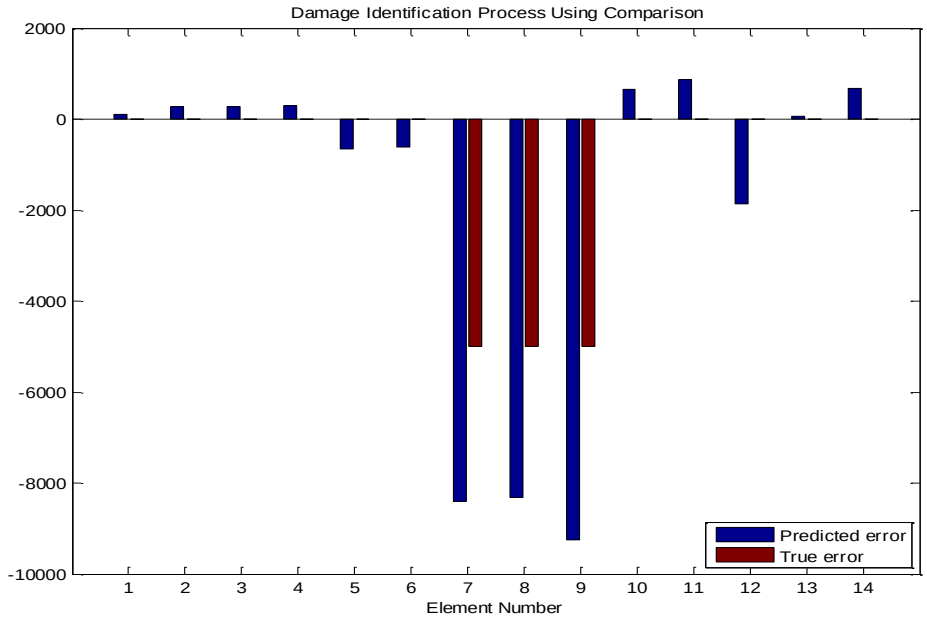

Figure 129. Multiple Damage Identification Using Comparison and the Sensitivity Matrix $[S_H]$, Applying 0.1% Damage at Elements 7, 8, 9.

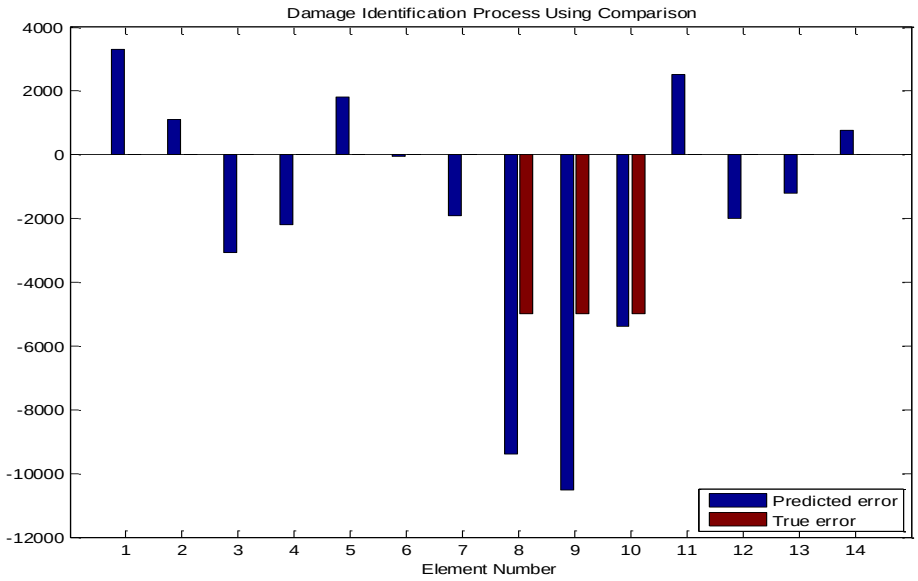

Figure 130. Multiple Damage Identification Using Comparison and the Sensitivity Matrix $[S_H]$, Applying 0.1% Damage at Elements 8, 9, 10.

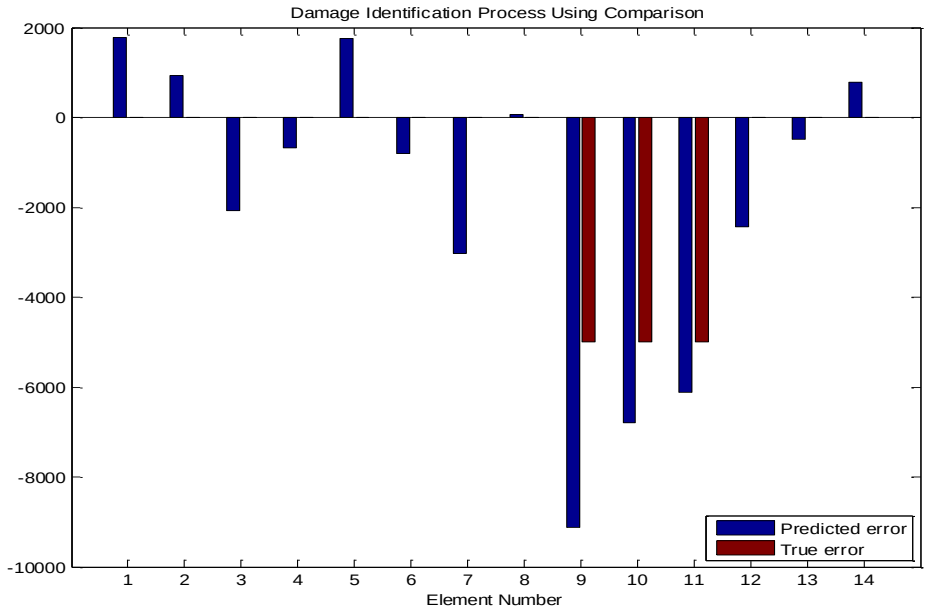

Figure 131. Multiple Damage Identification Using Comparison and the Sensitivity Matrix $[S_H]$, Applying 0.1% Damage at Elements 9, 10, 11.

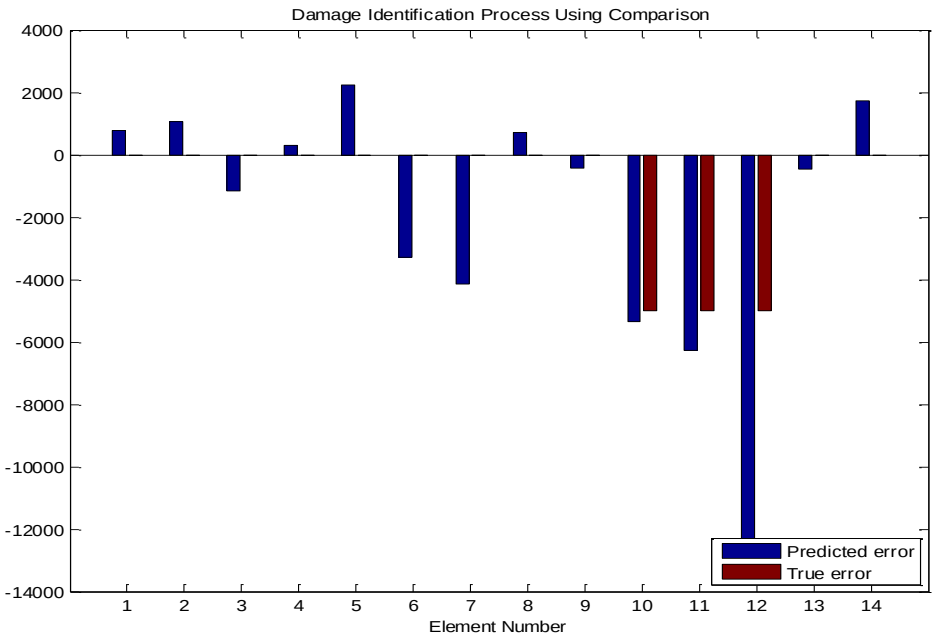

Figure 132. Multiple Damage Identification Using Comparison and the Sensitivity Matrix $[S_H]$, Applying 0.1% Damage at Elements 10, 11, 12.

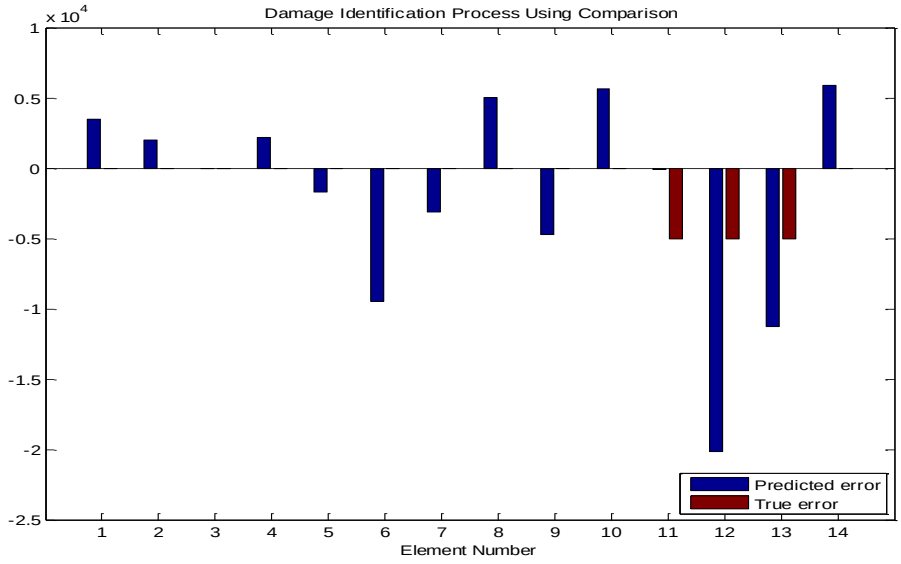

Figure 133. Multiple Damage Identification Using Comparison and the Sensitivity Matrix $[S_H]$, Applying 0.1% Damage at Elements 11, 12, 13.

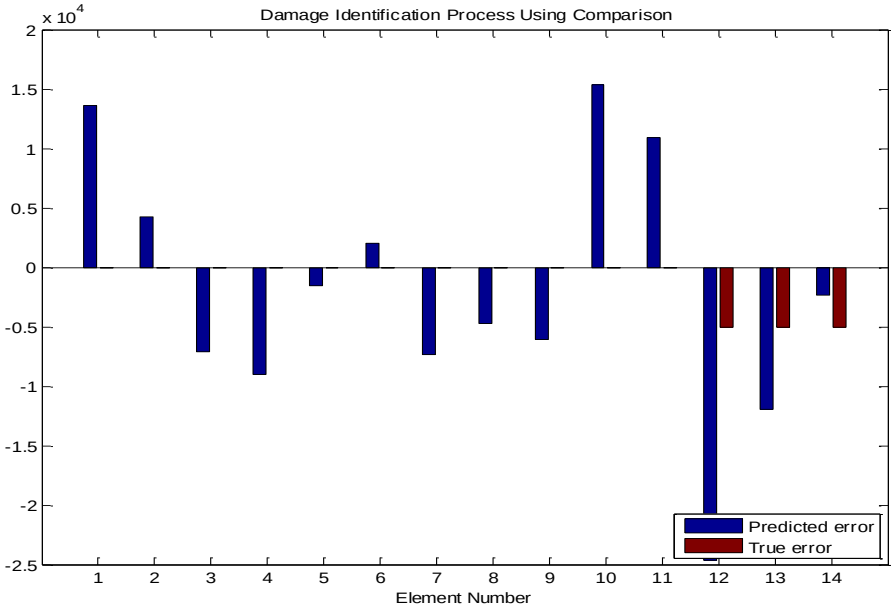

Figure 134. Multiple Damage Identification Using Comparison and the Sensitivity Matrix $[S_H]$, Applying 0.1% Damage at Elements 12, 13, 14.

Obviously, the damage identification process by comparison is not able to identify the damaged elements. Thus, the sensitivity matrix $[S_H]$ is not as effective as the sensitivity matrix $[S_G]$ for multiple damage identification purposes.

E. CONCLUDING REMARKS

In this chapter the damage identification process has been demonstrated. In order not to damage the real beam, the damage is applied to the finite element model by decreasing the stiffness of the corresponding element. Using Equation (5.2), which is the standard way of performing damage identification, we were not able to identify the damaged element in any case.

A new way to perform damage identification was proposed and investigated. The damage identification process using comparison can be summarized as follows:

$$
\begin{aligned}
\{\Delta EI_1\} &= [S] \setminus \{\omega^2_{\exp} - \omega^2_{upd\_Dam}\} \\
- \{\Delta EI_{RES}\} &= [S] \setminus \{\omega^2_{\exp} - \omega^2_{upd}\} \\
\{\Delta EI_1 - \Delta EI_{RES}\} &= [S] \setminus \{\omega^2_{upd} - \omega^2_{upd\_Dam}\}
\end{aligned}, \qquad (5.7)
$$

where $\{\Delta EI_1\}$ is the stiffness vector created by damage identification between the experimental data and the updated damaged finite element model, $\{\Delta EI_{RES}\}$ is the residual stiffness vector created by damage identification between the experimental data and the updated finite element model, $[S]$ is an arbitrary composite sensitivity matrix, $\{\omega^2_{\exp}\}$ is a vector created by the experimental natural frequencies, $\{\omega^2_{upd}\}$ is a vector created by the estimated natural frequencies of the updated finite element model, and $\{\omega^2_{upd\_Dam}\}$ is a vector created by the estimated natural frequencies of the updated damaged finite element model.

The residual stiffness of the updated damaged finite element model is subtracted from the stiffness of the updated finite element model. Thus, Equation (5.7) is used. In this research, the mean stiffness value was used to update the finite element model. This is the reason that the composite sensitivity matrix, which was used for the damage identification process, is the same as the composite sensitivity matrix of the baseline finite element model.

Using the composite sensitivity matrix made from higher modes, $[S_H]$, the damage identification process by comparison is not able to identify the damage at the last two elements. However, the damage at the rest of the elements can be identified. Moreover, the use of this matrix in multiple damage identification (three damaged elements) was not successful.

The composite sensitivity matrix $[S_G]$ has the best performance in damage identification using comparison. It can identify the damage at any element. This matrix also has the best performance in damage identification using computational data, as demonstrated in Chapter III. Furthermore, in

multiple damage identification, the use of this matrix can identify the damaged elements, even if the simulated damage is at three elements, which corresponds to almost 21 percent of the beam’s length.

THIS PAGE INTENTIONALLY LEFT BLANK

VI. CONCLUSIONS AND RECOMMENDATIONS

A. CONCLUSIONS

This research was mainly focused on the use of experimental data for model update and damage identification. The investigation process described in this thesis led to several important conclusions.

Initially, the use of the QR decomposition method to create the composite sensitivity method was verified using simulated data. An interesting result from this investigation, though, is that data from symmetrical structural configurations must not be used in the creation of the composite sensitivity matrix.

Next, it was demonstrated that the use of an experimentally measured frequency response function matrix can identify the resonant frequencies of any artificial boundary condition systems. The accuracy of those natural frequencies was validated using Cauchy's interlace theorem.

Furthermore, this research demonstrated that the natural frequencies of higher modes (in this case the seventh mode and higher) are more resistant to experimental error due to sampling. The reason for this is that the higher the mode is, the smaller the relative error is with respect to the frequency resolution of the measured frequency response functions.

Then, the standard method for model updating and the use of experimental data were shown to be inadequate for updating the finite element model. Therefore, this thesis introduced and demonstrated a new method for model update, the use of the mean value of the stiffness. Because the finite element model does not have the same dynamic behavior as the real structure, stiffness changes have to be applied at each element of the model to improve (update) that behavior. In general, these changes have a different value for each element. In the mean stiffness value method, the mean value of these changes in stiffness is applied at every element. It was demonstrated that using a composite sensitivity matrix made of higher modes would result in a successful update

process. In this research, however, the model could only be updated using this method once.

Another advantage of using the mean stiffness value method is that the sensitivity matrix does not change. Thus, its calculation is required only once, which decreases the required computation time.

Finally, it was found that using experimental data and the standard method for damage identification, the damaged element could not be identified. Again, this thesis introduced and demonstrated a new method for damage identification: the damage identification method using comparison, which is summarized in Equation (5.7). In this method, the residual stiffness errors are compared with the stiffness value of the damaged model. Any composite sensitivity matrix can be used for this process. However, if the finite element model has been updated using the mean stiffness value, the same sensitivity matrix can be used. It was found that the best performance in damage identification has been reached using a composite sensitivity matrix created by mixed artificial boundary condition sets and mixed modes, which had the best performance in damage identification using simulated data. Furthermore, this research demonstrated that using that sensitivity matrix could successfully identify multiple damages.

B. RECOMMENDATIONS

The findings of this research for model update and damage identification look promising. Nevertheless, there is a long way to go before these methods can be successfully used.

The use of the mean stiffness method for model update, for example, has been performed only on a simple and uniform structure, a beam, in this research. Subsequent studies should focus on validating this method on more complex structures that might not be uniform.

In this thesis, the damage identification using comparison has been performed damaging the finite element model. In a future research, the real structure should be damaged. Then, Equation (5.7), which was used for the damage identification process, will become:

$$\left\{\Delta EI_x - \Delta EI_{RES}\right\} = [S] \setminus \left\{\omega_{upd}^2 - \omega_{Dam}^2\right\},$$

where $\left\{\Delta EI_x\right\}$ is the stiffness vector created by damage identification between the intact structure and the damaged structure, $\left\{\Delta EI_{RES}\right\}$ is the residual stiffness vector created by damage identification between the intact structure and the updated finite element model, $[S]$ is an arbitrary composite sensitivity matrix, $\left\{\omega_{upd}^2\right\}$ is a vector created by the estimated natural frequencies of the updated finite element model, and $\left\{\omega_{Dam}^2\right\}$ is a vector created by the measured natural frequencies of the damaged structure.

Finally, the use of different composite sensitivity matrices is suggested to investigate the performance of these methods.

THIS PAGE INTENTIONALLY LEFT BLANK

LIST OF REFERENCES

[1] R. I. Levin and N. A. J. Lieven, “Dynamic finite element model updating using simulated annealing and genetic algorithms,” *Mech. Sys. and Signal Proc.*, vol. 12, no. 1, pp. 91–120, 1998.

[2] J. H. Gordis, “Artificial boundary conditions for model updating and damage detection,” *Mech. Sys. and Signal Proc.*, vol. 13, no. 3, pp. 437–48, 1999.

[3] P. Cawley and RD. Adams, “The location of defects in structures from measurements of natural frequencies,” *J. Strain Anal.*, vol. 14, pp. 49–57, 1979.

[4] S. Li, S. Shelley and D. Brown, “Perturbed boundary condition testing,” in *Proc. 13th Int. Modal Anal. Conf.*, 1955, vol. 1, pp. 902–7.

[5] J. H. Gordis, “Omitted coordinate systems and artificial constraints in spatially,” *Modal Anal.*, vol. 11, pp. 83–95, 1996.

[6] K. Jones and J. Turcotte, “Finite element model updating using anti-resonant frequencies,” *J. Sound Vib.*, vol. 252, no. 4, pp. 717–27, 2002.

[7] Z. Tu and Y. Lu, “FE model updating using artificial boundary conditions with genetic algorithms,” *Comput. and Structures*, vol. 86, pp. 714–727, 2007.

[8] Z. Tu and Y. Lu, “Dynamic model updating using combined genetic-eigensensitivity algorithm and application in seismic response prediction,” *Earthquake Eng. Structural Dyn.*, pp. 1149–70, 2004.

[9] J. H. Gordis and K. Papagiannakis, “Optimal selection of artificial boundary conditions for model update and damage detection,” *Mech. Sys. and Signal Process.*, vol. 25, pp. 1451–1468, 2011.

[10] S. Timoshenko, *Vibration Problems in Engineering.* New York: D. Van Nostrand, 1937.

[11] MATLAB R2014a, Mathworks, Inc.

[12] Pulse Reflex, version 20.0.0, Bruel &. Kjaer, 2016.

[13] Roy R. Craig, *Structural Dynamics: An Introduction to Computer Methods*. New York: John Wiley & Sons, Inc.1981, pp. 385–387.

[14] B. N. Parlett, *The Symmetric Eigenvalue Problem*. Prentice Hall, 1980.

[15] R. M. Lin, D. J. Ewins, “Model updating using FRF data,” in *Proc. 15th Int. Sem. on Modal Anal.—KULeuven,* 1990, pp. 141–162.

[16] C. Fritzen and T. Kiefer, “Localization and correction of errors in Finite Element models based on experimental data,” in *Proc. 17th Int. Sem. on Modal Anal.*, 1992, pp. 1581–1596.

[17] M. Imregun and W. J. Visser, “A technique to update finite element models using frequency response data,” in *Proc. 9th Int. Modal Anal. Conf.*, 1991, pp. 462–468.

[18] W. H. Wittrick, “Rates of change of eigenvalues with reference to buckling and vibration problems,” *J. Roy. Aeronaut. Soc.*, vol. 24, pp. 590–591, 1962.

[19] A. R. A. Lagunes, “Finite element based structural damage detection using artificial boundary conditions,” M.S. thesis, MEC, NPS, Monterey, CA, 2007.

[20] R. L. Fox and M. P. Kapoor, “Rate of change of eigenvalues and eigenvectors,” *AIAA*, vol. 6, p. 12, 1968.

[21] R. B. Nelson, “Simplified calculations of eigenvector derivatives,” *AIAA*, vol. 14, p. 9, 1976.

[22] J. H. Gordis, “Eigenvector sensitivity analysis: An informal survey of selected contributions to the literature,” Tech. Rep., SDRC Engineering Services, 1991.

[23] P. Blelloch, “Calculation of eigenvector derivatives for structural systems,” Tech. Rep., SDRC Engineering Services, 1990.

INITIAL DISTRIBUTION LIST

1. Defense Technical Information Center
   Ft. Belvoir, Virginia

2. Dudley Knox Library
   Naval Postgraduate School
   Monterey, California